CELLULOSE-BASED AEROGELS FOR HEAT INSULATION AND OIL SPILL–CLEANING APPLICATIONS

FENG JINGDUO

(B.Eng.(Hons.), NUS)

A THESIS SUBMITTED

FOR THE DEGREE OF DOCTOR OF PHILOSOPHY

DEPARTMENT OF MECHANICAL ENGINEERING

NATIONAL UNIVERSITY OF SINGAPORE

2015

DECLARATION

I hereby declare that this thesis is my original work and it has been written by me in its entirety. I have duly acknowledged all the sources of information which have been used in the thesis.

This thesis has also not been submitted for any degree in any university previously.

FENG Jingduo

25 December 2015

ACKNOWLEDGEMENTS

I would like to express my gratitude to everybody who has directly or indirectly helped me in completing my dissertation work.

First, I wish to express my heartfelt gratitude to my supervisors, Asst Prof. Hai Minh Duong and Assoc. Prof. Christina Lim, for their invaluable guidance and constant support throughout my PhD candidature.

I would like to convey my appreciation to my fellow group members, Dr Feng Gong, Dr Zeng Fan, Mr Hanlin Cheng, Ms Peng Liu, and Mr Thang Quyet Tran, and especially Dr Son Truong Nguyen, for their devoted help and, most importantly, for making my graduate life memorable.

My warm thanks to the technical staff in Materials Laboratory, Mr Thomas Tan, Mr Hongwei Ng, Mr Abdul Khalim Bin Abdul, Mr Juraimi Bin Madon, and Ms Ruey Na Lam, for their technical assistance.

I also wish to thank my parents and husband Wentao He for their love, understanding, encouragement, and support. Without their help, it would not have been possible to complete my graduate work.

Finally, I gratefully acknowledge the Environmental Technology Research Program Grant R-265-000-450-490, National Research Funding (NRF) Proof-of-Concept (POC) Grant R-265-000-514-281, and NUS Research Scholarship for providing financial support.

TABLE OF CONTENTS

SUMMARY

In this thesis research, recycled cellulose aerogels utilizing paper waste were successfully fabricated using two methods. The first approach uses a sodium hydroxide–urea aqueous solution, while the second uses a Kymene binder. The second method is novel and cost-effective. The second method needs only three days to fabricate the cellulose aerogels, compared with nine days for the first approach. The cellulose aerogels synthesized with a Kymene binder do not require any chemical dissolution steps or coagulation processes during their fabrication. The morphology of the cellulose aerogels could be controlled by changing the cellulose fibre concentration inside the initial cellulose aqueous suspension. Moreover, a simple and effective method for hydrophobic coating of the cellulose aerogels was successfully developed. The coated cellulose aerogels showed a stable hydrophobicity over the tested period (five months).

The crude-oil (Ruby, RB; Te Giac Trang, TGT; and Rang Dong, RD) absorption capacities of cellulose aerogels (cellulose fibre concentration: 2.0 wt. %) fabricated from a sodium hydroxide–urea aqueous suspension at three different temperatures (25, 40, and 60 ^{o}C) were investigated. The cellulose aerogels showed the highest absorption capacity (24.4 g/g) for Ruby (RB) crude oil at 40 ^{o}C, due to the optimum viscosity of the oil. The absorption properties of cellulose aerogels fabricated with a Kymene binder are explored in detail in the thesis. The maximum absorption capacity (95 g/g for 5w40 motor oil) was achieved by the cellulose aerogels with a low cellulose fibre

concentration (0.25 wt. %) inside the initial cellulose aqueous suspension, due to a high porosity (99.4 %) of the cellulose aerogels.

The oil absorption kinetics of the cellulose aerogels was investigated with the pseudo-first-order and pseudo-second-order models. The investigations provided the benchmark values for the absorption rate constant. The activation energy of the oil absorption behaviours of the cellulose aerogels fabricated with a Kymene binder was also provided. The pseudo-second-order model was more suitable for predicting the absorption behaviour of the cellulose aerogels because of its chemi-sorption nature.

Furthermore, the pH values of the artificial sea-water had a negligible effect on the oil absorption behaviours of the cellulose aerogels, and the result show the feasibility of applying the cellulose aerogels in future oil-spill accidents. The cellulose aerogels of industrial size (38cm×38cm×1cm) and fabricated with the Kymene binder method could also be bent and rolled without damaging their shape, which demonstrates their high flexibility.

The thermal conductivity and thermal stability of the cellulose aerogels fabricated with a sodium hydroxide–urea aqueous solution, the cellulose aerogels fabricated with a Kymene binder, and silica–cellulose aerogels were investigated. The cellulose aerogels fabricated with a sodium hydroxide–urea aqueous solution showed a thermal conductivity of 0.032 W/mK. However, a continuous weight loss was observed during thermogravimetric analysis. Although the thermal conductivity of the cellulose aerogels fabricated with a Kymene binder was 0.034–0.037 W/mK, the thermal stability was improved. The cellulose aerogels using Kymene binder decompose at a temperature of 300 ^{o}C. To improve the thermal stability of the cellulose-based aerogels

further, the silica–cellulose aerogels were successfully developed. A 25 ^{o}C delay of the decomposition of cellulose component (to 325 ^{o}C from 300 ^{o}C) was observed. Moreover, the silica–cellulose aerogels exhibited an inherent super-hydrophobicity and a better mechanical strength (Young's modulus: 86–169 KPa) than that of the cellulose aerogels (4–39 KPa). The cellulose-based aerogels developed for this thesis could therefore be used in oil spill–cleaning and thermal-insulation applications.

LIST OF TABLES

LIST OF FIGURES

CHAPTER 1: Introduction

This chapter presents the background of aerogels, highlights the drying techniques of aerogels, and describes the general properties and applications of aerogels. In addition, as a guideline, the objectives and organizational structure of this thesis are also provided.

1.1 Aerogels

1.1.1 Background

An aerogel is a highly porous solid that holds gas (usually air) inside the porosity of its solid network [1, 2]. Aerogels are well known in the scientific community for their low densities (typically from 0.00016 to 0.5 g/cm^3) and high porosities (typically from 95 to 99.9 %) [3–5]. Kistler *et al.* [6] invented the first aerogel in 1931, which was a relatively transparent silica aerogel. In the same year, they also prepared the alumina, nickel tartarate, stannic oxide, tungstic oxide, gelatine, agar, nitrocellulose, cellulose, and egg albumin aerogels [6]. Their aerogel inventions concerned both the organic and inorganic aspects of the solid substance. In later years, Kistler [7] also initialized the fabrication of aerogels at industrial scale.

Almost all aerogels can be categorized into the following two groups: single-component aerogels and composite aerogels, based on their composition [2]. The most famous single-component aerogels are the inorganic silica aerogels, carbon aerogels, and metal-oxide aerogels, while polysaccharide-based aerogels, resorcinol–formaldehyde (RF) aerogels, and melamine–formaldehyde (MF) aerogels are well known as organic aerogels.

The composite aerogels may be fabricated by post-synthesis doping or modification of the single-component aerogels [8]. However, a more advantageous approach is to integrate the different entities during the sol-gel processing, which opens more possibilities for composite-aerogel fabrication from various substances with different compositions [8]. Typical composite aerogels are metal oxide–silica aerogels, metal oxide–RF aerogels, and silica–polymer aerogels. There are other classification criteria for aerogel categorization, such as form (monolith, granular, powder, and film) and microstructure (microporous, mesoporous, and mixed-porous) [2].

Aerogels have many fascinating properties. The carbon aerogels fabricated by Sun *et al.* [5] have a bulk density of as low as 0.00016g/cm^3, making them some of the lightest materials. Additionally, the sound velocity in silica aerogels, as reported by Fricke [9], can be as low as 100 m/s, which is among the lowest of any solid material. Kabbour *et al.* [10] synthesized activated carbonized aerogels with a specific surface area of 3200 m^2/g, which is one of the largest of any non-powder material. Interestingly, aerogels have been awarded 15 entries in the Guinness World Record for their material properties [11].

Currently, the research front of aerogels is extremely diverse: carbon aerogels (such as graphene and carbon nanotube), diamond aerogels, carbide aerogels, chalcogenide aerogels, and single-metal-element aerogels are being studied for their novel compositions, and novel composite aerogels for their practical applications [2, 12–15]. Aerogels currently have a niche market. Today, the aerogel market is experiencing a fast growth: the global market value of

aerogel products was $110.5 million in 2011, and is estimated to be $332.2 million in 2017, with a compound annual growth rate of 19.3% [16].

1.1.2 Drying techniques for aerogels

Drying is the process that converts gels into aerogels, and most aerogels are the resultants of successful drying. During conventional drying, the surface tension of the evaporation liquids leads to cracks, distortion, and shrinkage, which should typically be minimized in aerogel fabrication. The two most widely used drying methods for the production of aerogels are 1) the supercritical-drying method and 2) the freeze-drying method. Both methods minimize the surface tension by avoiding crossing of the liquid/gas boundary during drying. The phase diagram presented in Figure 1.1 below illustrates the two processes.

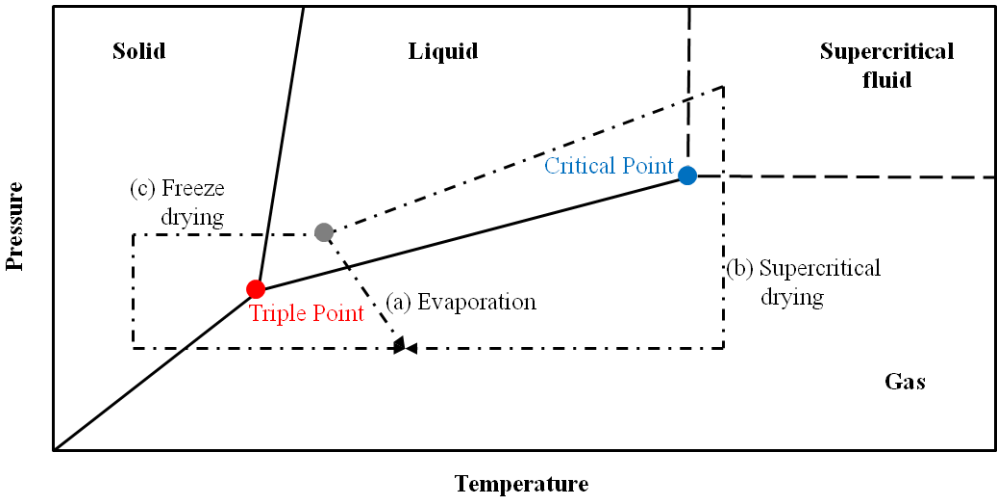

Figure 1.1 Phase diagram of (a) evaporation and the two drying methods, (b) supercritical drying and (c) freeze drying. Adapted from the thesis work of Mateusz B. Bryning [17].

Supercritical drying, also known as critical point drying (CPD), utilizes the supercritical fluid, which can effuse through a solid as a gas. When

temperature and pressure are raised above the critical point of a substance, the substance becomes a supercritical fluid, as no distinct liquid or gas phase can exist. As a supercritical fluid, when it leaves the pore walls, the evaporation of liquid does not occur (*i.e.*, there is no crossing of the liquid/gas boundary) [18]. Hence, the surface tension associated with the liquid evaporation is minimized [18, 19].

Supercritical carbon dioxide (CO_2) is the most commonly applied supercritical fluid for the supercritical drying, mainly due to its relatively easily accessible critical point (30.95 ^{o}C and 72.8 atm) [20]. Moreover, CO_2 is also non-toxic, non-flammable, and economical [21].

Freeze drying, also known as lyophilization, refers to a drying process in which the crystallized solvent below the triple point sublimes to a vapour phase [22]. As the freeze-dying method is used in this thesis, the history of freeze drying will be briefly reviewed. Freeze drying began in 1890. Altmann was the first to apply freeze drying to obtain the organs and tissues for a histological microscopy examination [23]. Later, in 1906, Bordas and d'Arsonval used a refrigerated condenser to remove the water vapour for the first time [24]. With the invention of the diffusion pump, Gersh added the effective vacuum concept to freeze drying in 1932 [25]. After World War II, accelerated freeze-drying (AFD) was developed by the Ministry of Food (UK), and commercial exploitation of this process started in 1960 [26]. In 1967, another breakthrough in freeze drying was reported by Mellor, who successfully developed a cyclic-pressure method by applying transfer effects of both the heat and vapour to reduce the drying time [27].

Freeze drying minimizes surface tension, since it avoids the boundary crossing of liquid and gas. Moreover, industrial freeze drying, as a standard industry process, and with the accumulated development of more than half a century, provides knowledge for its future applications [28]. Freeze drying is much more practical, economical, and scalable than supercritical drying, because supercritical drying, as a newly emerging industry process, with little public knowledge of its industrialization process, is well known for its high cost due to the high pressure and large amount of CO_2 involved. For this thesis, only water as a solvent for freeze drying was used, as water is cost-effective and eco-friendly. Moreover, all the cellulose aerogels synthesized in this thesis were fabricated from water-based solvents.

The freeze-drying process generally consists of three main stages: pre-freezing, primary drying, and secondary drying. During the pre-freezing stage, ice crystallizes from the free water, a critical step. This crystallization process may damage the network structures of the aerogels if the structures are not strong enough. The experimental results showed that our recycled cellulose-based samples were robust enough to withstand the formation of ice crystals [29–31]. The pre-freezing step for this thesis was carried out with a conventional refrigerator for 12 h, with the temperature approximately -18 ^{o}C.

After the pre-freezing stage, the frozen materials are taken out of the refrigerator, and then are transferred to the vacuum chamber (steady state pressure: below 0.1 mbar) of a freeze dryer. The temperature of the freeze dryer is approximately -90 ^{o}C. When the ice sublimes, the water vapour from sublimation is gathered by mounting a cold trap along its path. This is the

primary drying stage, also known as the sublimation drying stage, during which the majority of the water is removed from the samples. Two transport mechanisms are mainly involved in the primary drying: the energy transport, which transforms crystallized ice into water vapour, and the water vapour transport, which transports the water vapour from the surface of sublimation across the dried materials through the drying chamber to the cold trap [22]. Essentially, the driving force for the water sublimation relies on the vapour pressure difference between the sublimation surface and the cold trap.

Finally, the secondary drying stage, also known as desorption drying, commences after the disappearance of ice. During which stage, the moisture in the material is evaporated, and the heating rate and pressure must be reduced (temperature: approximately -95 ^{o}C; pressure: approximately 0.03 mbar) to successfully dry the materials, due to the upper safe temperature limit for the materials and low water vapour pressure in the chamber. For porous materials, such as the aerogels, the secondary drying may consume a third of the total drying time, due to the large surface area [32]. Moreover, over-drying is difficult to avoid at this stage, as it is difficult to judge whether the drying is finished or not, which further extends the drying time.

Ambient drying may reduce the time and energy consumptions of supercritical drying and freeze drying [33]. For the ambient-drying conditions, robust network structures need to be constructed to prevent collapse or irreversible shrinkage; another approach is to minimize the surface tension by chemically modifying the pore surface and carefully choosing the pore solvent [33]. At this point, both approaches are far from mature and are even

harmful to the environment, due to the large amount of chemicals and time required for aging or solvent exchange [34–36].

1.1.3 General properties and applications of aerogels

In this section, the discussion focuses on the porous, thermal, and mechanical properties of the various aerogels, which are well known in the scientific community [2, 8, 33]. The high surface areas and porosity make aerogels potential candidates for storage media, such as gas filters, absorption media, and hydrogen storage media [37]. Silica aerogels were used as gas filters to collect aerosols (viruses and bacteria in the size range of 20–2000 nm) for gas purification [38]. Moreover, aerogels were studied as absorption media, since the high porosity of aerogels leads to a large absorption capacity (14–743 g/g) [5, 39–42]. Many researchers have proposed to tailor silica aerogels to the host matrixes for long–life nuclear waste [40, 41]. In addition, aerogels such as carbon aerogels, silica aerogels, and cellulose aerogels have served as absorbents for oils and other organic pollutants [5, 39, 42].

One of the famous applications of aerogels is thermal insulation, as aerogels (thermal conductivity: 0.0089–0.05 W/mK) are among the best known thermal insulation materials [43–45]. Cohen *et al.* [45] reported a silica aerogel, fabricated by using separated catalysts for hydrolysis, condensation, and gelation steps, with a thermal conductivity of 0.0089 W/mK under ambient conditions. For comparison, air has a thermal conductivity of around 0.025 W/mK, which also implies that the low thermal conductivity of the silica aerogel is not the result of the high porosity [46, 47]. The low thermal conductivity of silica aerogels can be adequately explained by the Knudsen

effect. According to the Knudsen effect, when the pore size of a material is smaller than the mean free path of air, the thermal conductivity of the material is dramatically reduced [48].

Table 1.1 The economic relevance of typical aerogel insulation products [49]. (Reproduced with permission from Ref. 49. Copyright (2012) Springer.)

Application	Installation and assembly cost	Operating cost	Economic potential
Off-shore oil and gas	Smaller pipe diameter, lower weight, more pipes per round-trip installation, fewer trips	Superior lifetime, improved degradation resistance	High economic potential
Aeronautics/aerospace	Simplification of overall design, light construction, size reduction lowers materials/ assembly cost	Smaller gross weight results in fuel savings or additional capacity	Low economic potential
Building insulation	Comparable to conventional insulation, currently more elaborate due to lack of experience	Reduction of heating/cooling energy and/or larger useable building/exterior volume	Moderate economic potential
High temperature insulation	Smaller overall pipe diameter or exterior dimensions, easier installation	Reduced surface area per unit length, lower radiative losses, improved resistance and lifetime	Moderate economic potential
Cryogenic applications	Smaller overall pipe diameter or exterior dimensions, easier installation	Reduced sensitivity to cryo-embrittlement, increased lifetime, energy and/or space savings	Low economic potential
Appliances and apparel	Significantly more complex than standard technology	Energy savings/increased thermal comfort for lightweight extreme performance personal wear/gear	Low economic potential

Many commercial thermal products have been developed from silica aerogels, such as Thermal Wrap ™, Compression Pack ™, and Lumira ™ [49, 50]. Currently, North American industrials Cabot Corporation and Aspen Aerogels are the two main players in the global market for aerogel insulation, and their products are mainly sold in off-shore oil and gas, aerospace, building insulation, high temperature insulation, cryogenic applications, and apparel [49]. Some typical aerogel insulation products and their economic relevance are listed in Table 1.1 above.

The thermal stability of aerogels highly depends on the nature of their substance, for instance, the degradation temperatures of alumina aerogels (above 950 ^{o}C) are much higher than those of polymer aerogels (e.g. Resorcinol formaldehyde aerogels: 300–400 ^{o}C) [51, 52]. On the other hand, a slight improvement in the thermal stability of components with lower thermal stability has also been observed for composite aerogels, due to the interactions between the different components [53].

For the mechanical aspect, some aerogels are highly compressible materials (e.g. epoxy-clay aerogels can be compressed to a strain above 60%), and some elastic aerogels have been successfully synthesized (e.g. elastic graphene aerogels) [54, 55]. The silica aerogels with a reasonable compressible ability resulting from their low densities (0.13 g/cm^3) enable a large amount of kinetic energy to be absorbed (shock pressure: 6.7 GPa; shock density: 0.79 g/cm^3) when they are used as absorbers and experience shock compressions [56]. The low-shock-impedance silica and carbon aerogels are potentially applicable in generating thermodynamically confined plasma of few eV and capturing freezing states of minerals produced at 100 Mbar shock

pressure [56–58]. However, most aerogels are highly brittle materials (collapsed at a compressive strain below 5%), especially silica aerogels, and this characteristics limits their practical applications [59–61].

Table 1.2 A general summary of aerogel properties and applications [62]. (Reproduced with permission from Ref. 62. Copyright (1998) Elsevier.)

Property	Feature	Application
Thermal conductivity	• Best insulating solid • Transparent • High temperature • Lightweight	• Architectural and appliance insulation, portable coolers, transport vehicles, pipes, cryogenics, skylights • Space vehicles and probes, casting molds
Density/ porosity	• Lightest synthetic solid • Homogeneous • High specific surface area • Multiple compositions	• Catalysts, sorbers, sensors, fuel storage, ion exchange • Targets for ICF, X-ray lasers
Optical	• Low refractive index solid • Transparent • Multiple compositions	• Cherenkov detectors, lightweight optics, lightguides, special-effect optics
Acoustic	• Lowest sound speed	• Impedance matchers for transducers, range finders, speakers
Mechanical	• Elastic • Light weight	• Energy absorbers, hypervelocity particle traps
Electrical	• Lowest dielectric constant • High dielectric strength • High surface area	• Dielectrics for ICs, spacers for vacuum electrodes, vacuum display spacers, capacitors

Aerogels also have other extraordinary properties, such as acoustic, optical, and electronic properties. All these impressive properties enable them to have numerous practical and potential applications, as listed in Table 1.2 above.

1.2 Objectives of thesis

Large amounts of paper waste are constantly generated world-wide, and so paper waste should be recycled to preserve forests and reduce pollution

from landfills and incineration [63, 64]. Through separation processes, paper waste could be converted to recycled cellulose fibres [65]. These recycled cellulose fibres are a cost-effective and abundant raw material, and will be explored in this thesis [29–31]. The recycled cellulose fibres and general cellulose materials will be extensively discussed in Section 2.1.

This thesis aims to develop cellulose-based aerogels from recycled cellulose fibres of paper waste, and characterize the properties of these aerogels. The results of this thesis might help the environment in the following three ways:

- Finding new applications for recycled cellulose fibres, which would promote paper recycling.
- Introducing a promised sorbent material for oil-spill cleaning.
- Offering alternative materials for thermal insulation of buildings, which could help to save energy and reduce emissions of greenhouse gases.

The specific objectives of this research were to

(a) Propose a novel and cost-effective process for preparing highly flexible hydrophobic cellulose aerogels of an industrial size;

(b) Obtain cellulose aerogels with high absorption capacity for different oils, and investigate their oil absorption kinetics;

(c) Fabricate cellulose aerogels with low thermal conductivities;

(d) Develop cellulose composite aerogel to improve the thermal stability and mechanical strength of cellulose aerogels.

It should be noted that this thesis focuses on synthesizing the cellulose-based aerogels of recycled cellulose fibres from paper waste and testing their properties. Other cellulose resources, such as bacterial cellulose and plant

cellulose, are beyond the scopes of this thesis, due to the eco-friendliness of the recycled cellulose fibres. The fabrication of recycled cellulose fibres from paper waste was not attempted for this thesis, because the relevant technology is mature and well established [65]. Two methods for synthesizing recycled-cellulose aerogels have been developed. The first method uses sodium hydroxide–urea aqueous solutions. The second method, introduced for the first time in this thesis, is a novel method that works via the application of a Kymene binder. This thesis mainly deals with the oil absorption and thermal properties of the developed aerogels, rather than their other properties, because of its stated objectives and the high environmental potential of these two aspects.

1.3 Organization of thesis

This thesis is organized into the following chapters:

Chapter 1, *i.e.* this chapter, introduces the background of aerogels, discusses the drying techniques of aerogels, and presents the general properties and applications of aerogels. The motivations and contents of the thesis are also provided.

Chapter 2 presents a comprehensive literature review of cellulose, cellulose aerogels, and silica–cellulose composite aerogels, including their fabrication methods, morphology, and various properties.

Chapter 3 gives a summary of the materials, experimental methods, and characterization approaches of the cellulose-based aerogels in this thesis. In particular, the hydrophobic coating of recycled cellulose aerogels is discussed in detail.

Chapter 4 investigates the effects of cellulose concentrations, sodium-hydroxide concentrations, and urea concentrations on the morphologies of recycled cellulose aerogels using sodium hydroxide–urea aqueous suspensions. The oil absorption properties and mechanical properties of the cellulose aerogels are also presented. In addition, the oil absorption capacities of the different crude oils of cellulose aerogels are investigated for the first time.

Chapter 5 studies the morphologies, oil absorption properties, and mechanical properties of recycled cellulose aerogels synthesized using the Kymene-binder method, which is a novel approach. The absorption kinetics of two oils with different viscosities of the recycled cellulose aerogels at different temperatures are also investigated. In addition, activation energies are calculated from the change of the absorption-rate constant with temperature through the Arrhenius equation, which has never been done before for cellulose aerogels.

Chapter 6 focuses on the heat-insulation applications of recycled cellulose-based aerogels. The thermal stability and thermal conductivity of the recycled cellulose aerogels using sodium hydroxide–urea aqueous suspensions, of the recycled cellulose aerogels using a Kymene binder, and of the silica–cellulose aerogels are determined. In addition, the morphologies and mechanical properties of silica–cellulose aerogels are presented. This chapter highlights the fact that silica–cellulose aerogels show increased mechanical strength and improved thermal stability over the recycled cellulose aerogels.

Chapter 7 presents the main conclusions of this thesis and offers recommendations for further research.

References

[1] J. Cai, S. Kimura, M. Wada, S. Kuga, L. Zhang, Cellulose aerogels from aqueous alkali hydroxide-urea solution, *ChemSusChem*, 2008, **1**, 149-154.

[2] A. Du, B. Zhou, Z. Zhang, J. Shen, A Special Material or a New State of Matter: A Review and Reconsideration of the Aerogel, *Materials*, 2013, **6**, 941-968.

[3] I. M. El-Nahhal, N. M. El-Ashgar, A review on polysiloxane-immobilized ligand systems: Synthesis, characterization and applications, *J. Organomet. Chem.*, 2007, **692**, 2861-2886.

[4] V. M. Gun'ko, Competitive adsorption, *Theor. Exp. Chem.*, 2007, **43**, 139-183.

[5] H. Sun, Z. Xu, C. Gao, Multifunctional, ultra-flyweight, synergistically assembled carbon aerogels, *Adv. Mater.*, 2013, **25**, 2554-2560.

[6] S. S. Kistler, Coherent expanded aerogels and jellies, *Nature*, 1931, **127**, 741.

[7] S. S. Kistler, Treatment of aerogels to render them waterproof, U. S. Pat. No. 2,589,705, 1952.

[8] N. Hüsing, U. Schubert, Aerogels, 2006.

[9] J. Fricke, Aerogels-Highly tenuous solids with fascinating properties, *J. Non-Cryst. Solids*, 1988, **100**, 169-173.

[10] H. Kabbour, T. F. Baumann, J. H. Satcher, A. Saulnier, C. C. Ahn, Toward new candidates for hydrogen storage: high-surface-area carbon aerogels, *Chem. Mater.*, 2006, **18**, 6085-6087.

[11] S. Liu, Q. Yan, D. Tao, T. Yu, X. Liu, Highly flexible magnetic composite aerogels prepared by using cellulose nanofibril networks as templates, *Carbohydr. Polym.*, 2012, **89**, 551-557.

[12] S. K. Gill, P. Brown, L. J. Hope-Weeks, Gold modified cadmium sulfide aerogels, *J. Sol-Gel Sci. Technol.*, 2010, **57**, 68-75.

[13] Y. Kong, Y. Zhong, X. Shen, L. Gu, S. Cui, M. Yang, Synthesis of monolithic mesoporous silicon carbide from resorcinol-formaldehyde/silica composites, *Mater. Lett.*, 2013, **99**, 108-110.

[14] N. Leventis, A. Sadekar, N. Chandrasekaran, C. Sotiriou-Leventis, Click Synthesis of Monolithic Silicon Carbide Aerogels from Polyacrylonitrile-Coated 3D Silica Networks, *Chem. Mater.*, 2010, **22**, 2790-2803.

[15] Z. Li, J. Ding, H. Wang, K. Cui, T. Stephenson, D. Karpuzov, D. Mitlin, High rate SnO_2-graphene dual aerogel anodes and their kinetics of lithiation and sodiation, *Nano Energy*, 2015, **15**, 369-378.

[16] M. Gagliardi, Aerogels, http://www.bccresearch.com/market-research/advanced-materials/aerogels-markets-technology-avm052c.html, 2013 [assessed 16.03.11].

[17] M. B. Bryning, Carbon nanotube networks in epoxy composites and aerogels Physics and Astronomy, Master's Thesis, Physics and Astronomy, *University of Pennsylvania*, 2007.

[18] R. W. Pekala, Organic aerogels from the polycondensation of resorcinol with formaldehyde, *J. Mater. Sci.*, 1989, **24**, 3221-3227.

[19] Q. Tang, T. Wang, Preparation of silica aerogel from rice hull ash by supercritical carbon dioxide drying, *J. Supercrit. Fluids*, 2005, **35**, 91-94.

[20] P. Munshi, S. Bhaduri, Supercritical CO_2 : a twenty-first century solvent for the chemical industry, *Curr. Sci.*, 2009, **97**, 63-72.

[21] D. Sanli, S. E. Bozbag, C. Erkey, Synthesis of nanostructured materials using supercritical CO2: Part I. Physical transformations, *J. Mater. Sci.*, 2011, **47**, 2995-3025.

[22] G. W. Oetjen, P. Haseley, Freeze-drying, *WILEY-VCH*, Germany, 2004, p. 1.

[23] R. Altamann, Die Elementarorganismen und ihre Beziehungen zu den Zellen. Viet. Leipzig, 1890, **Viet**.

[24] F. Bordas, A. D. Arsonval, Les basses températures et l'analyse chimique, *C.r. hebd. Séanc. Acad. Sci. ,Paris*, 1906, **142**, 1058.

[25] I. Gersh, The Altmann technique for fixation by drying while freezing, *Anat. Rec*, 1932, **53**, 309.

[26] E. G. B. Gooding, E. J. Rolfe, Some recent work on dehydration in the United Kingdom, *Fd Technol*, 1957, **11**, 302.

[27] J. D. Mellor, Freeze-drying process with cyclic vacuum pressure, Brit. Pat. No. 1,083,244, 1967.

[28] A. Borisova, M. De Bruyn, V. L. Budarin, P. S. Shuttleworth, J. R. Dodson, M. L. Segatto, J. H. Clark, A sustainable freeze-drying route to porous polysaccharides with tailored hierarchical meso- and macroporosity, *Macromol. Rapid Commun.*, 2015, **36**, 774-779.

[29] J. Feng, S. T. Nguyen, Z. Fan, H. M. Duong, Advanced fabrication and oil absorption properties of super-hydrophobic recycled cellulose aerogels, *Chem. Eng. J.*, 2015, **270**, 168-175.

[30] S. T. Nguyen, J. Feng, N. T. Le, A. T. T. Le, N. Hoang, V. B. C. Tan, H. M. Duong, Cellulose Aerogel from Paper Waste for Crude Oil Spill Cleaning, *Ind. Eng. Chem. Res.*, 2013, **52**, 18386-18391.

[31] S. T. Nguyen, J. Feng, S. K. Ng, J. P. W. Wong, V. B. C. Tan, H. M. Duong, Advanced thermal insulation and absorption properties of recycled cellulose aerogels, *Colloids Surf., A*, 2014, **445**, 128-134.

[32] J. D. Mellor, Fundamentals of freeze-drying, *Academic Press*, London, 1978, p. 13.

[33] U. S. N. Hüsing, Aerogels-airy materials: chemistry, structure, and properties, *Angew. Chem. Int. Ed*, 1998, **37**, 22-45.

[34] P. J. Davis, C. J. Brinker, D. M. Smith, Pore structure evolution in silica gel during aging/drying I. temporal and thermal aging, *J. Non-Cryst. Solids*, 1992, **142**, 189-196.

[35] S. Haereid, M. Einarsrud, Mechanical strengthening of TMOS-based alcogels by aging in silane solutions *J. Sol-Gel Sci. Technol.*, 1994, **3**, 199-204.

[36] A. P. Rao, G. M. Pajonk, A. V. Rao, Effect of preparation conditions on the physical and hydrophobic properties of two step processed ambient pressure dried silica aerogels, *J. Mater. Sci.*, 2005, **40**, 3481-3489.

[37] C. Robertson, R. Mokaya, Microporous activated carbon aerogels via a simple subcritical drying route for CO_2 capture and hydrogen storage, *Microporous Mesoporous Mater.*, 2013, **179**, 151-156.

[38] S. Cao, K. L. Yeung, J. K. C. Kwan, P. M. T. To, S. C. T. Yu, An investigation of the performance of catalytic aerogel filters, *Appl. Catal., B*, 2009, **86**, 127-136.

[39] J. G. Reynolds, P. R. Coronado, L. W. Hrubesh, Hydrophobic Aerogels for Oil-Spill Cleanup? Intrinsic Absorbing Properties, *Energ. Source.*, 2001, **23**, 831-843.

[40] P. R. Aravind, L. Sithara, P. Mukundan, P. K. Pillai, K. G. K. Warrier, Silica alcogels for possible nuclear waste confinement-A simulated study, *Mater. Lett.*, 2007, **61**, 2398-2401.

[41] T. Woignier, J. Reynes, J. Phalippou, J. L. Dussossoy, N. Jacquet-Francillon, Sintered silica aerogel: a host matrix for log life nuclear wastes, *J. Non-Cryst. Solids*, 1998, **225**, 353-357.

[42] Z. Y. Wu, C. Li, H. W. Liang, Y. N. Zhang, X. Wang, J. F. Chen, S. H. Yu, Carbon nanofiber aerogels for emergent cleanup of oil spillage and chemical leakage under harsh conditions, *Sci. Rep.*, 2014, **4**, 4079.

[43] B. E. Yoldas, M. J. Annen, J. Bostaph, Chemical engineering of aerogel morphology formed under nonsupercritical conditions for thermal insulation, *Chem. Mater.*, 2000, **12**, 2475-2484.

[44] J. Cai, S. Liu, J. Feng, S. Kimura, M. Wada, S. Kuga, L. Zhang, Cellulose-Silica Nanocomposite Aerogels by In Situ Formation of Silica in Cellulose Gel, *Angew. Chem. Int. Ed.*, 2012, **51**, 2076-2079.

[45] E. Cohen, L. Glicksman, Thermal Properties of Silica Aerogel Formula, *J. Heat Transfer*, 2015, **137**, 081601-081601-081601-081608.

[46] A. A. Balandin, S. Ghosh, W. Bao, I. Calizo, D. Teweldebrhan, F. Miao, C. N. Lau, Superior thermal conductivity of single-layer graphene, *Nano Lett.*, 2008, **8**, 902-907.

[47] A.-M. Tang, Y.-J. Cui, T.-T. Le, A study on the thermal conductivity of compacted bentonites, *Appl. Clay Sci.*, 2008, **41**, 181-189.

[48] S. S. Kistler, A. G. Caldwell, Thermal conductivity of silica aerogel, *Ind. Eng. Chem.*, 1934, **26**, 658-662.

[49] M. Koebel, A. Rigacci, P. Achard, Aerogel-based thermal superinsulation: an overview, *J. Sol-Gel Sci. Technol.*, 2012, **63**, 315-339.

[50] E. Cuce, P. M. Cuce, C. J. Wood, S. B. Riffat, Toward aerogel based thermal superinsulation in buildings: A comprehensive review, *Renew. Sust. Energ. Rev.*, 2014, **34**, 273-299.

[51] J. F. Poco, J. H. Satcher, L. W. Hrubesh, Synthesis of high porosity, monolithic alumina aerogels, *J. Non-Cryst. Solids*, 2001, **285**, 57-63.

[52] M. Reuß, L. Ratke, Subcritically dried RF-aerogels catalysed by hydrochloric acid, *J. Sol-Gel Sci. Technol.*, 2008, **47**, 74-80.

[53] S. Sequeira, D. V. Evtuguin, I. Portugal, Preparation and properties of cellulose/silica hybrid composites, *Polym. Compos.*, 2009, **30**, 1275-1282.

[54] E. M. Arndt, M. D. Gawryla, D. A. Schiraldi, Elastic, low density epoxy/clay aerogel composites, *J. Mater. Chem.*, 2007, **17**, 3525.

[55] J.-Y. Hong, B. M. Bak, J. J. Wie, J. Kong, H. S. Park, Reversibly Compressible, Highly Elastic, and Durable Graphene Aerogels for Energy Storage Devices under Limiting Conditions, *Adv. Funct. Mater.*, 2015, **25**, 1053-1062.

[56] N. C. Holmes, H. B. Radousky, M. J. Moss, W. J. Nellis, S. Henning, Silica at ultrahigh temperature and expanded volume, *Appl. Phys. Lett.*, 1984, **45**, 626.

[57] P. Amendt, S. G. Glendinning, B. A. Hammel, O. L. Landen, T. J. Murphy, L. J. Suter, S. Hatchett, M. D. Rosen, S. Lafitte, D. Desenne, J. P.

Jadaud, New methods for diagnosing and controlling hohlraum drive asymmetry on Nova, *Phys. Plasmas*, 1997, **4**, 1862.

[58] P. Amendt, S. G. Glendinning, B. A. Hammel, O. Landen, L. J. Suter, Direct measurement of X-ray drive from surrogate targets in nova hohlraums, *Phys. Rev. Lett.*, 1996, **77**, 3815-3818.

[59] Y. Kobayashi, T. Saito, A. Isogai, Aerogels with 3D ordered nanofiber skeletons of liquid-crystalline nanocellulose derivatives as tough and transparent insulators, *Angew. Chem. Int. Ed. Engl.*, 2014, **53**, 10394-10397.

[60] H. Maleki, L. Durães, A. Portugal, An overview on silica aerogels synthesis and different mechanical reinforcing strategies, *J. Non-Cryst. Solids*, 2014, **385**, 55-74.

[61] R. Saliger, V. Bock, R. Petricevic, T. Tillotson, S. Geis, J. Fricke, Carbon aerogels from dilute catalysis of resorcinol with formaldehyde, *J. Non-Cryst. Solids*, 1997, **221**, 144-150.

[62] L. W. Hrubesh, Aerogel applications, *J. Non-Cryst. Solids*, 1998, **225**, 335-342.

[63] A. Nourbakhsh, A. Ashori, Particleboard made from waste paper treated with maleic anhydride, *Waste Manage. Res.*, 2010, **28**, 51-55.

[64] L. Szabó, A. Soria, J. Forsström, J. T. Keränen, E. Hytönen, A world model of the pulp and paper industry: Demand, energy consumption and emission scenarios to 2030, *Environ. Sci. Policy*, 2009, **12**, 257-269.

[65] C. J. Biermann, Chapter 10: Fiber from recycled paper, Handbook of pulping and papermaking, 2 nd ed., *Academic Press*, San Diego, 1996, pp. 263-282.

CHAPTER 2: Literature Review

This literature-review chapter presents the basic facts about cellulose materials and comprehensive information about cellulose aerogels and silica–cellulose composite aerogels. Both the fabrication methods and properties of cellulose aerogels and silica–cellulose aerogels are discussed in detail.

2.1 Cellulose materials

2.1.1 Introduction

Cellulosic materials have a long history in human civilization, dating back to prehistoric times. When mankind discovered the technology to generate fire, it is very possible that cellulosic materials served as the fuel. In 4500 BC, human beings had already cultivated hemp for rope and cordage production in China and Southeast Asia. Five hundred years later, in 4000 BC, garments containing cellulosic materials were fabricated. In AD 105, Ts'ai Lun in China was the first to make paper sheets, and since then cellulose has been used extensively in the writing of documents. Later in history, cellulose was also involved in propellants and gun-powder production, which was significant in exploration and trade [1].

French chemist Anselme Payen was the first to separate cellulose, *i.e.* an isomeric form of starch (44.4 wt%, C; 6.2 wt%, H), from other substances; it was later named 'cellulose' by the French Academy in 1839 [2]. About 100 years later, cellulose was proven by the works of Staudinger and other scientists to be a covalently linked macromolecule [3]. This fact is thought to

be the foundation of polymer science [1]. In 1953, Staudinger received the Nobel Prize for his contributions to the polymer molecular structure field.

Cellulose has the advantages of biodegradability, non-toxicity, and high chemical durability, and is the most abundant organic polymer [4]. The annual production rate of cellulose by photosynthesis is approximately 1.5×10^{12} tons, which guarantees its renewability and sustainability [4–7]. Moreover, cellulose is biodegradable in the natural environment. Cellulolytic microorganisms are commonly found in soils, and they degrade cellulose completely with the help of other non-cellulolytic microorganisms [8]. Under aerobic conditions, the end products of the degradation of cellulose are normally carbon dioxide and water, while under anaerobic conditions, the end products are methane and carbon dioxide [8, 9]. Furthermore, cellulose is not toxic to living organisms, because of its high chemical durability [10, 11].

Cellulose is produced by the condensation polymerization of glucose [12]. Wood, plants, tunicates, several species of algae, and some bacteria (e.g. Gluconacetobacter xylinus) can convert glucose to cellulose [13]. The secondary wall of cotton-seed hairs contains nearly 100% cellulose, while in many other plant products, such as wood, straw, and bamboo, the cell wall is constructed of a combination of cellulose, hemi-cellulose, and lignin [9].

The major source of cellulose for paper production is wood. As recycled cellulose fibres from paper waste were used for this thesis, the pulping process is briefly discussed. Wood is converted into pulp for the purposes of dispersion in water and reformation of webs by the pulping process. The four industrial categories for wood pulping are chemical pulping, semi-chemical pulping, chemi-mechanical pulping, and mechanical pulping,

categorized by the dependency on chemicals and mechanical energy [14]. The method with higher dependency on mechanical energy and lower dependency on chemicals results in a higher fibre yield and fibres of lower mechanical strength, because of the increased amount of lignin and cleavages in the cellulose fibres, which are associated with the increased usage of mechanical energy [14].

2.1.2 Structure of cellulose

The unit of cellulose is the D-anhydroglucopyranose unit (AGU), and the AGUs are linked by β-(1→ 4)-glycosidic bonds in cellulose, as displayed in Figure 2.1below. Cellulose could also be viewed as an isotactic polymer of the dimer cellobiose. The cellulose chain has a reducing C-1 end and a non-reducing C-4 end with regard to the hydroxyl group behaviour. Three hydroxyl groups are located at the C-2, C-3, and C-6 positions of each of the AGUs. As confirmed by X-ray diffraction (XRD) and nuclear magnetic resonance (NMR), the AGUs in a cellulose chain normally follow a $^4C_1$ chair conformation. In the $^4C_1$ chair conformation, the free hydroxyl groups are on the ring plane (equatorial), whereas the hydrogen atoms are located in a vertical position (axial).

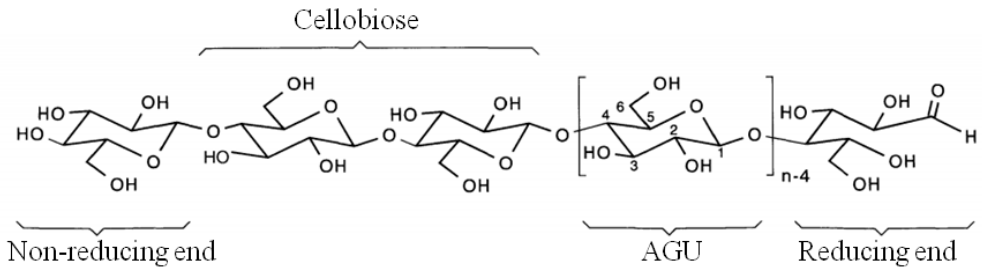

Figure 2.1 The primary structure of cellulose [15]. (Reproduced with permission from Ref. 15. Copyright (2004) John Wiley and Sons.)

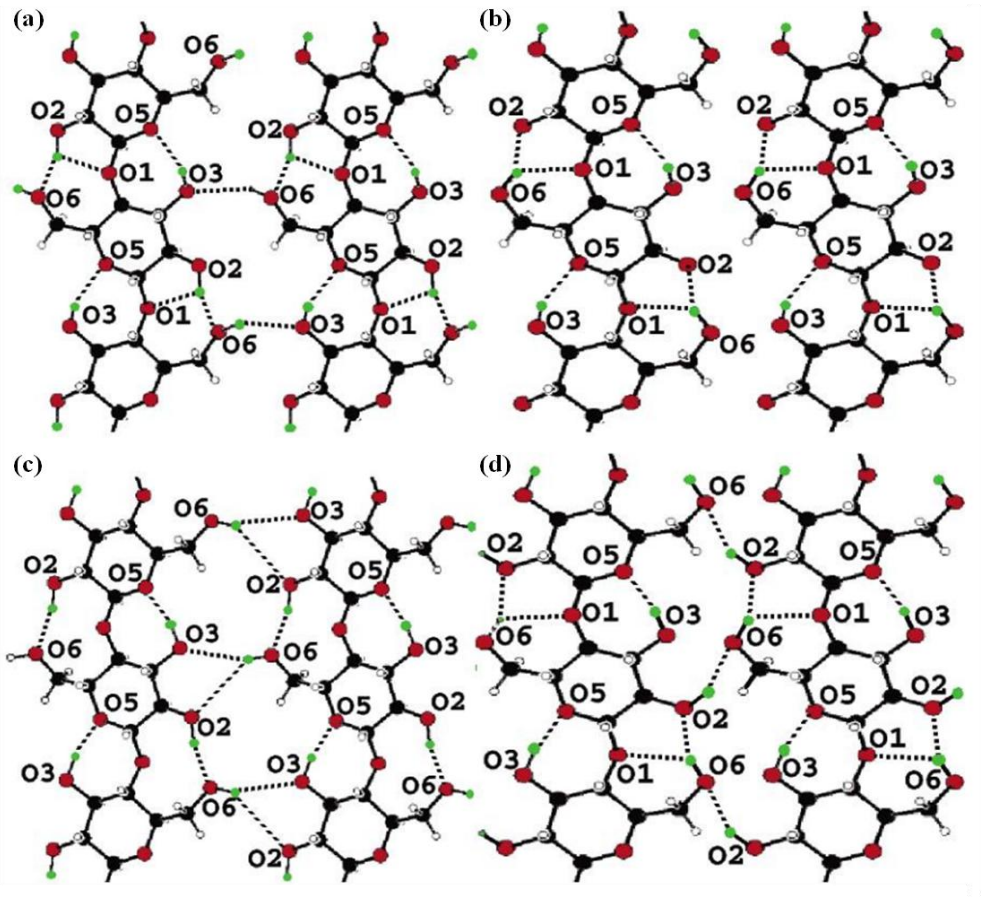

Figure 2.2 Hydrogen-bonding patterns in cellulose I_β investigated by deuterium atom location [16]. Carbon, oxygen, hydrogen, and deuterium atoms are in black, red, white, and green, respectively. (a) and (b) show the cellulose chain at the corner of the unit cell parallel to the *c* axis, while (c) and (d) display the chain passing through the centre of the *a*-*b* plane of the unit cell. (a) and (c) present the calculation results based on Fourier difference analysis, whereas in (b) and (d), the second disordered deuterium atom components are considered. (Adapted with permission from Ref. 16. Copyright (2002) American Chemical Society.)

The hydroxyl groups facilitate the formation of hydrogen bonds. There are two types of hydrogen bonds: intramolecular and intermolecular hydrogen bonds [13]. The intramolecular hydrogen bonds that are between O-3-H and O-5', and between O-2-H and O-6' are suggested by XRD and NMR [17, 18]. There are currently a number of hypotheses about intermolecular hydrogen bonds. One such hypothesis, made by Nishiyama *et al.* [16], is presented in Figure 2.2 above. The hydrogen bonds contribute to the stiffness of the cellulose chain and the stability of the crystalline conformation. Moreover, the

micro-fibrils formation of cellulose also needs the cooperation of hydrogen bonds and the van der Waals forces [9].

The fringed fibril model is well established for the supramolecular structure of cellulose [19]. This model shows the coexistence of the amorphous regions and crystalline regions, while neglecting the small amount of substances that have minor influence in an intermediate state of order [19]. This two-phase model is widely used to adequately explain the heterogeneous reaction process of cellulose [15]. An illustration of this model is shown in Figure 2.3 below [15, 19]. The crystalline degree of native cellulose is approximately 60–90% [20].

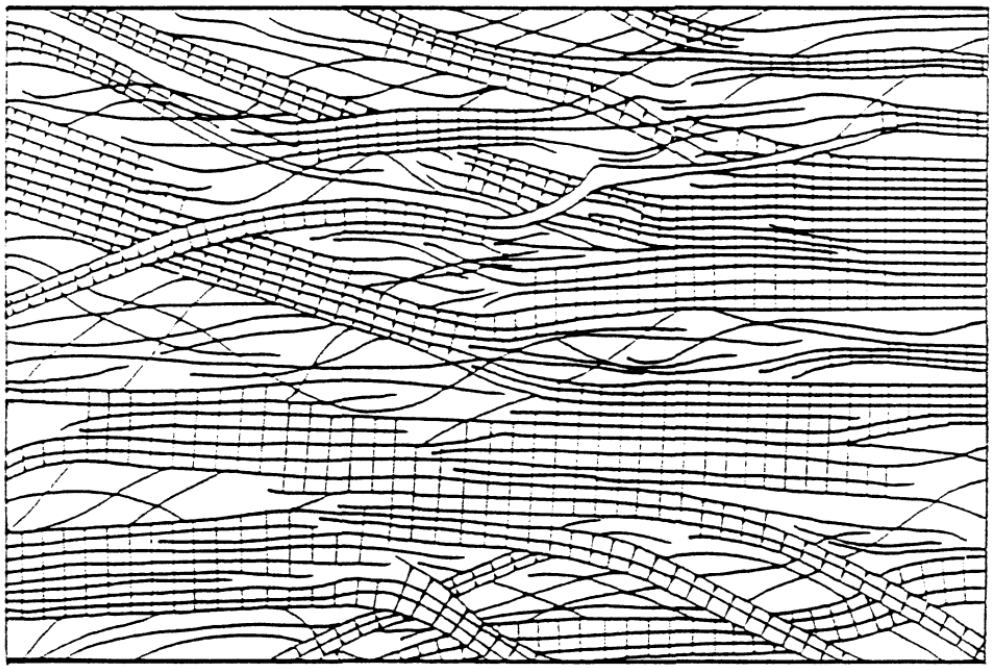

Figure 2.3 The supramolecular structure of cellulose according to the fringed fibril model [15, 19]. The fringed fibril model shows the coexistence of the amorphous regions and crystalline regions of cellulose. (Reproduced with permission from Ref. 15. Copyright (2004) John Wiley and Sons.)

Four different cellulose crystalline allomorphs (cellulose I, II, III, and IV) have been well known for a long time [13, 21]. Natural cellulose is cellulose I, while cellulose II commonly results from the regeneration of a

cellulose I solution inside an aqueous medium at room temperature or slightly higher temperatures [4]. The conversion of cellulose I to cellulose II is usually irreversible. Generally, cellulose III is obtained from cellulose I or II via treatment with liquid ammonia below -30 ^{o}C, and subsequent evaporation of the ammonia [15]. For cellulose IV, one of the methods for generating it is to soak the cellulose inside a suitable liquid at a high temperature under tension [15]. The unit cell of native cellulose (cellulose I), defined by the Meyer–Misch model, is shown in Figure 2.4 below, and its lattice lengths a, b, and c, as well as lattice angle β, are indicated [22]. The parameters of the unit cells of various cellulose allomorphs are listed in Table 2.1 below [22].

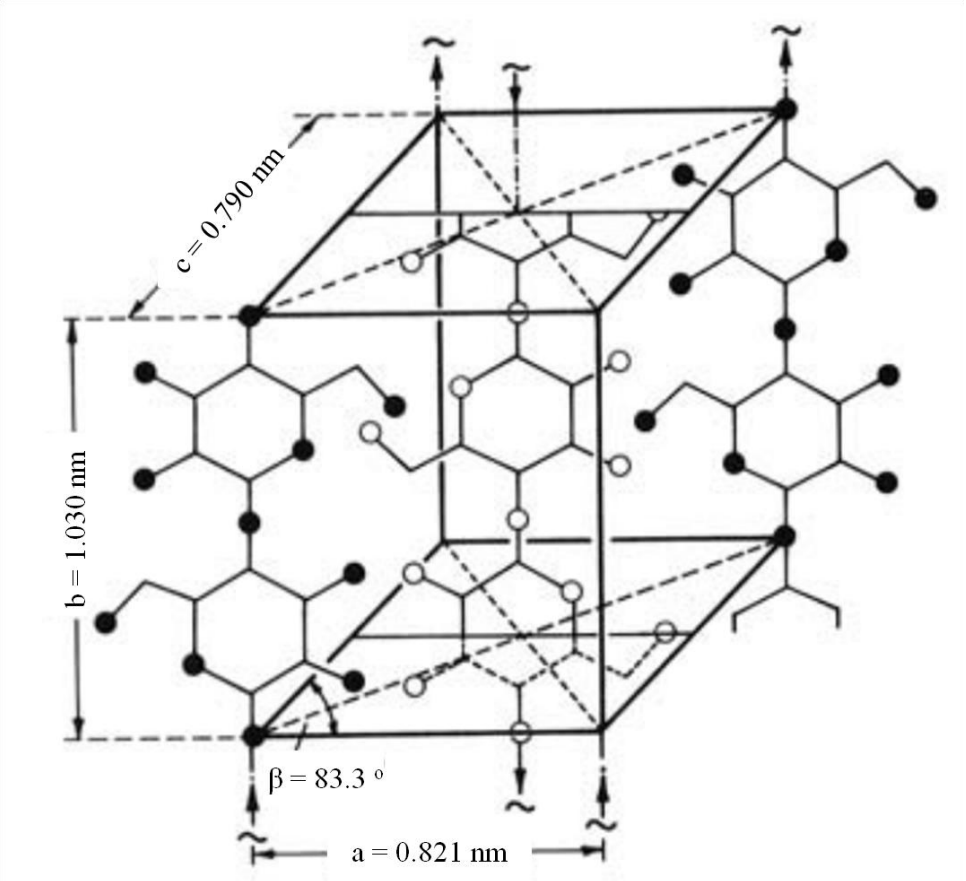

Figure 2.4 shows the unit cell of native cellulose (cellulose I) defined by the Meyer–Misch model, with dots representing oxygen atoms [22]. (Reproduced with permission from Ref. 22. Copyright (2012) Wiley-VCH Verlag GmbH & Co. KGaA.)

Table 2.1 A comparison of different parameters for the unit cells of various cellulose allomorphs[22]. (Reproduced with permission from Ref. 22. Copyright (2012) Wiley-VCH Verlag GmbH & Co. KGaA.)

Polymorph	a (nm)	b (nm)	c (nm)	β (^{o})
Cellulose I	0.821	1.030	0.790	83.3
Cellulose II	0.802	1.036	0.903	62.8
Cellulose III	0.774	1.030	0.990	58.0
Cellulose IV	0.812	1.030	0.799	90.0

Based on recent studies conducted by synchrotron X-ray and neutron fibre diffraction, cellulose I is a mixture of the two polymorphs (I_α & I_β), and the parameters of the unit cells of these two polymorphs are known [13, 16, 23, 24]. The structures of I_α and I_β are triclinic and monoclinic, respectively [13, 21]. The lattice lengths a, b, and c of I_α are 0.596, 1.040, and 0.672 nm, and the lattice angles α, β, and γ are 114.80, 80.375, and 118.08 ^{o}, respectively [24]. The lattice lengths a, b, and c of I_β are 0.820, 1.038, and 0.778 nm, respectively, and the lattice angle β is 96.3 ^{o} [16]. Native cellulose produced from bacteria and algae consists mainly of I_α, while native cellulose from ramie, cotton, and wood sources usually has a higher I_β content [25, 26]. I_α is metastable and can be transformed to I_β by annealing, which has led to the conclusion that I_β is more thermodynamically stable [27].

The natural morphological structures (texture) of the cellulose fibres strongly depend on the cellulose sources, and can normally be described as a hierarchy of fibrous elements. The hierarchies of wood and flax are displayed in Figures 2.5 and 2.6 below, which show how cellulose fibres are organized according to wood and plants [28, 29]. Their hierarchical structures span from nanoscopic dimensions to macroscopic dimensions, from a few nanometres to micrometers, millimetres, and even meters.

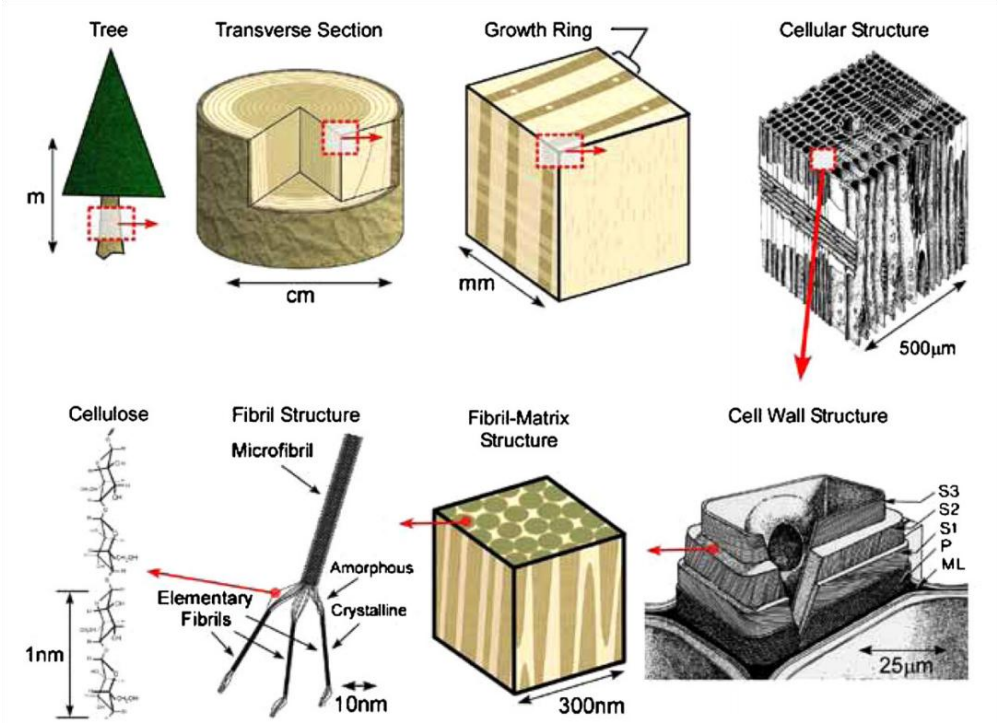

Figure 2.5 The hierarchical structure of wood with the dimensions [29]. (© IOP Publishing. Reproduced with permission. All rights reserved.)

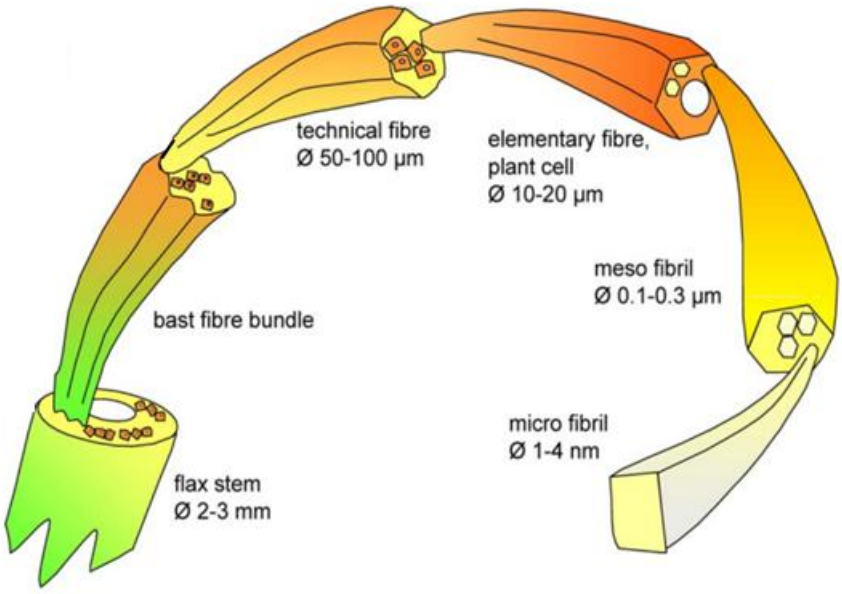

Figure 2.6 The hierarchy of flax fibres with the dimensions [28]. (Reproduced with permission from Ref. 28. Copyright (2006) Elsevier.)

The different microfibril structures of the different cellulose sources are the result of the different configurations of the terminal enzyme complexes (TCs) for cellulose microfibril biosynthesis in the cell wall [30]. The

different TC configurations are listed in Figure 2.7 below, and categorized into the two general structures (rosette and linear) [30]. Each grey dot of a single configuration in Figure 2.7 represents an identical subunit, which has multiple catalytic sites and is capable of producing a cellulose minisheet. The minisheet is a cellulose chain, a layer of parallel stacked cellulose chains, or multiple layers of parallel stacked cellulose chains, depending on the number and arrangement of the catalyst sites inside the subunit [13]. Figure 2.8 below illustrates how the TCs form a microfibril (wood): a TC subunit fabricates a layer of six paralleled cellulose chains bonded by van der Waals forces, and a TC containing six subunits produces a cellulose elementary fibril with 36 cellulose chains [13].

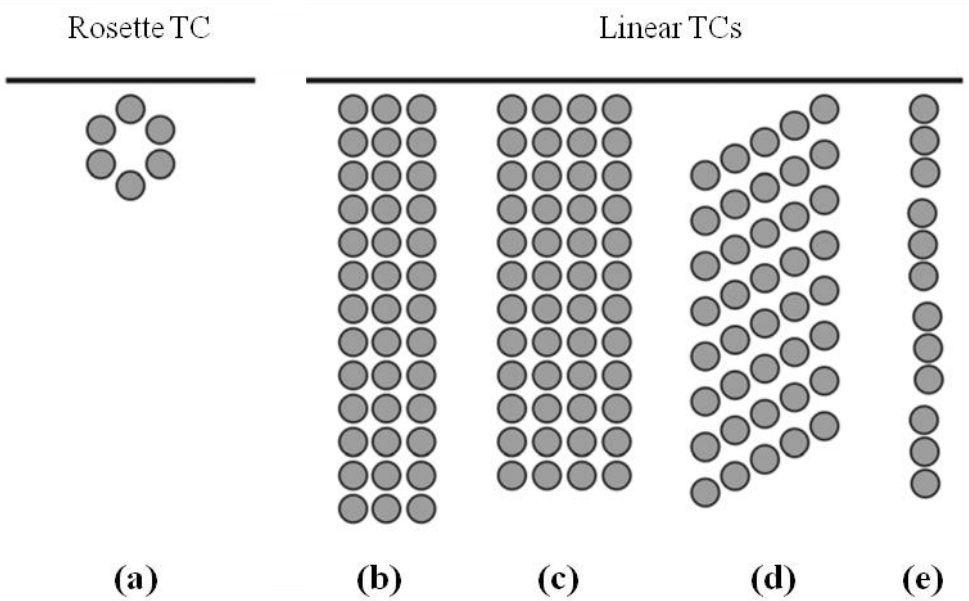

Figure 2.7 Configurations of different terminal enzyme complexes (TCs) of (a) wood, plants, and green algae (Micrasterias) (6 chains/subunit), (b) green algae (Valonia) (10–12 chains/subunit), (c) red algae (Erythrocladia) (4 chains/subunit), (d) yellow-green algae (Vaucheria) (1 chain/subunit), and (e) bacteria (Acetobacter) (16 chains/subunit) [13, 30, 31]. Each grey circle represents a subunit. (Reproduced with permission from Ref. 13. Copyright (2011). Royal Society of Chemistry.)

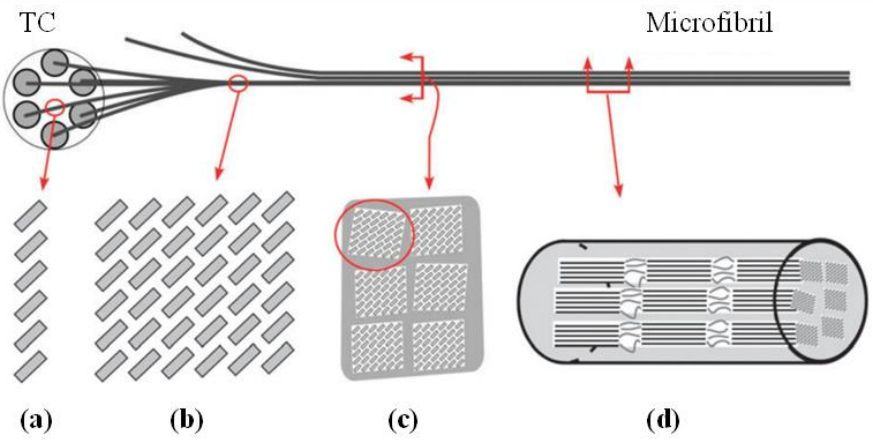

Figure 2.8 The hierarchical structure of wood microfiber, from the (a) terminal enzyme complex (TC) for synthesis from a mainsheet to the (b) elementary fibril (the assembly of 6 minisheets into an elementary fibre with dimensions approximately 3–5 nm), (c) microfibril cross-section (composed of 6 elementary fibrils, according to the modified Frey–Wysling model), and (d) microfibril lateral section (suggesting the arrangement of crystalline and amorphous regions) [13, 32]. Each grey rectangle represents a cellulose chain. (Reproduced with permission from Ref. 13. Copyright (2011). Royal Society of Chemistry.)

Table 2.2 The general characterization methods for the cellulose fibres [33].

Parameter		Characterization method
Degree of crystallinity		Wide-angle X-ray scattering (WAXS)
		^{13}C high-resolution CP-MAS solid-state NMR spectrum
Inner surface area		Water-vapor sorption
Pore size/volume		Mercury porosimetry
		Small-angle X-ray scattering (SAXS)
Degree of polymerization	The number-average molecular mass (M_n)/ The number-average degree of polymerization (DP_n)	Vapor pressure osmometry (low molecular mass)
	The weight-average molecular mass (M_w) / The weight-average degree of polymerization (DP_w)	Light scattering, sedimentation/diffusion measurements
	M_η/DP_η (the values are similar to M_w/DP_w, based on the Staudinger-Kuhn-Mark-Houwink law)	Viscosity measurements (widely used at commercial and laboratory scale)
Molecular weight distribution		Gel permeation chromatography (GPC)

The pore and void system contributes significantly to the inner surface area of the cellulose fibres. Furthermore, the inner surface area, supramolecular order, and fibril morphology strongly influence the accessibility of the cellulose, which is highly relevant to the various physical and chemical properties [15]. Table 2.2 above lists the primary parameters of cellulose fibres and their corresponding characterization methods [15].

2.1.3 Recycled cellulose fibres

The increase in paper consumption has been creating huge amounts of paper waste, which accounts for 25–40 % of global municipal solid waste [34]. In 2004 alone, 360 million tonnes of paper-related waste was generated worldwide. Moreover, paper and paperboard consumption will increase the amount of waste produced by 2.1% each year until 2020, which suggests that more than 500 million tonnes of paper waste can be expected in 2020 [35]. In addition, incineration or landfill of the paper waste could damage the environment further with toxic emissions and groundwater contamination.

Recycling paper waste will help to preserve forests and solve the environmental problem. Therefore, it is important to recycle or convert this enormous amount of waste into useful products. Several efforts have been made to solve this problem. For instance, in 2010, 63% of paper waste was recycled in the US [36]. Paper waste has also been investigated as a raw material for production of bioethanol, polymer precursors, particleboard etc. [34, 37, 38]. Commercially, recycled paper is mainly converted into other paper commodities of lower quality grades than the original products [39]. In addition, the maximum conversion rate from paper waste to other paper

products is only approximately 65% [39]. This low conversion rate is due to the length degradation of the cellulose fibres during the recycling processes, which also compromises the quality of the end product [39]. In addition, waste fibres of short lengths generated during recycling are discarded, since they are not suitable for further recycling [39]. It is therefore necessary to develop alternative commodities from paper waste.

The conversion of paper waste into recycled cellulose fibres is mainly a separation process, which removes the contaminants from the cellulose fibres [40]. The floating, heavy, and stringy items of a repulper need to be removed during the pulping process [40]. After this, screening (with coarse and fine screens) and removal of small contaminants such as plastic bits and glue globes is performed [40]. The deinking process is then carried out to remove the ink, glue, and other adhesive residues [40]. Later, the refining, colour-stripping, and bleaching processes are conducted, depending on the requirements of the end products [40]. The benefit of such waste-paper recycling is the reduction of landfills and of the incineration of paper waste. However, the disadvantage of cellulose-fibre recycling is the dependency on the sorting of the paper waste (e.g. the separation of newspapers from magazines), which has a significant influence on the quality of the recycled cellulose fibres that are produced.

Recycled cellulose fibres from paper waste are a cheap and abundant resource; the price of scrap paper was approximately $100/ton in 2015 [41]. A combination of aerogel structure and recycled cellulose fibre constitute a new material – called the recycled cellulose aerogel – which is cost-effective and has potential for oil absorption [42–44]. The recycled cellulose aerogel and its silica composite aerogel can also potentially be used as thermal-insulation

materials for buildings [44]. Therefore, all the practical applications developed by this thesis work may contribute to the recycling of paper-related waste.

Although some studies have examined the use of cellulosic materials for oil absorption, none have covered the fabrication of aerogels from paper-waste cellulose fibres, and investigated the aerogels as absorbents for the cleaning of crude-oil spills [45–51]. For this thesis, a fabrication procedure for making cellulose aerogels from paper-waste cellulose fibres was developed successfully, and the materials showed high absorption capacity for different crude oils, such as Ruby (RB), Te Giac Trang (TGT), and Rang Dong (RD) [43].

The recycled cellulose fibre used for this study was donated by Insul-Dek Engineering Pte Ltd (Singapore) [42–44]. The thermal conductivity of the recycled cellulose fibre was approximately 0.050 w/mK, and was measured with the heat-flow-meter method of ASTM C518-91, provided by their manufacturer [52]. The density of the bulk recycled-cellulose fibre mass was approximately 0.15 g/cm^3 [52]. As a result of the fire retardant, the recycled cellulose fibre was non-combustible in accordance with BS476 Part 4:1970 [53]. To measure the acoustic performance of the fibre mass, the fibres were applied to a solid backing with a thickness of 2.54 cm, achieving a noise-reduction coefficient (NRC) of 0.83 [53].

2.2 Cellulose aerogels

2.2.1 Synthesis of cellulose aerogels

As mentioned in Section 2.1.1, natural cellulose sources could be wood, plants, tunicates, several species of algae, and some bacteria [13]. According to

the previous literature, almost all the natural cellulose sources have been explored in the field of cellulose aerogels, with the exception of algae [54–57]. Compared with plant cellulose sources, bacterial cellulose sources have advantages, such as high purity, high average molecular strength, and high fibre strength [57]. However, harvesting bacterial cellulose fibres involves the production of cellulose, which is highly time-consuming. It usually takes 30 days to produce a bacterial cellulose mass with a thickness of 3–4 cm [57]. In contrast, wood cellulose fibres can be produced at a large scale via well-developed-wood industry methods [46]. For this research, recycled cellulose fibres were explored, and the reasons have been explained in detail in Section 2.1.3 above. The main goals of this research into recycled cellulose fibres are to help save the environment and to produce cost-effective cellulose-based aerogels.

With regard to the size of cellulose fibres, the most popular type in the literature is cellulose nanofibres (CNFs), which can be fabricated by a wide variety of methods [45, 46, 54–56, 58–63]. Mechanical methods, such as homogenization of wood pulp and ultrafine frication grinding of macroscopic cellulose fibres, can successfully fabricate CNFs [45, 46, 58, 64]. Acid hydrolysis of cotton wool, as a chemical method, has also been proven to be workable [56]. In addition, integrated approaches, such as acid pre-treatment combined with ultrasonication, and enzymatic hydrolysis combined with shearing and homogenization, have been advocated by several authors [55, 65, 66]. CNFs can also be grown directly by the bacterial strain Acetobacter xylinum, using a culture mainly consisting of coconut and sucrose, instead of disintegrating CNFs from the large fibres by chemical and/or mechanical approaches [61].

However, CNFs have their disadvantages. The mechanical-based approaches are highly energy-consuming [67]. Moreover, the acid treatments reduce the degree of polymerization and produce fibres with a low aspect ratio, due to the extensive hydrolysis [66]. As a result, the acid treatments may lead to fragile cellulose aerogels [66]. The fabrication processes of bacterial CNFs hinder the variation of cellulose concentration inside the cellulose hydrogels, which results in cellulose aerogels with an uncontrollable density [67]. Hence, for this thesis, the popular CNF-based aerogels were not used, but cellulose aerogels with adjustable densities and better oil absorption capacities were successfully created.

The common steps involved in the fabrication of cellulose aerogels are dissolution, gelation, coagulation, and drying. All these steps will be comprehensively discussed in their natural sequence. One of the major problems in the fabrication of cellulose aerogels is the insolubility of cellulose in most solvents. The insolubility of cellulose in nonpolar solvents is easily understandable, as cellulose is a considerably polar molecule with several hydroxyl groups [68]. Traditional viewpoints hold that the insolubility of cellulose is due to the strong intermolecular and intramolecular hydrogen bonds, which are difficult to break by the solvents [69–71].

Recently, Lindman *et al.* [68] claimed that cellulose is a significantly amphiphilic polymer, and the hydrophobic interactions contribute to the insolubility of cellulose in the aqueous solutions. More specifically, the flat ribbon structures of cellulose molecules formed by hydrogen bonding have sides of different polarities [72, 73]. The hydrophobic sides tend to assemble together, which results in the low solubility [68]. Moreover, the chain structure

of cellulose is inherently stiff due to the $^4C_1$ conformation of anhydroglucopyranse units (AGUs) in cellulose. As a result, it is difficult for the cellulose to adjust its conformation to minimize the contacts between its hydrophobic side and water, which promotes the insolubility [68].

The solvent systems for cellulose have been divided into derivatizing and non-derivatizing solvent systems [68]. The non-derivatizing solvent systems are preferred, since the final products are without chemical changes. A lithium chloride (LiCl)/dimethylacetamide (DMAc) solvent system can dissolve cellulose with a wide range of molecular weight (DP_n: 100–4000), and the resulting solutions are colourless and homogeneous [68, 74]. However, the LiCl/DMAc solvent system needs to work at a temperature of 150 ^oC to swell the cellulose, and requires an activation step [75]. During the dissolution process, the Cl^- is bonded with the activated cellulose hydrogen, and the anhydrous Li^+ is considered to associate with the carbonyl-oxygen of DMAc. When the temperature of the systems decreases, the thermal movement is reduced and the intermediate complex forms, which leads to the dissolution of cellulose [68].

Ionic liquids (ILs) are miscible with water, non-explosive, and non-volatile. However, their high viscosity, reactivity, and toxicity, and relatively high cost are their shortcomings [68]. Moreover, the dissolved amount of cellulose inside ILs is quite limited (up to 3%), and the cellulose needs to have a low molecular weight. Heavy degradation of cellulose is sometimes observed during cellulose dissolution in ILs [76]. According to Lindman *et al.* [68], the successful dissolution of cellulose inside ILs is because of the fact that both ILs and cellulose are amphiphilic.

The N-methylmorpholine N-oxide (NMMO) dissolution system does not generate hazardous by-products [77]. High-molecular cellulose can also be dissolved inside the NMMO solution to form a clear solution. However, the NMMO solution system only works at optimal parameters, such as limited temperature and NMMO concentration range, and requires a relatively high temperature. Moreover, recycling NMMO from the diluted solutions incurs high energy costs [68]. As a relatively strong oxidant, NMMO solutions become unstable above 130 ^{o}C, and thus spontaneous and uncontrollable blasts or exothermic events may occur [68, 78]. When propyl gallate serves as the stabilizer, it is difficult to remove the coloured side products from oxidation and degradation [78, 79]. The dissolution of cellulose inside NMMO has two main steps. In the first step, when the system is heated to 100 ^{o}C, the NMMO molecules become mobile and the crystalline celluloses transform to an amorphous state [74]. When the system temperature is subsequently elevated to 150 ^{o}C, the NMMO begins to bond to the cellulose that replaces the water [74]. With regard to amphiphilicity, the solubility of cellulose in NMMO systems is due to the amphiphilic property of NMMO [68].

The alkali/urea (urea derivatives) solution systems have become popular in recent years [7, 54, 80–84]. In this thesis, one of the dissolution methods is the application of a NaOH/urea aqueous solution. The NaOH/urea solutions have the advantages of low cost and relative non-toxicity. The alkali hydrates and urea hydrates penetrate the cellulose and break the hydrogen bonding at low temperature. During this process, some of the NaOH hydrates bond to the cellulose, as confirmed by differential scanning calorimetry (DSC) and nuclear magnetic resonance (NMR) [80]. Urea hydrates (the lone-pair electron on the

oxygen atom of urea) act as hydrogen-bonding donors and receptors to help the cellulose units keep some distance from each other [80]. Lindman *et al.* [68] also believe that urea, as a cosolute, serves to weaken the hydrophobic interactions. However, the Kymene approach used for this thesis does not require any solvent systems, which further simplifies the fabrication process of cellulose aerogels. The Kymene approach utilizes mechanical energy (sonication) to disperse the cellulose fibres uniformly and help the reformation the of hydrogen bond [55, 56].

In the gelation step, cellulose-based gels are formed. This step usually involves changing the temperature of the cellulose solution/suspension systems [85]. For the 7 wt. % NaOH/12 wt. % urea solution bath, the gelation processes can be fulfilled either by lowering the temperature to -20 ^{o}C or by increasing the temperature to 50 ^{o}C [82]. According to Cai *et al.* [82], the stability of the cellulose solution is destroyed by the temperature change. Because of the temperature change, the strength of the hydrogen bonds between the cellulose and the solvent are weakened [82]. As a result, the self-association tendency leads to the formation of intra- and intermolecular hydrogen bonds in the cellulose, which leads to gelation [82]. Without any temperature changes, the sonication methods cause the cellulose nanofibres (CNFs) in water to undergo gelation, as has been reported [55, 56]. Heath *et al.* [56] have suggested that the low-power sonication processes supply the cavitation energy in the same order of the hydrogen bonds, which helps the cellulose hydrogel formation. In the case of high-power sonication, the sonication processes could disturb or destroy the hydrogen bonds between the cellulose fibres. After the sonication, the hydrogen bonds could reform

uniformly to construct the cellulose hydrogels. Similarly, a CNF hydrogel can also be formed by the ultrafine fraction grinder treatments [58]. However, the bacterial cellulose hydrogels are fabricated directly by the bacteria inside the cultures, without requiring any further treatments [61].

Coagulation is one of the crucial steps in the synthesis of cellulose aerogels [63], and the coagulation process usually takes several hours to several days [54, 57, 59, 75, 76], mainly depending on the thickness of the gels. For most cases, coagulation is achieved by immersing the cellulose hydrogels inside the regeneration baths. However, this step is difficult to identify in some situations, because of the difficulties in distinguishing it from the pre-drying solvent-exchange step or gelation step [56, 63]. In fact, some of the solvent-exchange processes could serve the function of coagulation, and some of the regeneration baths could serve as pre-drying solvent-exchange liquids. The regeneration and gelation of cellulose could also be achieved together, with one bath [63].

The regeneration baths have a wide variation, mainly depending on the nature of the cellulose solvent systems. For the ionic-liquid (IL) solvent systems, the regeneration bath could be water, ethanol, or acetone [67]. For the N-methylmorpholine N-oxide (NMMO) solvent systems, the regeneration bath could be water, ethanol, isopropanol, hexanol, and dimethyl sulfoxide (DMSO) [76, 86–88]. Schimper *et al.* [87] have claimed that the less polar regeneration baths, such as isopropanol and hexanol, are better than their more polar counterparts, such as water and ethanol. The less polar regeneration baths yield the rigid shape and high porosity of the resulting cellulose aerogels [87]. In addition, increasing the temperature of the

regeneration baths could effectively reduce the cracks of the cellulose aerogels [87]. The regeneration bath for the NaOH aqueous solutions could be water or ethanol [86, 88]. For the NaOH/urea solvent systems, as reported, the regeneration bath could be water, ethanol, n-propanol, acetone, H_2SO_4 aqueous solutions, and NH_4Cl aqueous solutions [54, 89].

The mechanisms of the coagulation of the cellulose from the alkali/urea solvent systems are discussed in depth because of their great relevance to this thesis. The coagulation processes of these systems are dominated by the counter-diffusion process (a two-phase separation process) [89]. During this process, the regeneration bath components diffuse inside the cellulose solution, while the solvents of the cellulose solution diffuse into the regeneration bath [89]. To enable this counter-diffusion process, the regeneration baths must be miscible with NaOH/urea aqueous solutions, and be the cellulose precipitant. Zhang *et al.* [89] confirmed the counter-diffusion theory by experiments. They observed that the thicknesses of the coagulation layers were proportionally correlated with the square root of time in the non-reactive regeneration baths (water, ethanol, and n-propanol), which follows Fick's law [89]. For the H_2SO_4 and NH_4Cl aqueous regeneration baths, the diffusion-controlled chemical reaction kinetic dominates the coagulation processes [89]. The OH^- in the cellulose solvents and the H^+ in the precipitants undergo a neutralization reaction, which results in a more rigid coagulation skin with a slightly higher rate of coagulation, compared with a pure counter-diffusion process discussed above (water, ethanol, and n-propanol) [89].

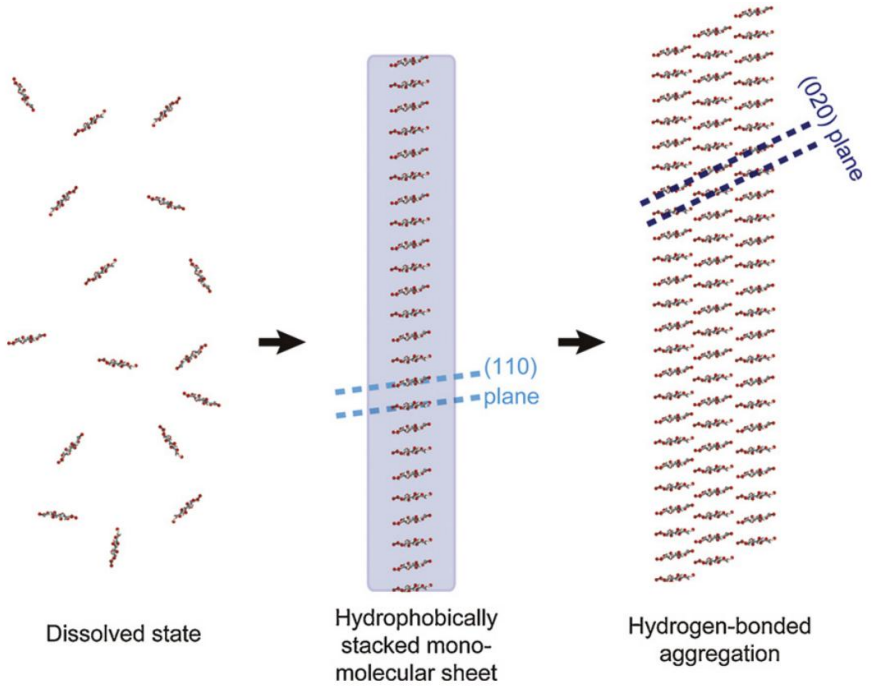

Figure 2.9 The coagulation process of the alkali/urea solution, investigated by synchrotron-radiation X-ray. The coagulation process began as the polar regeneration solution surrounded the cellulose. After being surrounded, the cellulose molecules tended to hide the hydrophobic glucopyanoside ring planes, which led to the aggregation of the cellulose molecules. With the aggregation, the cellulose molecules formed stacked monomolecular sheets, promoting the development of hydrogen-bonded aggregation [81]. The (1 1 0) plane suggests the lattice spacing of the hydrophobically stacked mono-molecular sheet, while the (0 2 0) plane implies the lattice spacing transverse to the ring plane of the cellulose molecules inside the hydrogen-bonded aggregation [81]. (Reproduced with permission from Ref. 81. Copyright (2012). Elsevier.)

The gelation and coagulation processes were analytically studied by Isobe *et al.* [81] using a synchrotron-radiation X-ray. The coagulation process (regeneration solutions: 5 wt. % Na_2SO_4 aqueous solution; dissolution solvent systems: 4.6 wt. % LiOH/15 wt. % urea aqueous solution) began with the polar regeneration solutions surrounding the cellulose [81]. The cellulose tended to hide the hydrophobic glucopyanoside ring planes, which led to the aggregation of the cellulose [81]. With the aggregation, the cellulose molecules formed stacked monomolecular sheets; this was observed by a (1 1 0) peak [81]. The stacked sheets promoted the development of hydrogen bonds in the

cellulose [81]. As a consequence of the hydrogen bonding, the monomolecular sheets lined up, which was observed by a (0 2 0) peak [81]. The coagulation process is schematically shown in Figure 2.9 above. The heat-induced gelation showed an X-ray profile similar to that of the coagulation process [81]. However, the peaks were much weaker, indicating a limited crystalline order [81]. These phenomena might be explained by the more random association of cellulose induced by the enhanced thermal motion [81].

Supercritical drying is associated with higher costs than freeze drying, due to the high pressure and supercritical carbon dioxide involved [66]. The Brunauer–Emmett–Teller (BET) surface areas of the freeze-dried cellulose aerogels (80–160 m^2/g) were much lower than those of the supercritical dried samples (200–220 m^2/g), although both processes were applied to the same cellulose gels [85]. The same cellulose hydrogel could form a rigid structure with supercritical drying, as opposed to a fissured and partially broken structure with freeze drying [85]. Hence, freeze drying requires cellulose gels with higher integrity and strength. However, freeze drying is also considered a safer and much more cost-effective drying method than supercritical drying [90] because of the availability and maturity of the relevant industrial knowledge, and the preclusion of supercritical carbon dioxide. The cellulose aerogels for this thesis had rigid structures after freeze drying, proving their high integrity and strength.

The general freeze-drying processes are discussed comprehensively in Section 1.1.2. In this section, only the most relevant information for cellulose-aerogel fabrication is presented. During the pre-drying step, liquid-nitrogen immersion is quite popular with researchers [45, 85]. However,

the liquid-nitrogen treatments might only be suitable for thin samples (e.g. membranes). Non-uniformity has been observed with the bulk cellulose aerogels: the outside layers had a smaller pore size and a more compacted structure than the inner layers [64]. This phenomenon might result from the faster freezing rate of the outside layers of the cellulose hydrogels than the inner layers, due to the formed ice crystals hampering the heat transfer [64]. The faster freezing rate leads to small crystal sizes and pores, giving a denser shell [64].

Film-like structures have been observed in several freeze-dried cellulose samples [54, 55, 59, 60]. These film-like structures might be formed by the fine cellulose fibres that are expelled by the growth of the large ice crystals during the slow cooling processes [59, 60, 66]. An interesting alternative to water freeze drying is tert-butanol freeze drying. Tert-butanol has a weaker surface tension, which might lead to larger surface areas, smaller pores, and more rigid structures of the cellulose aerogels [62]. However, the toxicity of tert-butanol is higher than that of water, and the pre-requirements of the tert-butanol solvent exchanges are time-consuming and expensive. The processes of cellulose-aerogel synthesis described in the literature so far consume a large amount of chemicals. The processes are not favourable in industrial-scale production, as they will damage the environment and increase the cost. Moreover, the synthesis of cellulose aerogels with an industrial size has not been attempted.

2.2.2 Properties of cellulose aerogels

2.2.2.1 Morphologies and hydrophobicity of cellulose aerogels

The morphologies (density, porosity, and BET surface area) of cellulose aerogels vary widely. Extensive acid-treated cellulose fibres with a width of 2–4 nm could form a hydrogel with a cellulose content of 0.1 wt. %, and after drying, a cellulose aerogel with a density as low as 0.0013 g/cm^3 could be fabricated [55]. The tunicate cellulose aerogels with a density of 0.01g/cm^3 and a BET surface area of 481 m^2/g can be fabricated from a cellulose solution with a 0.5 wt. % cellulose fibre concentration [54]. Cellulose aerogels with densities of 0.01–0.06 g/cm^3 and BET surface areas of 200–220 m^2/g are synthesized from 0.5–3 wt. % cellulose calciumthiocyanate solutions [85].

Obtained by a similar approach to that of the tunicate cellulose aerogel synthesis, the filter paper pulp cellulose aerogels (1–7 wt. % cellulose content in the dissolved solutions) have densities ranging from 0.03 to 0.14 g/cm^3 and BET surface areas ranging from 329 to 430 m^2/g [54]. Bacterial cellulose aerogels with an average density of 0.08 g/cm^3 and a BET surface area of approximately 200 m^2/g are produced [57]. Cellulose aerogels with densities of 0.12–0.35 g/cm^3 are fabricated from LiCl/DMAc solution (cellulose content: 5–20 wt. %) [75]. Almost all the reported porosities of the cellulose aerogels are calculated from the densities, which are always higher than 98%. The lowest reported BET surface area of a cellulose aerogel is 20 m^2/g, with a density of 0.03 g/cm^3 [60], while the highest reported BET surface area of a cellulose aerogel is 605 m^2/g, and its corresponding cellulose hydrogel was fabricated by a low-power sonication method using CNFs [56].

Hydrophilicity is an inherent property of cellulose materials, due to the hydroxyl groups. However, the sorbent materials that can clean oil spills

should be hydrophobic and oleophilic, so as to absorb oil rather than seawater. Moreover, thermal-insulation materials in buildings should not absorb moisture, as it will increase the thermal conductivity of the materials. This implies that hydrophobicity is also a requirement for thermal-insulation materials. Hence, for cellulose aerogels to be used in oil-spill cleaning and thermal insulation, the cellulose aerogels should be modified to be hydrophobic materials.

According to the literature, researchers have used several methods to hydrophobize the surface of cellulose materials. The graft-copolymerisation method employs by atom-transfer radical polymerization of glycidyl methacrylate (GMA) and other chemical modifications, which results in a fluorinated surface with a water contact angle of 170^{o} [91]. Surface silylation by chlorodimethyl isopropylsilane (CDMIPS) involves multiple steps of solvent exchange and chemical reactions in an argon atmosphere [92]. Similarly, surface esterification by pentafluorobenzoyl chloride requires a multiple-step solution-immersion process and a nitrogen atmosphere [93]. Cellulose fibre can be coated with five layers of titanium film via a complicated sol-gel process, and further modified with octyltrimethoxysilane (OTMS) via a solution-immersion method, which yields a water contact angle of 154.8 ± 1.5^{o} [94]. All these methods require multiple-step processes, expensive equipment, or excess chemicals.

Recently, a number of new hydrophobization methods have been developed for cellulose aerogels. Korhonen *et al.* [46] applied atomic layer deposition (ALD), using titanium isopropoxide as the titanium precursor and water as the oxygen source, to achieve a water contact angle of more than 90^{o}.

Interestingly, a photoswitchable titanium dioxide–coated surface has been successfully developed by a chemical vapour deposition (CVD) method using titanium isopropoxide vapour [60]. The CVD process was conducted at a temperature of 190 ^{o}C and a pressure of 1–5 KPa for 2h [60]. After the coating was applied, the water contact angle of the cellulose aerogel was 140^{o}, and UV illumination could have changed the hydrophobicity back to hydrophilicity [60]. However, the water contact angle of the UV illuminated sample recovered to 135^{o} after two weeks of dark treatment [60].

Jin *et al.* [58] used a simplified CVD method involving a bottle-in-bottle approach. In this approach, an open vial containing a small amount of fluorosilanes (FTCS) and the pre-coated samples was put inside a bigger airtight container [58]. The coating system was heated to 70 ^{o}C for 2h, followed by vacuum drying of the coated samples [58]. The resulting cellulose aerogels had a water contact angle of 160^{o}, a paraffin-oil contact angle of 153^{o}, and a mineral-oil contact angle of 158^{o} [58]. Moreover, the droplets were pinned at tilted angles, demonstrating high adhesive superhydrophobic properties and high adhesive superoleophobic properties [58]. A modified version of this approach was adopted for this thesis, due to its high efficiency, low cost, and simplicity. However, the coating chemical FTCS was not suitable for this thesis, because the research aims of this thesis required the aerogels to have oleophilic properties.

The stability of the hydrophobic coatings is crucial for industrial applications. For an illustrative example of the stability issue, the pentadecafluorooctanoyl chloride–coated cellulose surface exhibited a water contact angle of 150^{o} immediately after modification, while the water contact

angle decreased to 128^{o} in 20 minutes and below 90^{o} in 50 minutes [91]. However, only a few reports have addressed the stability issue. In this thesis, the stability of the hydrophobic coating of the cellulose aerogels over a five-month time span will be explored and documented.

2.2.2.2 Absorption properties of cellulose aerogels

The water sorption capacities of cellulose aerogels have been studied by a few groups. Uncoated cellulose aerogels with a density of 0.03 g/cm^3 and a water sorption capacity of 35 $\pm$ 2 g/g were synthesized by Kettunen *et al.* [60]. Zhang *et al.* [64] fabricated cellulose aerogels with a water sorption capacity of 98 g/g and demonstrated their reusability. Cellulose aerogels fabricated by Chen *et al.* [55] had densities of 0.0013–0.017 g/cm^3 and water absorption capacities ranging from 54 to 155 g/g. For comparison, commercial cellulosic pulp and commercial super-absorbents (sodium polyacrylate polymer) have water absorption capacities of approximately 1.5 and 172 g/g, respectively [95]. The water absorption capacity of commercial cellulosic pulp is lower than that of cellulose aerogels, while the water absorption capacity of commercial super-absorbents is slightly higher than that of cellulose aerogels [55, 60, 64, 95].

Hydrophobic and oleophilic cellulose aerogels have been successfully synthesized, and their oil spill–cleaning abilities explored [42–44]. Korhonen *et al.* [46] prepared cellulose aerogels with densities of 0.02–0.03 g/cm^3; the maximum absorption capacity of the paraffin oil was 40 g/g. The cellulose aerogel containing oil could float on the water surface without releasing the oil [46]. The reusability of the cellulose aerogels was demonstrated by an immersion–drying method: after the aerogel absorbed the

oil, the aerogel was immersed in an organic solvent, such as ethanol or octane, and subsequently dried [46]. This process was repeated 20 times without a significant decrease in absorption capacity and dry weight [46]. A similar hydrophobic and oleophilic cellulose-based aerogel with an oil sorption capacity of 45 g/g was obtained by Cervin *et al.* [45]. According to the literature, the oil sorption capacities of hydrophobic cellulose aerogels are low compared with the water absorption capacities of hydrophilic cellulose aerogels. However, the absorption capacities of cellulose aerogels are still higher than those of commercial polypropylene fibrous mats (approximately 10 g/g) [96–100].

For this thesis, an oil sorption capacity of 95 g/g for cellulose aerogels was achieved, which is comparable to the water absorption capacities for cellulose aerogels mentioned in the literature [42]. Various authors have tested the absorption capacity of cellulose aerogels with water or light oils other than crude oil, which is the main substance in oil spills in the sea [45, 46]. Moreover, studies of the absorption rate, which is important in determining the efficiency of the absorbent, of cellulose aerogels are not available in the literature.

2.2.2.3 Thermal properties of cellulose aerogels

The thermal conductivities of cellulose aerogels are between 0.0295 and 0.033 W/mK [90, 101], and are comparable to those of conventional thermal-insulation materials, such as cork (0.043 W/mK), polyurethane foams (0.02-0.04 W/mK), and silica aerogels (0.026 W/mK) [102]. The low thermal conductivities are due to the porous structure of the cellulose aerogels.

The cellulose aerogels start degrading at temperatures ranging from 270 to 330 ^{o}C, according to various reports [55, 64, 103, 104]. The cellulose

aerogels fabricated from microsize and nanosize cellulose fibres have a decomposition temperature of 303.8 ^{o}C, compared with 327.9 ^{o}C for the pulp-fibre cellulose aerogels fabricated with the same synthesis method [64]. This decrease in decomposition temperature is due to the high specific surface area of the cellulose aerogels fabricated from microsize and nanosize cellulose fibres, which assists the thermal degradation of the cellulose-fibre surface [64].

2.2.2.4 Mechanical properties of cellulose aerogels

The mechanical properties of cellulose aerogels, such as the tensile, compressive, and flexible properties, are discussed below. An interesting mechanics-related property of the cellulose aerogel membrane synthesized by Jin *et al.* [58] is that the membrane, with a diameter of 19 mm and a weight of 3 mg, could support 960 or 1658 mg of weight on oil and water, with a dimple of 2.7 or 3.7 mm respectively.

The only reported tensile properties of unmodified cellulose aerogels are from the aerogels synthesized by Cai *et al.* [54] via an alkali/urea dissolution method. The tensile Young's moduli and the breaking strengths of those aerogels were approximately 200–300 MPa and 10–20 MPa, respectively [54]. The magnetic paper synthesized from magnetic nanoparticle-enhanced bacterial cellulose aerogels had a tensile modulus and strength of 3GPa and 25 MPa respectively [61].

With regard to the compressive properties, the bacterial cellulose aerogels had a compressive modulus of 0.15 MPa, a collapse stress of 0.04 MPa, and a maximum strain of more than 90% [61]. The good mechanical properties of the bacterial cellulose aerogels were due to the bacterial cellulose

fibres involved. The CNF aerogels synthesized from the tert-butanol freeze drying had compressive moduli of 35–2800 KPa and compressive strengths of 3.2–238 KPa [62]. These CNF aerogels could be compressed to more than 80% strain without yield points being detected, and with energy absorptions of 10.8–720 KJ/m^3 observed [62]. The high mechanical strengths of the CNF aerogels were a result of the high mechanical strength of the raw cellulose nanofibres [62]. With the enzymatic treatments and mechanical shearing, the resultant CNF aerogels showed linear compressive behaviour (up to a strain of approximately 40%), and had a maximum compressive strength of approximately 200 KPa [66]. The CNF aerogels achieved a maximum compressive strain of 70% [66]. These two types of CNF aerogels mentioned above had similar mechanical properties, due to the similar size of the cellulose fibres and the similar enzymatic treatments involved. The CNF aerogels synthesized from the hydrated calciumthiocyanate ($Ca(SCN)_2$ $4H_2O$) solution had a 2 MPa elastic bending strength at a 6% pseudo-elastic deflection, and were fabricated by supercritical drying, as freeze drying would have made them brittle [85]. This phenomenon could be explained by the large pore and fibre sizes caused by freeze drying. For the high-density cellulose aerogels (0.12–0.35 g/cm^3), the maximum flexural strength and stiffness were 8.1 and 250 MPa respectively [75], and the improved mechanical strength was due to the high density [105].

Most cellulose aerogels are brittle and dusty, and in industrial usage, high flexibility is a desired property, as cellulose aerogels with high flexibility are convenient to store, transport, and use for various applications, such as oil-spill cleaning and thermal insulation. Thicker aerogels can also absorb

more solvents and provide a better insulation effect due to their large volume and thickness, which is also highly desirable. There are a few examples of successfully synthesized flexible cellulose aerogels in the literature [55, 61, 64, 66], although their thicknesses are rather limited. General descriptions of selected cases are given here. A 0.25 mm–thick cellulose composite aerogel with cobalt ferrite ($CoFe_2O_4$) embedded in it could be bent 180^o without apparent damage [7]. Similarly, bacterial cellulose composite aerogels with cobalt ferrite nanoparticle embedded in them were also found to be quite flexible, although the sample that could withstand repeated bending was of a rather limited thickness [61].

Besides magnetic cellulose composite aerogels, some pure cellulose aerogels have also been demonstrated to be flexible. A 1 mm–thick cellulose aerogel fabricated by Pääkkö *et al.* [66] could be folded into a loop. A CNF aerogel treated with acid and low-power ultrasonication, with a thickness of 5.9 mm, withstood repeated bending without significant structural changes [55]. Zhang *et al.* [64] produced a highly flexible cylindrical cellulose aerogel, which could be bent without cracking. However, the exact thickness of this flexible cylindrical cellulose aerogel was not given, and other structural damage, such as plastic deformation, might have resulted from the bending. Highly flexible cellulose aerogels with large thicknesses will be discussed in this thesis.

2.3 Silica–cellulose aerogels

Silica–cellulose aerogels, as inorganic–organic composite materials, have received considerable attention in recent years [90, 101, 103, 104, 106]. The silica modification of the cellulose materials improves the mechanical and

thermal properties of the materials [90, 101, 103, 104, 107], which has great potential for thermal-insulation applications [90, 101, 107].

2.3.1 Synthesis of silica–cellulose aerogels

Silica–cellulose aerogels have been fabricated from a wide range of cellulose sources, such as fibrous native cellulose, microcrystalline cellulose, cellulose powder, bacterial cellulose, and cotton linter [90, 101, 103, 104, 106]. However, silica–cellulose aerogels fabricated from recycled cellulose fibres had not been reported when the synthesis approach for this thesis was initiated.

The main silica precursors to silica–cellulose aerogels are tetraethyl orthosilicate (TEOS) and polyethoxydisiloxane (PEDS: the pre-polymerized oligomers of TEOS) [90, 101, 103, 104, 107]. 3-chloropropyltrimethoxysilane CPTMS) and sodium silicate have also been reported as silica precursors to silica–cellulose aerogels [104, 106]. However, attempts to create methyltrimethoxysilane (MTMS)-based silica–cellulose aerogels have not yet been made. The main advantage of silica–cellulose aerogels fabricated from an MTMS precursor is the potentially inherent hydrophobic property [108].

Silica-embedded cellulose aerogels are created by immersing the cellulose gels in solvents containing the silica precursors [90, 101, 103, 104, 107]. The silica precursors and the catalysts are separated in some cases, as described below [101, 103]. The cellulose gels are first immersed inside the silica-precursor solutions, and then soaked in the catalyst solutions to enable the gelation of the silica [101, 103]. However, some researchers mixed the silica precursor and the silica gelation catalyst together in one solution, and immersed the cellulose gel in the solution [90, 104, 107]. The differences in the properties, such as

morphology, thermal, and mechanical properties, of the silica–cellulose aerogels produced by these two approaches are not significant [90, 101, 103, 104, 107]. Some later procedures simplified the process and reduced the synthesis time, which is considered more advantageous. Hence, this thesis work used a silica precursor and catalyst mixtures as the impregnation solvents.

One type of modification of the gel-impregnation processes is directly immersing the cellulose aerogels in solutions containing the silica precursors [90]. This approach seems to be inefficient because the dryings need to be done twice. However, if the cellulose aerogels are commercial products with a reasonable cost, it will be much easier and more convenient to handle the commercial cellulose aerogels than the commercial cellulose gels at industrial scale, as the aerogels are in the dry state. Moreover, this aerogel-based approach of silica–cellulose aerogel fabrication could significantly reduce the silica-impregnation duration, because the diffusion rates in the aerogels are higher than in the gels. However, this approach has only been attempted by Sai *et al.* [90], with no justification given. In this thesis, the cellulose aerogel–based impregnation approach of silica–cellulose aerogel fabrication will be explored further.

Demilecamps *et al.* [106] used inorganic sodium silicate as the silica precursor, and used a mixed aqueous solution of cellulose, sodium hydroxide (NaOH), and sodium silicate (Na_2SiO_3) during the synthesis. Although the immersion process was eliminated, the fabrication process was prolonged. This prolongation was because the formation of silica from the Na_2SiO_3 requires the renewal of the acid baths several times, and the removal of the by-product salts is time-consuming [106].

Most silica–cellulose aerogels are synthesized by supercritical drying methods [101, 103, 104, 106]. Sai *et al.* [90] applied freeze drying that involved a tert-butanol and water mixture instead of pure water. Shi *et al.* [107] successfully used the freeze-drying (pure water–based) method to fabricate silica–cellulose aerogels, but the silica loadings of these silica aerogels were relatively low (up to 16%). Silica–cellulose aerogels with a high silica loading could be more thermally stable, as the silica component tends to degrade at a high temperature [108]. The advantages of water-based freeze drying have been comprehensively discussed in Section 1.1.2 and Section 2.2.1. However, monolithic silica–cellulose aerogels with a high silica loading (more than 50%) and fabricated by pure water–based freeze drying have not yet been reported elsewhere.

2.3.2 Properties of silica–cellulose aerogels

Hydrophobicity can help materials withstand moisture, which contributes to the stability of their thermal-insulation performance [107]. To improve the hydrophobicity of silica–cellulose aerogels, a multi-step approach was taken by Sai *et al.* [90]. First, a mixture of MTMS, methanol, and oxalic was obtained, and after 24 h the dilute ammonia was added to the bath [90]. The silica–cellulose aerogels were immersed in the bath for 30 min, then aged for 24 h [90]. The aged composites then underwent solvent exchange with a water/tert-butanol mixture [90]. Finally, the composites were freeze-dried [90]. With this approach, a water contact angle of 133^{o} for the silica–cellulose aerogels was achieved [90]. However, this approach requires a large number of chemicals, and is highly time- and energy-consuming. Shi *et al.* [107] used a

different approach to modify the surface of the silica–cellulose aerogels with CCl_4 cold plasma. The plasma is produced by gas ionization, and the large number of active particles both chemically and physically modify the surface material of the silica–cellulose aerogels, which results in a water contact angle of 132^o for the silica–cellulose aerogels [107]. The main disadvantages of this approach are the expensive equipment and complicated technique.

The thermal conductivities of silica–cellulose aerogels have been studied by various research groups. Cai *et al.* [103] reported that the thermal conductivity of silica–cellulose aerogels increased from 0.025 to 0.045 W/mK when the density of the composite increased from 0.14 to approximately 0.6 g/cm^3. This observation could be explained by the improved phonon conduction via the solid backbone of the aerogels with high density [109]. Shi *et al.* [107] synthesized a silica–cellulose aerogel with a thermal conductivity of 0.026 W/mK, which is similar to the findings of Cai *et al.* [103]. Demilecamps *et al.* [101] fabricated a silica–cellulose aerogel with a thermal conductivity of approximately 0.027 W/mK, while the thermal conductivities of its silica and cellulose counterparts were 0.015 and 0.033 W/mK, respectively. The thermal conductivity of the silica–cellulose aerogels was therefore between those of its silica and cellulose counterparts; this was because the silica aerogels were partially filling the macropores of the cellulose matrix, and because of the increased density of the composite [101]. Sai *et al.* [90] observed that the thermal conductivity of the composite increases from 0.0295 to 0.0368 W/mK with the increased density, which is similar to the observation made by Cai *et al.* [103].

The thermal stability of silica–cellulose aerogels is slightly better than that of their cellulose counterparts [103, 104]. Litschauer *et al.* [104] observed that the cellulose degradation temperature shifted from 270 ^{o}C for the cellulose aerogels to 282 ^{o}C for the silica–cellulose aerogels. Similarly, Cai *et al.* [103] found that the silica embedment stabilized the cellulose aerogels, as the differential thermal analysis (DTA) peaks were at 318 and 346 ^{o}C before and after the silica embedment, respectively. These observations could possibly be explained by the interactions between the cellulose and silica components at high temperatures, and the reduced exposure surface of the cellulose fibres due to the silica-particle coverage.

The silica embedment is considered an effective way to enhance the mechanical properties of cellulose aerogels, as the mechanical properties of silica–cellulose aerogels are significantly improved with its addition, which is not the case for their counterparts (pure cellulose aerogels and silica aerogels) [90, 101]. For example, the compressive Young's modulus was approximately 11.5 MPa for the silica–cellulose aerogels synthesized by Demilecamps *et al.* [101], while those for the cellulose aerogels and the silica aerogels were 2.8 and 1.8 MPa, respectively [101]. The increase in the modulus could be explained by the increase in density [101]. Moreover, the compressive strain of the silica–cellulose aerogel could reach up to 60% without the aerogel breaking down into pieces [101], possibly due to the interconnected cellulose matrix.

In another demonstration, Sai *et al.* [90] fabricated silica–cellulose aerogels with the compressive Young's modulus ranging from 1.23 to 16.9 MPa, and the modulus increased with the silica loading (65–97 wt. %).

For comparison, the bacterial cellulose aerogel had a modulus of 0.27 MPa, and the silica aerogel was brittle without a monolithic form [90]. According to the authors, the increase in the modulus was due to the inorganic silica network, which supports the cellulose matrix to withstand the compressive pressure [90]. Moreover, no breakpoint for these silica–cellulose aerogels was observed under compression when the silica loading was lower than 95.5 wt. %. [90]. This observation could possibly be explained by the flexible cellulose matrix, that restricts the silica components, interconnected by a large amount of hydrogen bonds [90].

However, a softening effect was also observed by Cai *et al.* [103]; for example, the tensile and compressive modulus decreased from 72 and 12 MPa for the cellulose aerogel to 10.8 and 7.9 MPa for the silica–cellulose aerogel, respectively. This softening effect could have been the result of poor integration between the cellulose and silica components.

The fabrication of cellulose-based aerogels with recycled cellulose fibres from paper waste has not yet been attempted in the literature. The dissolution and coagulation processes of cellulose aerogel synthesis are time-consuming and generate a large amount of chemical waste, which should be avoided in the industrial development of cellulose aerogels. The efficient method of improving the hydrophobicity of cellulose aerogels developed by Jin *et al.* [58] cannot be applied directly due to the resultant superoleophobic properties of the aerogels, and the method needs to be modified for aerogels in oil spill–cleaning applications. The crude-oil absorption properties and the oil absorption kinetics of cellulose aerogels have not been investigated in the literature.

The inherently superhydrophobic silica–cellulose aerogels derived from the MTMS precursor are worth more attention. The method of developing silica–cellulose aerogels with a high silica loading (>50%) from the direct immersion of cellulose aerogels inside the silica precursor solutions and water-based freeze drying is also of interest. The experimental part of these topics is presented in the next chapter.

References

[1] D. N. S. Hon, Cellulose: a random walk along its historical path, *Cellulose*, 1994, **1**, 1-25.

[2] A. Brongniart, T. J. Pelouze, A. B. Dumas, C. R. Hedb, Rapport sur un mémoire de M. Payen, relatif à la composition de la matière ligneuse, *Seances Acad. Sci*, 1839, **8**, 51.

[3] H. Staudinger, J. Fritschi, Über die Hydrierung des. Kautschuks und über seine Konstitution, *Helv. Chim. Acta*, 1922, **5**, 785-806.

[4] D. Klemm, B. Heublein, H. P. Fink, A. Bohn, Cellulose: fascinating biopolymer and sustainable raw material, *Angew. Chem. Int. Ed. Engl.*, 2005, **44**, 3358-3393.

[5] S. Cao, K. L. Yeung, J. K. C. Kwan, P. M. T. To, S. C. T. Yu, An investigation of the performance of catalytic aerogel filters, *Appl. Catal., B*, 2009, **86**, 127-136.

[6] S. J. Eichhorn, Cellulose nanowhiskers: promising materials for advanced applications, *Soft Matter*, 2011, **7**, 303-315.

[7] S. Liu, Q. Yan, D. Tao, T. Yu, X. Liu, Highly flexible magnetic composite aerogels prepared by using cellulose nanofibril networks as templates, *Carbohydr. Polym.*, 2012, **89**, 551-557.

[8] P. Béguin, J. P. Aubert, The biological degradation of cellulose, *FEMS Microbiol. Rev.*, 1994, **13**, 25-58.

[9] S. B. Leschine, Cellulose degradation in anaerobic environments, *Annu. Rev. Microbiol.* , 1995, **49**, 399-426.

[10] T. Miyamoto, S. Takahashi, H. Ito, H. Inagaki, Tissue biocompatibility of cellulose and its derivatives, *J. Biomed. Mater. Res.*, 1989, **23**, 125-133.

[11] N. Jia, S. Li, M. Ma, J. Zhu, R. Sun, Synthesis and characterization of cellulose-silica composite fiber in ethanol/water mixed solvents, *BioResources*, 2011, **6**, 1186-1195.

[12] M. Kumar, S. Turner, Plant cellulose synthesis: CESA proteins crossing kingdoms, *Phytochemistry*, 2015, **112**, 91-99.

[13] R. J. Moon, A. Martini, J. Nairn, J. Simonsen, J. Youngblood, Cellulose nanomaterials review: structure, properties and nanocomposites, *Chem. Soc. Rev.*, 2011, **40**, 3941-3994.

[14] C. J. Biermann, Chapter 3: Pulping fundamentals, Handbook of pulping and papermaking, 2nd ed., *Academic Press*, San Diego, 1996, pp. 55-100.

[15] D. Klemm, B. Philipp, T. Heinze, U. Heinze, W. Wagenknecht, Volume 1 Fundamentals and analytical methods, Comprehensive cellulose chemistry, *John Wiley and Sons*, Weinheim, 2004, pp. 9-29.

[16] Y. Nishiyama, P. Langan, H. Chanzy, Crystal structure and hydrogen-bonding system in cellulose I_β from synchrotron X-ray and neutron fiber diffraction *J. Am. Chem. Soc*, 2002, **124**, 9074-9082.

[17] K. H. Gardner, J. Blackwell, The structure of native cellulose, *Biopolymers*, 1974, **13**, 1975-2001.

[18] D. W. Jones, Crystalline modifications of cellulose. Part III. The derivation and preliminary study of possible crystal structure, *J. Polym. Sci.*, 1958, **32**, 371-394.

[19] J. W. S. Hearle, A fringed fibril theory of structure in crystalline polymers, *J. Polym. Sci.*, 1958, **28**, 432-435.

[20] C. Louime, H. Uckelmann, Cellulosic ethanol: securing the planet future energy needs, *Int. J. Mol. Sci.*, 2008, **9**, 838-841.

[21] A. C. O'sullivan, Cellulose: the structure slowly unravels, *Cellulose*, 1997, **4**, 173-207.

[22] H. Krässig, J. Schurz, R. G. Steadman, K. Schliefer, W. Albrecht, M. Mohring, H. Schlosser, Cellulose, Ullmann's encyclopedia of industrial chemistry, *Wiley-VCH*, Weinheim, 2012, pp. 279-332.

[23] R. H. Atalla, D. L. Vanderhart, Native cellulose: a composite of two distinct crystalline forms, *Science*, 1984, **223**, 283-285.

[24] Y. Nishiyama, J. Sugiyama, H. Chanzy, P. Langan, Crystal structure and hydrogen bonding system in cellulose Iα from synchrotron X-ray and neutron fiber diffraction, *J. Am. Chem. Soc*, 2003, **125**, 14300-14306.

[25] P. Belton, S. F. Tanner, N. Cartier, H. Chanzy, High-resolution solid-state ^{13}C nuclear magnetic resonance spectroscopy of tunicin, an animal cellulose, *Macromolecules*, 1989, **22**, 1615-1617.

[26] H. Yamamoto, F. Horii, In Situ crystallization of bacterial cellulose I. influences of polymeric additives, stirring and temperature on the formation celluloses I_α and I_β as revealed by cross polarization/magic angle spinning (CP/MAS) ^{13}C NMR spectroscopy, *Cellulose*, 1994, **1**, 57-66.

[27] H. Yamamoto, F. Horii, CP/MAS I3C NMR analysis of the crystal transformation induced for vdonia cellulose by annealing at high temperatures, *Macromolecules*, 1993, **26**, 1313-1317.

[28] H. L. Bos, J. Müssig, M. J. A. van den Oever, Mechanical properties of short-flax-fibre reinforced compounds, *Compos. Part A-Appl. S.*, 2006, **37**, 1591-1604.

[29] M. T. Postek, A. Vladár, J. Dagata, N. Farkas, B. Ming, R. Wagner, A. Raman, R. J. Moon, R. Sabo, T. H. Wegner, J. Beecher, Development of the metrology and imaging of cellulose nanocrystals, *Meas. Sci. Technol.*, 2011, **22**, 024005.

[30] R. M. Brown, The Biosynthesis of Cellulose, *J. Macromol. Sci., Pure Appl. Chem.*, 2006, **33**, 1345-1373.

[31] S. Kimura, T. Itoh, New cellulose synthesizing complexes (terminal complexes) involved in animal cellulose biosynthesis in the tunicate Metandrocarpa uedai, *Protoplasma*, 1996, **194**, 151-163.

[32] A. Sarko, R. H. Marchessault, Supermolecular structure of polysaccharides *J. Polym. Sci. Pol. Sym.*, 1969, **28**, 317-331.

[33] D. Klemm, B. Philipp, T. Heinze, U. Heinze, W. Wagenknecht, Volume 1 Fundamentals and analytical methods, Comprehensive cellulose chemistry, *John Wiley and Sons*, Weinheim, 2004, pp. 167-217.

[34] A. Nourbakhsh, A. Ashori, Particleboard made from waste paper treated with maleic anhydride, *Waste Manage. Res.*, 2010, **28**, 51-55.

[35] L. Szabó, A. Soria, J. Forsström, J. T. Keränen, E. Hytönen, A world model of the pulp and paper industry: Demand, energy consumption and emission scenarios to 2030, *Environ. Sci. Policy*, 2009, **12**, 257-269.

[36] Paper Recycling, http://www.epa.gov/osw/conserve/materials/paper/basic_info.htm.

[37] D. Mishra, S. Vijay Kumar, Value-based Polymer Precursors from Paper Waste and its Application in Polyurethane Foams, *J. Cell. Plast.*, 2009, **46**, 15-30.

[38] L. Wang, R. Templer, R. J. Murphy, High-solids loading enzymatic hydrolysis of waste papers for biofuel production, *Appl. Energ.*, 2012, **99**, 23-31.

[39] Y. Ikeda, E. Y. Park, N. Okuda, Bioconversion of waste office paper to gluconic acid in a turbine blade reactor by the filamentous fungus Aspergillus niger, *Bioresour. Technol.*, 2006, **97**, 1030-1035.

[40] C. J. Biermann, Chapter 10: Fiber from recycled paper, Handbook of pulping and papermaking, 2 nd ed., *Academic Press*, San Diego, 1996, pp. 263-282.

[41] The paper stock report: Paper recycling online, http://www.recycle.cc/freepapr.htm, 2015.

[42] J. Feng, S. T. Nguyen, Z. Fan, H. M. Duong, Advanced fabrication and oil absorption properties of super-hydrophobic recycled cellulose aerogels, *Chem. Eng. J.*, 2015, **270**, 168-175.

[43] S. T. Nguyen, J. Feng, N. T. Le, A. T. T. Le, N. Hoang, V. B. C. Tan, H. M. Duong, Cellulose Aerogel from Paper Waste for Crude Oil Spill Cleaning, *Ind. Eng. Chem. Res.*, 2013, **52**, 18386-18391.

[44] S. T. Nguyen, J. Feng, S. K. Ng, J. P. W. Wong, V. B. C. Tan, H. M. Duong, Advanced thermal insulation and absorption properties of recycled cellulose aerogels, *Colloids Surf., A*, 2014, **445**, 128-134.

[45] N. T. Cervin, C. Aulin, P. T. Larsson, L. Wågberg, Ultra porous nanocellulose aerogels as separation medium for mixtures of oil/water liquids, *Cellulose*, 2011, **19**, 401-410.

[46] J. T. Korhonen, M. Kettunen, R. H. Ras, O. Ikkala, Hydrophobic nanocellulose aerogels as floating, sustainable, reusable, and recyclable oil absorbents, *ACS Appl. Mater. Inter.*, 2011, **3**, 1813-1816.

[47] D. Li, F. Z. Zhu, J. Y. Li, P. Na, N. Wang, Preparation and characterization of cellulose fibers from corn straw as natural oil sorbents, *Ind. Eng. Chem. Res.*, 2013, **52**, 516-524.

[48] K. C. Payne, C. D. Jackson, C. E. Aizpurua, O. J. Rojas, M. A. Hubbe, Oil spills abatement: factors affecting oil uptake by cellulosic fibers, *Environ. Sci. Technol.*, 2012, **46**, 7725-7730.

[49] J. Wang, Y. Zheng, Y. Kang, A. Wang, Investigation of oil sorption capability of PBMA/SiO2 coated kapok fiber, *Chem. Eng. J.*, 2013, **223**, 632-637.

[50] J. Wang, Y. Zheng, A. Wang, Effect of kapok fiber treated with various solvents on oil absorbency, *Ind. Crop. Prod.*, 2012, **40**, 178-184.

[51] J. Wang, Y. Zheng, A. Wang, Coated kapok fiber for removal of spilled oil, *Mar. Pollut. Bull.*, 2013, **69**, 91-96.

[52] T. K. Chuan, Thermal conductivity test, *PSB Corporation*, 2004.

[53] Insul-Dek Engineering Pte. Ltd., Cell-Spray Catalogue: The high performance multi-function insulation system, Singapore, 2015, p. 2.

[54] J. Cai, S. Kimura, M. Wada, S. Kuga, L. Zhang, Cellulose aerogels from aqueous alkali hydroxide-urea solution, *ChemSusChem*, 2008, **1**, 149-154.

[55] W. Chen, H. Yu, Q. Li, Y. Liu, J. Li, Ultralight and highly flexible aerogels with long cellulose I nanofibers, *Soft Matter*, 2011, **7**, 10360-10368.

[56] L. Heath, W. Thielemans, Cellulose nanowhisker aerogels, *Green Chem.*, 2010, **12**, 1448-1453.

[57] F. Liebner, E. Haimer, M. Wendland, M. A. Neouze, K. Schlufter, P. Miethe, T. Heinze, A. Potthast, T. Rosenau, Aerogels from unaltered bacterial cellulose: application of $scCO_2$ drying for the preparation of shaped, ultra-lightweight cellulosic aerogels, *Macromol. Biosci.*, 2010, **10**, 349-352.

[58] H. Jin, M. Kettunen, A. Laiho, H. Pynnonen, J. Paltakari, A. Marmur, O. Ikkala, R. H. Ras, Superhydrophobic and superoleophobic nanocellulose aerogel membranes as bioinspired cargo carriers on water and oil, *Langmuir*, 2011, **27**, 1930-1934.

[59] H. Jin, Y. Nishiyama, M. Wada, S. Kuga, Nanofibrillar cellulose aerogels, *Colloids Surf., A*, 2004, **240**, 63-67.

[60] M. Kettunen, R. J. Silvennoinen, N. Houbenov, A. Nykänen, J. Ruokolainen, J. Sainio, V. Pore, M. Kemell, M. Ankerfors, T. Lindström, M. Ritala, R. H. A. Ras, O. Ikkala, Photoswitchable Superabsorbency Based on Nanocellulose Aerogels, *Adv. Funct. Mater.*, 2011, **21**, 510-517.

[61] R. T. Olsson, M. A. Azizi Samir, G. Salazar-Alvarez, L. Belova, V. Strom, L. A. Berglund, O. Ikkala, J. Nogues, U. W. Gedde, Making flexible magnetic aerogels and stiff magnetic nanopaper using cellulose nanofibrils as templates, *Nat. Nanotechnol.*, 2010, **5**, 584-588.

[62] H. Sehaqui, Q. Zhou, L. A. Berglund, High-porosity aerogels of high specific surface area prepared from nanofibrillated cellulose (NFC), *Compos. Sci. Technol.*, 2011, **71**, 1593-1599.

[63] Z. Wang, S. Liu, Y. Matsumoto, S. Kuga, Cellulose gel and aerogel from LiCl/DMSO solution, *Cellulose*, 2012, **19**, 393-399.

[64] W. Zhang, Y. Zhang, C. Lu, Y. Deng, Aerogels from crosslinked cellulose nano/micro-fibrils and their fast shape recovery property in water, *J. Mater. Chem.*, 2012, **22**, 11642-11650.

[65] M. Pääkkö, M. Ankerfors, H. Kosonen, A. Nykänen, S. Ahola, M. Österberg, J. Ruokolainen, J. Laine, P. T. Larsson, O. Ikkala, T. Lindström, Enzymatic hydrolysis combined with mechanical shearing and high-pressure homogenization for nanoscale cellulose fibrils and strong gels, *Biomacromolecules*, 2007, **8**, 1934-1941.

[66] M. Pääkkö, J. Vapaavuori, R. Silvennoinen, H. Kosonen, M. Ankerfors, T. Lindström, L. A. Berglund, O. Ikkala, Long and entangled native cellulose I nanofibers allow flexible aerogels and hierarchically porous templates for functionalities, *Soft Matter*, 2008, **4**, 2492-2499.

[67] R. Sescousse, R. Gavillon, T. Budtova, Aerocellulose from cellulose–ionic liquid solutions: Preparation, properties and comparison with cellulose–NaOH and cellulose–NMMO routes, *Carbohydr. Polym.*, 2011, **83**, 1766-1774.

[68] B. Lindman, G. Karlström, L. Stigsson, On the mechanism of dissolution of cellulose, *J. Mol. Liq.*, 2010, **156**, 76-81.

[69] R. Bodvik, A. Dedinaite, L. Karlson, M. Bergström, P. Bäverbäck, J. S. Pedersen, K. Edwards, G. Karlsson, I. Varga, P. M. Claesson, Aggregation and network formation of aqueous methylcellulose and hydroxypropylmethylcellulose solutions, *Colloids Surf., A*, 2010, **354**, 162-171.

[70] K. J. Edgar, C. M. Buchanan, J. S. Debenham, P. A. Rundquist, B. D. Seiler, M. C. Shelton, D. Tindall, Advances in cellulose ester performance and application, *Prog. Polym. Sci.*, 2001, **26**, 1605-1688.

[71] L. Zhang, D. Ruan, S. Gao, Dissolution and regeneration of cellulose in NaOH/thiourea aqueous solution, *J. Polym. Sci., Part B: Polym. Phys.*, 2002, **40**, 1521-1529.

[72] O. Biermann, E. Hädicke, S. Koltzenburg, F. M. Plathe, Hydrophilicity and lipophilicity of cellulose crystal surfaces, *Angew. Chem. Int. Ed*, 2001, **40**, 3822-3825.

[73] C. Yamane, T. Aoyagi, M. Ago, K. Sato, K. Okajima, T. Takahashi, Two Different Surface Properties of Regenerated Cellulose due to Structural Anisotropy, *Polym. J.*, 2006, **38**, 819-826.

[74] C. Chang, L. Zhang, Cellulose-based hydrogels: Present status and application prospects, *Carbohydr. Polym.*, 2011, **84**, 40-53.

[75] B. J. C. Duchemin, M. P. Staiger, N. Tucker, R. H. Newman, Aerocellulose based on all-cellulose composites, *J. Appl. Polym. Sci.*, 2010, **115**, 216-221.

[76] F. Liebner, A. Potthast, T. Rosenau, E. Haimer, M. Wendland, Ultralight-Weight Cellulose Aerogels from NBnMO-Stabilized Lyocell Dopes, *Res. Lett. Mater. Sci.*, 2007, **2007**, 1-4.

[77] H. P. Fink, P. Weigel, H. J. Purz, J. Ganster, Structure formation of regenerated cellulose materials from NMO-solutions, *Prog. Polym. Sci.*, 2001, **26**, 1473-1524.

[78] T. Rosenau, A. Potthast, I. Adorjan, A. Hofinger, H. Sixta, H. Firgo, P. Kosma, Cellulose solutions in N-methylmorpholine-N-oxide (NMMO)-degradation processes and stabilizers, *Cellulose*, 2002, **9**, 283-291.

[79] I. Adorjan, A. Potthast, T. Rosenau, H. Sixta, P. Kosma, Discoloration of cellulose solutions in N-methylmorpholine-N-oxide (Lyocell). Part 1: Studies on model compounds and pulps, *Cellulose*, 2005, **12**, 51-57.

[80] J. Cai, L. Zhang, Rapid dissolution of cellulose in LiOH/urea and NaOH/urea aqueous solutions, *Macromol. Biosci.*, 2005, **5**, 539-548.

[81] N. Isobe, S. Kimura, M. Wada, S. Kuga, Mechanism of cellulose gelation from aqueous alkali-urea solution, *Carbohydr. Polym.*, 2012, **89**, 1298-1300.

[82] J. Cai, L. Zhang, Unique Gelation Behavior of Cellulose in NaOH/Urea Aqueous Solution, *Biomacromolecules*, 2006, **7**, 183-189.

[83] J. Innerlohinger, H. K. Weber, G. Kraft, Aerocell aerogels from cellulosic materials, *Lenzinger Berichte*, 2006, **86**, 137-143.

[84] J. Rooke, C. de Matos Passos, M. Chatenet, R. Sescousse, T. Budtova, S. Berthon-Fabry, R. Mosdale, F. d. r. Maillard, Synthesis and Properties of Platinum Nanocatalyst Supported on Cellulose-Based Carbon Aerogel for Applications in PEMFCs, *J. Electrochem. Soc.*, 2011, **158**, B779.

[85] S. Hoepfner, L. Ratke, B. Milow, Synthesis and characterisation of nanofibrillar cellulose aerogels, *Cellulose*, 2007, **15**, 121-129.

[86] C. K. Liu, J. A. Cuculo, B. Smith, Coagulation studies for cellulose in the ammonia/ammonium thiocyanate direct solvent system, *J. Polym. Sci., Part B: Polym. Phys.*, 1989, **27**, 2493-2511.

[87] C. Schimper, E. Haimer, M. Wendland, A. Potthast, T. Rosenau, F. Liebner, The effect of different process parameters on the properties of cellulose arogels obtained via the lyocell route, *Lenzinger Berichte*, 2011, **89**, 109-117.

[88] R. Gavillon, T. Budtova, Kinetics of cellulose regeneration from cellulose-NaOH-water gels and comparison with cellulose-N-methylmorpholine-N-oxide-water solutions, *Biomacromolecules*, 2007, **8**, 424-432.

[89] S. Zhang, F. X. Li, J. Y. Yu, Kinetics of cellulose regeneration from cellulose NaOH/thiourea/urea/H_2O system, *Cellulose Chem. Technol.*, 2011, **45**, 593-604.

[90] H. Sai, L. Xing, J. Xiang, L. Cui, J. Jiao, C. Zhao, Z. Li, F. Li, Flexible aerogels based on an interpenetrating network of bacterial cellulose and silica by a non-supercritical drying process, *J. Mater. Chem.*, 2013, **1**, 7963-7970.

[91] D. Nystrom, J. Lindqvist, E. Ostmark, A. Hult, E. Malmstrom, Superhydrophobic bio-fibre surfaces via tailored grafting architecture, *Chem. Commun.*, 2006, 3594-3596.

[92] M. Andresen, L.-S. Johansson, B. S. Tanem, P. Stenius, Properties and characterization of hydrophobized microfibrillated cellulose, *Cellulose*, 2006, **13**, 665-677.

[93] A. G. Cunha, C. S. R. Freire, A. J. D. Silvestre, C. P. Neto, A. Gandini, E. Orblin, P. Fardim, Highly hydrophobic biopolymers prepared by the surface pentafluorobenzoylation of cellulose substrates, *Biomacromolecules*, 2007, **8**, 1347-1352.

[94] S. Li, Y. Wei, J. Huang, Facile fabrication of superhydrophobic cellulose materials by a nanocoating approach, *Chem. Lett.*, 2010, **39**, 20-21.

[95] K. Ramzi, F. Ikhlass, M. h. M. Farouk, Study of liquids absorption and retention capacities of new cellulosic materials and sodium cellulose carboxylmethylate prepared from Posidonia, *Fiber. Polym.*, 2010, **11**, 593-597.

[96] C. Teas, S. Kalligeros, F. Zanikos, S. Stournas, E. Lois, G. Anastopoulos, Investigation of the effectiveness of absorbent materials in oil spills clean up, *Desalination*, 2001, **140**, 259-264.

[97] A. Bayat, S. F. A. A. Moheb, G. R. Vakili-Nezhaad, Oil spill cleanup from sea water by sorbent materials, *Chem. Eng. Technol.*, 2005, **28**, 1525-1528.

[98] M. O. Adebajo, R. L. Frost, J. T. Kloprogge, O. Carmody, S. Kokot, Porous materials for oil spill cleanup: a review of synthesis and absorption properties, *J. Porous Mater.*, 2003, **10**, 159-170.

[99] J. Lin, Y. Shang, B. Ding, J. Yang, J. Yu, S. S. Al-Deyab, Nanoporous polystyrene fibers for oil spill cleanup, *Mar. Pollut. Bull.*, 2012, **64**, 347-352.

[100] Q. F. Wei, R. R. Mather, A. F. Fotheringham, R. D. Yang, Evaluation of nonwoven polypropylene oil sorbents in marine oil-spill recovery, *Mar. Pollut. Bull.*, 2003, **46**, 780-783.

[101] A. Demilecamps, C. Beauger, C. Hildenbrand, A. Rigacci, T. Budtova, Cellulose-silica aerogels, *Carbohydr. Polym.*, 2015, **122**, 293-300.

[102] S. Sequeira, D. V. Evtuguin, I. Portugal, Preparation and properties of cellulose/silica hybrid composites, *Polym. Compos.*, 2009, **30**, 1275-1282.

[103] J. Cai, S. Liu, J. Feng, S. Kimura, M. Wada, S. Kuga, L. Zhang, Cellulose-silica nanocomposite aerogels by in situ formation of silica in cellulose gel, *Angew. Chem. Int. Ed. Engl.*, 2012, **51**, 2076-2079.

[104] M. Litschauer, M.-A. Neouze, E. Haimer, U. Henniges, A. Potthast, T. Rosenau, F. Liebner, Silica modified cellulosic aerogels, *Cellulose*, 2010, **18**, 143-149.

[105] T. Clyne, A. Markaki, J. Tan, Mechanical and magnetic properties of metal fibre networks, with and without a polymeric matrix, *Compos. Sci. Technol.*, 2005, **65**, 2492-2499.

[106] A. Demilecamps, G. Reichenauer, A. Rigacci, T. Budtova, Cellulose–silica composite aerogels from "one-pot" synthesis, *Cellulose*, 2014, **21**, 2625-2636.

[107] J. Shi, L. Lu, W. Guo, J. Zhang, Y. Cao, Heat insulation performance, mechanics and hydrophobic modification of cellulose-SiO2 composite aerogels, *Carbohydr. Polym.*, 2013, **98**, 282-289.

[108] A. Venkateswara Rao, M. M. Kulkarni, D. P. Amalnerkar, T. Seth, Superhydrophobic silica aerogels based on methyltrimethoxysilane precursor, *J. Non-Cryst. Solids*, 2003, **330**, 187-195.

[109] M. C. Kiran, A. Nandanwar, M. V. Naidu, K. C. V. Rajulu, Effect of density on thermal conductivity of bamboo mat board, *Int. J. Agr. Forest.*, 2012, **2**, 257-261.

CHAPTER 3: Experiments

This chapter presents information about the raw materials, the fabrication approaches, and the characterization methods used for this thesis. After the raw materials are listed, the fabrication approaches of recycled cellulose aerogels using both a sodium hydroxide–urea aqueous solution and a Kymene binder will be discussed. Following the discussions on fabrication approaches, the hydrophobic modification method used will be described. Subsequently, the synthesis procedures of the silica–recycled-cellulose aerogels will be described. Finally, the characterization methods, such as X-ray diffraction, scanning electron microscopy, and water contact angle measurements, will be presented.

3.1 Materials

Sodium hydroxide (NaOH), urea ($CO(NH_2)_2$), ethanol (CH_3CH_2OH), methoxytrimethylsilane (MTMS), ammonium hydroxide (NH_4OH), and ammonium fluoride (NH_4F), all of analytical grade, were purchased from Sigma-Aldrich. All the solutions were made with deionized (DI) water. Recycled cellulose fibres and Kymene 557H were obtained from Insul-Dek Engineering Pte Ltd (Singapore) and Ashland (Taiwan) respectively. Motor oils of 5w40 and 5w50 were purchased from Carlube, and Singer machine oil was purchased from the commercial market. Three crude oils were used for the absorption tests: Ruby (RB), Te Giac Trang (TGT), and Rang Dong (RD). The crude oils were supplied by the Petrovietnam Research and Development

Centre for Petroleum Processing (PVPro). All the chemicals were used as received, without further purification.

3.2 Experimental techniques

For this thesis, recycled cellulose fibres were directly purchased from the market because the established raw–paper waste recycling methods are mature, and using commercial recycled cellulose fibres is cost-effective and time-saving.

3.2.1 Synthesis of recycled cellulose aerogels using sodium hydroxide–urea aqueous solutions

Recycled cellulose fibres (2 wt. %) were dispersed in a NaOH/urea solution (1.9 wt. %/10 wt. %) by sonication for 10 min. The mixture was then placed in a refrigerator for more than 24 h to allow gelation. After the mixture was frozen, it was thawed at room temperature (25 ^{o}C), followed by immersion in ethanol (99 vol. %) for coagulation. The specimen thickness of the cellulose hydrogels was controlled to be approximately 1 cm with a diameter of 3.8 cm, using a beaker as a mould. After coagulation, solvent exchange was carried out by immersing the gel in DI water for two days. Freeze drying was carried out on the frozen cellulose hydrogels for two days at -98 ℃ with a ScanVac CoolSafe 95-15 Pro freeze-dryer (Denmark), after the hydrogels were prefrozen at -18 ℃ for 12 h. The details of the parameter changes (the amounts of cellulose, NaOH and urea) will be presented in Section 4.2.1 for referral convenience.

3.2.2 Synthesis of recycled cellulose aerogels using Kymene binder

The recycled cellulose fibres from paper waste (0.075–0.3 g) and Kymene (5–20 μl) were first dispersed in 30 ml of DI water by sonicating the mixtures for 10 min. The suspensions were then placed in a refrigerator at -18 ^{o}C for more than 12 h to allow the gelation. The cellulose aerogels were obtained by freeze drying the obtained gels at -98 ^{o}C for two days using a Scan Vac CoolSafe 95-15 Pro freeze dryer (Denmark). Thereafter, the cellulose aerogels were further cured at 120 ^{o}C for another 3 h to completely cross-link the Kymene molecules.

3.2.3 Hydrophobic coating of the recycled cellulose aerogels

As the recycled cellulose aerogels whose development is described in Section 3.2.1 and 3.2.2 were hydrophilic, the highly porous networks of the as-prepared cellulose aerogels were coated with MTMS, to form super-hydrophobic cellulose aerogels for oil absorption and thermal insulation, in accordance of the aims of this thesis. The proposed coating mechanism of the silanation reaction between the cellulose and MTMS is illustrated in Figure 3.1 below.

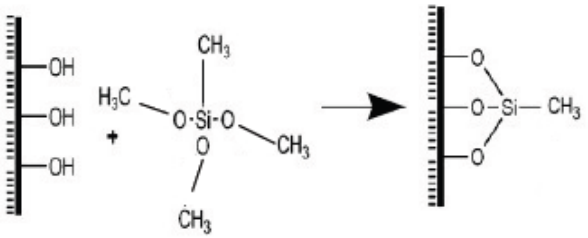

Figure 3.1 The proposed silanation reaction between cellulose and MTMS, which results in super-hydrophobic cellulose aerogels [1, 2].

The cellulose aerogels and open glass vials containing MTMS (0.5 ml) were placed in big containers. The containers were then capped and heated at 70 ^{o}C for 3 h for the silanation reaction. After the aerogel structure was coated

completely, excessive MTMS was removed by placing the aerogel in a vacuum oven until the pressure decreased to below 0.03 mbar.

3.2.4 Synthesis of silica–cellulose aerogels

The catalyst solution was prepared by mixing 10.250 g of ammonium hydroxide and 0.927 g of ammonium fluoride in 50 ml of DI water. After that, 6 ml of MTMS solution was mixed with 11 ml of ethanol and stirred for 5 min (forming an MTMS/ethanol solution). Then, 7 ml of DI water, 11ml of ethanol, and 0.5 ml of the catalyst solution were mixed in another beaker (forming a water/ethanol/catalyst solution). While the MTMS/ethanol mixture was still being stirred, the obtained DI water/ethanol/catalyst solution was poured slowly into the MTMS/ethanol mixture and stirred for another 15 min to form the sol. The sol was poured into a mould that contained the cellulose aerogel (as described in Section 3.2.2), and the gelation and aging process were conducted at room temperature (25 ^{o}C) for three days. After solvent exchange between the gel and DI water, the obtained hydrogel was frozen and dried using a Scan Vac CoolSafe 95-15 Pro freeze dryer (Denmark) for 24 h. Different silica–cellulose aerogels were synthesized from the different cellulose aerogel matrixes with varied cellulose fibre concentrations inside the initial cellulose aqueous suspensions; the details will be presented in Section 6.4.

3.3 Characterization

3.3.1 X-ray diffraction (XRD)

X-ray diffraction (XRD) can identify and characterize materials based

on their diffraction patterns, which revealing the chemical composition and crystallographic structure of the materials [3]. In crystals, the scattered X-rays interfere with the materials constructively and destructively, forming the diffraction pattern. This process is described by the famous Bragg's law:

$$n\lambda = 2d\sin\theta \quad (3.1)$$

in which n is an integer, λ is the wavelength of the X-ray (nm), d is the distance between the lattice planes (nm), and θ is the angle between the incidence X-ray and lattice planes (^{o}).

For this thesis, the chemical composition of the aerogels was investigated by X-ray diffraction (XRD, 6000 Shimadzu, Japan). An X-ray beam generated by a Cu-Kα radiation source with a wave length of 0.1506 nm was used. The continuous scan was recorded from 5 to 45^o (2θ), and the scan step and scan rate were 0.02^o and 0.6^o/min respectively. Before being characterized, the aerogels were ground and pressed into a glass holder to ensure a flat surface.

3.3.2 Scanning electron microscopy (SEM)

Scanning electron microscopy (SEM) can observe the surface morphologies and features and obtain the elemental identification and quantitative composition of a specimen [4]. When a finely focused high-energy electron beam scans the surface of the sample, the interaction between the electrons and atoms (in the sample) produces several detective signals, such as those of secondary electrons and backscattered electrons. The signals are usually collected by an Everhart-Thornley detector, which is a positively

biased scintillator-photomultiplier, and then amplified and displayed through intensity modulation [4].

For this thesis, all the SEM images were obtained by field emission scanning electron microscopy (FESEM, Model S-4300 Hitachi, Japan) and scanning electron microscopy (SEM, Model JSM-600LV, Japan), with the field emission guns operating at 15 KV. As both cellulose and silica have low electrical conductivity, all the aerogels were gold-coated by sputtering before characterization. The coating of the cellulose aerogels was performed under 10 mA for 30 s, while the silica–cellulose aerogels were gold-coated at 20 mA for 15 s.

3.3.3 Surface-area determination

The Brunauer–Emmett–Teller (BET) theory studies the physical adsorption of gas molecules on the surface of solids, which is widely accepted in specific surface-area analysis [5]. This theory adopts the Langmuir mechanism with three simplifying hypotheses: (i) the heat of adsorption is equal to the condensation molar heat in all layers except the first layer; (ii) the evaporation–condensation conditions of all layers are identical except the first layer; (iii) the number of adsorbed layers is infinite [6]. The BET equation is as follows:

$$\frac{1}{v((P_0/P)-1)} = \frac{1}{v_m C} + \frac{C-1}{v_m C}\left(\frac{P}{P_0}\right) \tag{3.2}$$

in which C is the BET constant, P is the equilibrium pressure of the adsorbent at the test temperature (Pa), P_0 is the saturation pressure of the adsorbent at the test temperature (Pa), V is the volume of gas absorbed at a relative pressure

(mm^3), and V_m is the volume of adsorbate constituting a monolayer of surface coverage (mm^3).

The BET constant can be practically simplified to the following expression:

$$C=\exp((E_1-E_L)/RT) \tag{3.3}$$

in which E_1 is the heat of adsorption for the first layer (J/mol), E_L is the heat of adsorption for the second and upward layers (J/mol), R is the gas constant (J/K. mol), and T is the test temperature (K).

Furthermore, the total surface area S_t of the sample can be calculated from the obtained V_m via a linear interpretation:

$$S_t = \frac{V_m N A_{cs}}{V} \tag{3.4}$$

in which A_{cs} is the adsorbate molecular cross-section (nm^2/molecule), N is the Avogadro's number (6.022×10^{23} molecule/mol), and V is the molar volume of the adsorbate (m^3/mol).

It is then straightforward to calculate the specific surface area S_{BET} from S_t using the following equation:

$$S_{BET} = \frac{S_t}{W_{sample}} \tag{3.5}$$

in which W_{sample} (g) is the sample weight.

For this thesis, the BET specific surface areas of the aerogels were obtained with a Nova 2200e (Quantachrome) analyzer, with nitrogen serving as the absorbate. Before characterization, the aerogels were cut into small pieces and degassed in a vacuum at 80 ^oC for 24h.

3.3.4 Water contact angle

The contact angle refers to the angle made by the intersection of the

liquid/solid interface and liquid/air interface. The water contact angle measurements are useful in determining the solid surface energy, chemical affinity, and wettability [7]. Two common methods of water contact angle measurement are the goniometer method and the Wilhelmy method [8, 9]. In the goniometer method, a motor-driven syringe deposits the droplets onto the sample surface, and the image, captured by a camera, is displayed on the screen visually. Further analysis of images generates the water contact angles directly with software [10]. The Wilhelmy method requires a small plate-shaped sample and measures the force experienced by the sample via the liquid [9]. The value of the water contact angle shows the hydrophobicity of the material surface: a material surface with a water contact angle of less than 90^o is considered hydrophilic, while a material surface with a water contact angle larger than 90^o is considered hydrophobic; moreover, a material surface with a water contact angle larger than 150^o is considered superhydrophobic [11]. Under laboratory conditions, the water contact angles can be measured more accurately, with a small derivation (a few degrees).

For this thesis, the water contact angle values were measured with a VCA Optima goniometer (AST Products Inc., USA), to investigate the water repellency of the aerogels. The volume (0.5 uL) of the dispensed water droplets was accurately controlled using the syringe-control function of the software. The contact angle values were calculated using contact angle meter software, on the basis of the droplet shape in the image, and displayed on the saved images. For each aerogel, measurements were repeated at several different positions, and the contact angle of the aerogel was finally determined by averaging these contact angle values from various measurements.

3.3.5 Oil absorption capacity

The oil absorption capabilities of the cellulose aerogels were investigated using a modified ASTM F726-06 test method [12–15]. Three crude oils were used for the absorption tests of the recycled cellulose aerogels using a NaOH–urea aqueous solution: Ruby (RB), Te Giac Trang (TGT), and Rang Dong (RD). The specifications of the crude oils will be presented in Section 4.2.2.1. The dry aerogel sample for oil absorption had dimensions of 38 mm (diameter) by 11 mm (thickness). The aerogel was weighed and placed in 300 mL of crude oil for a certain period of time. The wet aerogel was then removed from the liquid using a stainless steel mesh basket and drained for 1 min. The wet aerogel was weighed.

For the recycled cellulose aerogel fabricated using a Kymene binder, dry aerogels with dimensions of 45 mm (diameter) by 11 mm (thickness) were first weighed, and then immersed in oil for 2 h to reach a swelling equilibrium. Thereafter, the gels were lifted up from the oil container with a stainless steel mesh basket, drained in air for 30 s, and weighed again.

The oil absorption capacity of the aerogels was calculated using the following formula:

$$Q_t = \frac{m_w - m_d}{m_d} \tag{3.6}$$

in which Q_t (g/g) is the oil absorption capacity of the aerogel at a certain time t (s), m_d is the weight of the aerogel before absorption (g), and m_w is the weight of the aerogel after absorption (g).

To qualitatively evaluate the oil absorption ability of the aerogel in a crude oil/water mixture, 40 mL of deionized (DI) water and 5 mL of RB oil were added to a Petri dish. An MTMS-coated aerogel was used for the

absorption test. Similar studies were carried to test the oil absorption ability of the cellulose aerogels in motor oil/water mixtures. Moreover, environmental factors were also taken into consideration while testing the aerogels in the motor oil/water mixtures, with the different pH values (pH = 3, 5, 7 and 9) of the artificial seawater (3.5 wt. % NaCl).

3.3.6 Reusability

The reusability of cellulose aerogels was evaluated by the changes on absorption capacity, on squeezed ratio of the absorbed oils, and on volume during cycles of sorption. After the first sorption cycle, the cellulose aerogel was weighted, as described in Section 3.3.5, and then its dimensions were measured. The cellulose aerogel was then squeezed, and weighted again. The test was repeated several times to assess the reusability of the cellulose aerogels.

The ratio of the aerogel volume before the absorption test to its original volume was calculated with the following equation:

$$V_n = \frac{V_d}{V_i} \tag{3.7}$$

in which V_n is the ratio of the aerogel volume before the absorption test to its original volume, V_d is the volume of the aerogel before the absorption test (cm^3), and V_i is the original volume of the aerogel (cm^3).

The squeezed ratio (Q_s) of oil was calculated using the following formula:

$$Q_s = \frac{\text{squeezed amount of oil}}{\text{absorbed amount of oil}} = \frac{m_w - m_s}{m_w - m_d} \tag{3.8}$$

in which m_s (g) was the weight of the aerogel after squeezing.

3.3.7 Oil absorption kinetics

To study the oil absorption kinetics of these cellulose aerogels, the immersed aerogels were lifted up from the oil, drained, and weighed at several time intervals (0, 2, 5, 7, 10, 15, 20, 30, and 60 s). The motor oil (5w50) and Singer machine oil, with different viscosities of 0.14 and 0.026 Pa. s respectively, were used for the absorption kinetics tests to investigate the effects of the oil viscosity on the absorption kinetics.

Various kinetics models have been suggested for absorption kinetics analysis [16–18]. Pseudo-first-order and pseudo-second-order models are commonly used for the oil absorption [19–23]. The pseudo-first-order model can be used in many absorption cases, such as systems close to equilibrium, systems with time-independent solute concentrations, or linear equilibrium absorption isotherms, while the pseudo-second-order model is used to describe the sorption process controlled by chemisorption [16, 18, 19, 24–27].

In this work, both these models were used to fit the experimental absorption kinetics data. After integration, the pseudo-first-order equation can be obtained [23]:

$$\ln \frac{Q_m}{Q_m - Q_t} = k_1 t \tag{3.9}$$

in which Q_m (g/g) is the maximum oil absorbency, Q_t (g/g) is the oil absorbency at time t (s), and k_1 (1/s) is the absorption rate constant determined from the slope of $\ln[Q_m/(Q_m-Q_t)]$ versus t (s) plot. On the other hand, the pseudo-second-order equation can be converted into a linear form [16]:

$$\frac{t}{Q_t} = \frac{1}{Q_m} t + \frac{1}{k_2 {Q_m}^2} \tag{3.10}$$

By plotting (t/Q_t) (s) versus t (s), the absorption rate constant k_2 (1/s) can be determined.

3.3.8 Thermal gravimetric analysis (TGA)

Thermal gravimetric analysis (TGA) measures the mass of a sample as a function of sample temperature or time [28]. During dynamic measurement, the sample is normally treated with a constant heating rate. Moreover, the analysis atmosphere could be reactive, oxidising, or inert depending on the analytical purposes. To minimize the effects of gas density change (resulting from the temperature changes), thermal gravimetric analysis is normally equipped with buoyancy corrections [28]. These corrections are performed by subtracting the baseline (generated in the blank measurement) from the sample measurement curve [28]. Thermal gravimetric analysis could provide useful information, such as degradation temperatures and the decomposition point. Differential thermal analysis (DTA) could be conducted simultaneously with TGA to detect the exothermic/endothermic reactions and the enthalpy change [29].

For this thesis, the TGA and DTA were performed by a DTG60H thermogravimetric analyzer (Shimadzu, Japan). The aerogel was heated up in air from room temperature to 800 ^{o}C at a rate of 10 ^{o}C/min. During the test, the aerogel was kept at 150 ^{o}C for 1 h to ensure that the adsorbed water was removed.

3.3.9 Thermal conductivity

Thermal conductivity measures the ability of a material to transfer heat. All the available methods can be categorized into two groups: (i) steady-state methods and (ii) transient methods. One of the transient methods is the modified transient plane source (MTPS) method developed by Nancy

Mathis [30]. In this method, a heat reflectance sensor provides a momentary and constant heat (generated by a known current), which induces a temperature difference of less than 2 ^{o}C between the sensor and the sample at the interface. The rate of the sample voltage increment resulting from the temperature rise determines the thermal conductivity: the steeper the voltage rise, the lower the thermal conductivity. This method is considered rapid and non-destructive.

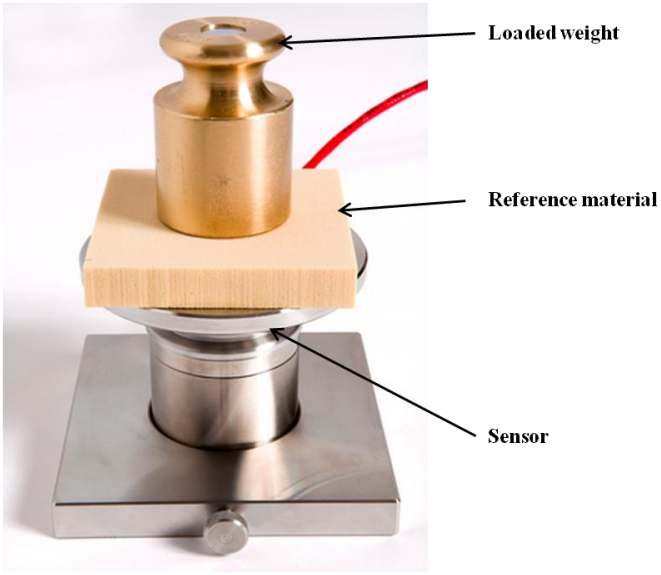

Figure 3.2 The set-up of thermal conductivity measurement with a C-Therm TCi Thermal Conductivity Analyzer (C-Therm Technologies, Canada).

For this thesis, the thermal conductivities of the aerogels were measured under ambient conditions using a C-Therm TCi Thermal Conductivity Analyzer (C-Therm Technologies, Canada), with the MTPS method. The sensor of the equipment was put on a stable and flat table with the sensor head facing upwards. The aerogel was placed directly on the top of the sensor with a loaded weight to ensure good surface contact between the aerogel and the sensor, as shown in Figure 3.2 above. During the test, the foam method was selected, and three measurements were made. After the test, the results were directly displayed on the screen with the TCi 3.0 software.

3.3.10 Compression test

The compressive test examines the behaviour of a material responding to an applied compression. The test can determine various important mechanical properties, such as compressive modulus, compressive strength, yield strength, and yield point. During the test, a specimen is deformed with a gradually increasing compressive load generated by the testing machine. The compressive testing machine contracts the specimen at a constant rate, and the instantaneously applied load and contraction are measured with a load cell and an extensometer, respectively. Although the compressive test is destructive, it is highly desirable when it is necessary to know the behaviour of a material under large and permanent strains [31]. For this thesis, only the compressive properties of the aerogels were investigated as compression is more likely to occur in thermal and oil spill–cleaning applications.

For this thesis, the compressive tests were carried out on an Instron 5500 microtester (USA), according to ASTM D1621-10 [32]. Before the measurements, the dimensions of the samples were recorded for the subsequent data analysis. The load and the gauge length needed to be balanced and reset before compression. During the tests, the aerogels were subjected to a loading of 1 mm/min. After every single run, the data was manually saved before the next test was started.

References

[1] A. V. Rao, S. D. Bhagat, H. Hirashima, G. M. Pajonk, Synthesis of flexible silica aerogels using methyltrimethoxysilane (MTMS) precursor, *J. Colloid Interf. Sci.*, 2006, **300**, 279-285.

[2] L. Xu, W. Zhuang, B. Xu, Z. Cai, Fabrication of superhydrophobic cotton fabrics by silica hydrosol and hydrophobization, *Appl. Surf. Sci.*, 2011, **257**, 5491-5498.

[3] J. Als-Nielsen, D. McMorrow, Elements of modern X-ray physics *John Wiley and Sons Pte. Ltd.*, 2011.

[4] J. I. Goldstein, C. E. Lyman, D. E. Newbury, E. Lifshin, P. Echlin, L. Sawyer, D. C. Joy, J. R. Michael, Scanning electron microscopy and X-ray microanalysis, *Springer*, New York, 2003.

[5] S. Brunauer, P. H. Emmett, E. Teller, Adsorption of gases in multimolecular layers, *J. Am. Chem. Soc.*, 1938, **60**, 309-319.

[6] S. J. Gregg, K. S. W. Sing, Adsorption, surface area and porosity, *Academic Press Inc.*, London, 1982.

[7] W. A. Zisman, Contact angle, wettability and adhesion, *ACS*, Washington, 1964.

[8] W. C. Bigelow, D. L. Pickett, W. A. Zisman, Oleophobic monolayers: I. Films adsorbed from solution in non-polar liquids, *J. Coll. Sci. Imp. U. Tok.* , 1946, **1**, 513-538.

[9] H. M. Princen, Capillary phenomena in assemblies of parallel cylinders I. Capillary rise between two cylinders, *J. Colloid Interf. Sci.*, 1969, **30**, 69-75.

[10] D. Y. Kwok, R. Lin, M. Mui, Low-rate dynamic and static contact angles and the determination of solid surface tensions *Colloid. Surface. A*, 1996, **116**, 63-77.

[11] T. R. L. Y. Yuan, Contact angle and wetting properties, in: B.H. G. Bracco (Ed.), Surface science techniques *Springer-Verlag Berlin Heidelberg*, 2013, pp. 3-34.

[12] ASTM Standard F726, Standard test method for sorbent performance of adsorbents, ASTM Internatinal, West Conshohocken, PA, 2006.

[13] C. Cojocaru, M. Macoveanu, I. Cretescu, Peat-based sorbents for the removal of oil spills from water surface: Application of artificial neural network modeling, *Colloid. Surface. A*, 2011, **384**, 675-684.

[14] V. Singh, R. J. Kendall, K. Hake, S. Ramkumar, Crude Oil Sorption by Raw Cotton, *Ind. Eng. Chem. Research*, 2013, **52**, 6277-6281.

[15] X. Yuan, T. C. M. Chung, Novel Solution to Oil Spill Recovery: Using Thermodegradable Polyolefin Oil Superabsorbent Polymer (Oil–SAP), *Energ. Fuel.*, 2012, **26**, 4896-4902.

[16] Y. Chen, D. Zhang, Adsorption kinetics, isotherm and thermodynamics studies of flavones from Vaccinium Bracteatum Thunb leaves on NKA-2 resin, *Chem. Eng. J.*, 2014, **254**, 579-585.

[17] P. Sharma, B. K. Saikia, M. R. Das, Removal of methyl green dye molecule from aqueous system using reduced graphene oxide as an efficient adsorbent: Kinetics, isotherm and thermodynamic parameters, *Colloid. Surface. A*, 2014, **457**, 125-133.

[18] A. M. M. Vargas, A. L. Cazetta, M. H. Kunita, T. L. Silva, V. C. Almeida, Adsorption of methylene blue on activated carbon produced from

flamboyant pods (Delonix regia): Study of adsorption isotherms and kinetic models, *Chem. Eng. J.*, 2011, **168**, 722-730.

[19] D. Bastani, A. A. Safekordi, A. Alihosseini, V. Taghikhani, Study of oil sorption by expanded perlite at 298.15K, *Sep. Purif. Technol.*, 2006, **52**, 295-300.

[20] X. Gui, H. Li, K. Wang, J. Wei, Y. Jia, Z. Li, L. Fan, A. Cao, H. Zhu, D. Wu, Recyclable carbon nanotube sponges for oil absorption, *Acta Mater.*, 2011, **59**, 4798-4804.

[21] H. H. Sokker, N. M. El-Sawy, M. A. Hassan, B. E. El-Anadouli, Adsorption of crude oil from aqueous solution by hydrogel of chitosan based polyacrylamide prepared by radiation induced graft polymerization, *J. Hazard. Mater.*, 2011, **190**, 359-365.

[22] N. E. Thompson, G. C. Emmanuel, K. J. Adagadzu, N. B. Yusuf, Sorption studies of crude oil on acetylated rice husks, *Arch. Appl. Sci. Res.* , 2010, **2**, 142-151.

[23] B. Wu, M. H. Zhou, Recycling of waste tyre rubber into oil absorbent, *Waste Manage.*, 2009, **29**, 355-359.

[24] H. K. Boparai, M. Joseph, D. M. O'Carroll, Kinetics and thermodynamics of cadmium ion removal by adsorption onto nano zerovalent iron particles, *J. Hazard. Mater.*, 2011, **186**, 458-465.

[25] Y. S. Ho, G. McKay, A Comparison of Chemisorption Kinetic Models Applied to Pollutant Removal on Various Sorbents, *Process. Saf. Environ.*, 1998, **76**, 332-340.

[26] Y. S. Ho, G. McKay, Pseudo-second order model for sorption processes *Process Biochem.,* 1999, **34**, 451-465.

[27] D. Robati, Pseudo-second-order kinetic equations for modeling adsorption systems for removal of lead ions using multi-walled carbon nanotube, *J. Nanostruct. Chem.*, 2013, **3**, 55.

[28] P. Gabbott, Thermogravimetric analysis, Principles and applications of thermal analysis, *Blackwell Publishing Ltd.*, 2008, pp. 87-118.

[29] P. Gabbott, A practical introduction to differential scanning calorimetry, Principles and applications of thermal analysis, *Blackwell Publishing Ltd.*, 2008, pp. 2-49.

[30] N. Mathis, C. Chandler, Direct thermal conductivity measurement technique, *Mathis Instruments Ltd.* , United States, 2004.

[31] W. D. Callister, Materials science and engineering: an introduction, *John Wilney and Sons Pte. Ltd.*, Asia, 2007.

[32] ASTM Standard D1621, Standard test method for compressive properties of rigid cellular plastics, ASTM International, West Conshohocken, PA, 2010.

CHAPTER 4: Recycled Cellulose Aerogels Using Sodium Hydroxide–Urea Aqueous Solutions for Oil Spill–Cleaning Applications

4.1 Introduction

This chapter presents the oil spill–cleaning applications of the recycled cellulose aerogels synthesized with a sodium hydroxide/urea method. Oil spills have been considered one of the most serious disasters threatening the marine ecosystem. Recently, the explosion of a drilling rig in the Gulf of Mexico caused significant environmental damage [1]. Oil spills are usually related to accidents during oil production, storage, and transportation. As long as fossil fuels are needed, oil spills will remain a significant problem that human beings will have to face [2–8]. Therefore, it is essential to solve, or at least alleviate, this environmental problem.

Several methods of oil spill–cleaning have been developed, and can be classified as chemical, biological, and physical methods. Dispersion, in-situ burning, and solidification are considered chemical methods that are complicated and expensive [9–11]. The use of microorganisms via biological methods is effective but requires a long time, and the microorganisms are affected by environmental factors, such as pH, temperature, and oxygen content [12]. Moreover, the oil spills cleaned with the chemical and the biological methods are difficult to recover, and recoverability is a crucial factor for oil spill–cleaning applications. With the physical methods, booms and skimmers are often used, but cannot remove oil from the sea

effectively [13]. Of these methods, sorption has been considered one of the most effective ways for oil-spill cleaning, as it enables the collection and complete removal of oil from oil-spill sites [2, 11, 14–20].

Several materials have been used as sorbents for oil-spill cleaning in research and practical applications. The oil absorbents can be categorized into inorganic minerals, natural organic materials, and synthetic organic materials [11, 16, 17, 19]. Inorganic materials, such as clay, vermiculite, exfoliated graphite, diatomite, and fly ash, have low oil absorption capacities (4–20 g/g) [21–23]. Furthermore, some of these inorganic materials, such as clay and vermiculite, are harmful when inhaled by human beings under windy conditions, due to the loose structures of these materials. Natural organic materials from plant and animal residues, such as kapok fibre, sugar-cane bagasse, rice husk, coconut husk, cotton, wool, sawdust, and chitosan, have been examined for oil absorption capabilities [24–26]. However, most of the materials have low oil absorption abilities (3–15 g/g), and also absorb water.

On the other hand, synthetic organic materials, such as polypropylene, polystyrene, and polyurethane, possess a high affinity with oil and high oil absorption capacities (4.5–100 g/g), but cause waste problems after use due to their slow rates of degradation [11, 16, 19]. Therefore, there is high demand for new environmentally friendly absorbents with high oil absorption capacity, good selectiveness, and low cost for oil-spill removal.

A combination of an aerogel structure and recycled cellulose fibres from paper waste can be used to form an advanced material, called a recycled cellulose aerogel, which is cost-effective and a promising material for oil

absorption. Although some studies have investigated the use of cellulosic materials for oil absorption, none have fabricated aerogels from paper-waste cellulose fibres and investigated them as absorbents for crude oil-spill cleaning [2, 5, 27–31].

In this chapter, the fabrication procedure for making cellulose aerogels from paper-waste cellulose fibres using the sodium hydroxide–urea method will be discussed; the materials have been found to have high absorption capacities for different crude oils. Other properties of the cellulose aerogels created with the sodium hydroxide–urea aqueous solution, such as morphology, hydrophobicity, oil absorption kinetics, and compressive mechanical property, will also be explored in this chapter.

4.2 Results and discussion

4.2.1 Morphology and hydrophobicity of the recycled cellulose aerogels

Recycled cellulose aerogels are synthesized with the method described in Section 3.2.1. In the literature, most research on cellulose aerogels used high-quality cellulose, bacterial cellulose, or wood powder [27, 32–35]. For this study, recycled cellulose fibres, as shown in Figure 4.1(a) below, from paper waste were chosen as raw materials for the first time. The cellulose aerogels were prepared using a sodium hydroxide–urea method, due to the low cost and convenience of the technique [32, 36, 37]. To dry the frozen cellulose hydrogel samples, the freeze-drying method was used to prevent the pores of the cellulose aerogels from collapsing. The freeze-drying process was discussed in detail in Section 1.1.2.

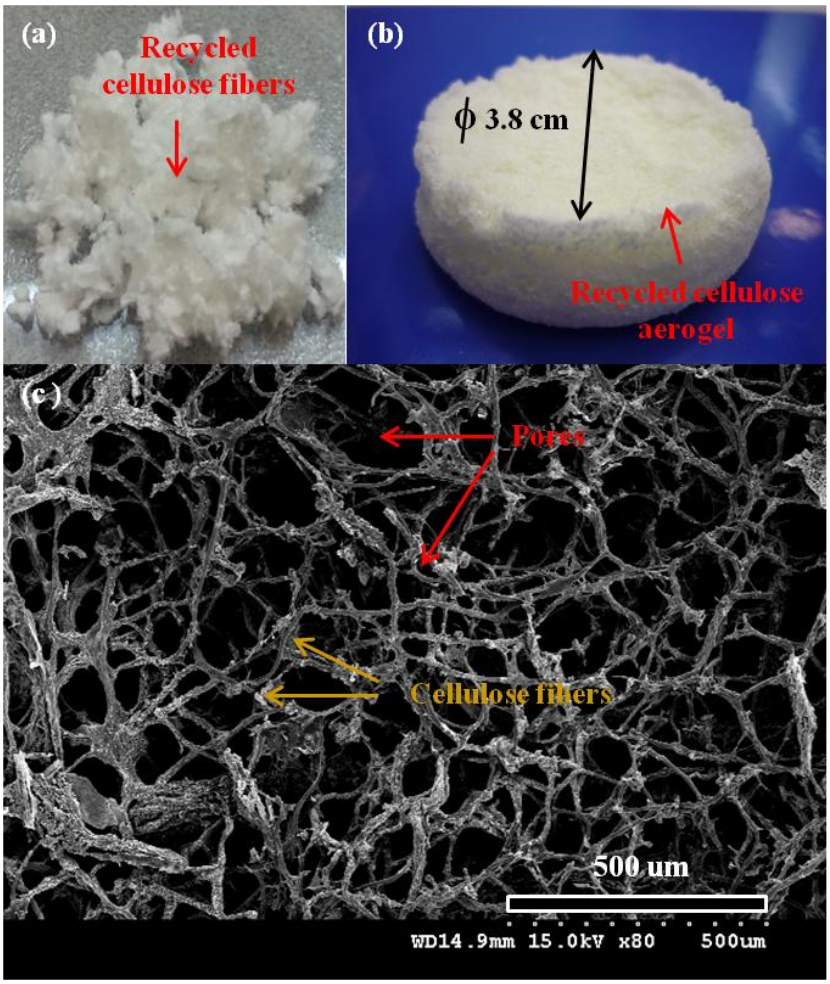

Figure 4.1 (a) Recycled cellulose fibres, (b) A recycled cellulose aerogel with a diameter of 3.8 cm, and (c) A FE-SEM image of a recycled cellulose aerogel before MTMS-coating.

As shown in Figure 4.1(b) above, a porous aerogel with a cellulose concentration of 2.0 wt. % was formed after the freeze-drying process. The FE-SEM was used to investigate the morphology of the cellulose aerogel prepared from recycled cellulose fibres. Figure 4.1(c) above shows an image of the internal structure of the material with a cellulose concentration of 2.0 wt. %. It can be observed that the aerogel had an open porous network structure of uniform fibres (about 8 μm wide), indicating that recycled cellulose fibres were successfully self-assembled via hydrogen bonding to form a three-dimensional porous network [37]. The width of the recycled cellulose fibres was much larger than that of the nanocellulose

fibres (2–100 nm) [33, 38–40]. The micro-sized cellulose fibres were consistent with the sizes of the recycled cellulose fibres as recorded in the literature [41–43]. From Figure 4.1(c) above, it can be observed that the pore size of the aerogel could be estimated to be in the range of 40–200 μm, indicating the macroporous property of the material. The sample with a cellulose concentration of 2.0 wt. % had a density of 0.040 g/cm^3, calculated from the weight and volume of the aerogel. With a cellulose fibre density of 1.5 g/cm^3 [44], the porosity of the aerogel sample with a cellulose concentration of 2.0 wt. % was calculated to be 97.3% by the sample mixing rule, neglecting the air density [33]. The low density and high porosity, which are essential for a good absorbent, were comparable to those of the nanocellulose aerogels (0.03 g/cm^3, 95–98 %) [45].

The effects of chemical compositions, such as cellulose concentrations, urea concentrations, and sodium-hydroxide concentrations, on the densities and porosities will be systematically investigated in the following sections.

4.2.1.1 Effects of the cellulose concentration

The morphology control of the cellulose aerogels was successfully achieved by changing the cellulose fibre concentration. As shown in Table 4.1 below, the density increased (0.03–0.10 g/cm^3) as the cellulose concentration in the hydrogel increased (1.5–4.0 wt. %), as more cellulose fibres were packed inside the aerogel. The increase in the density (0.03–0.10 g/cm^3) also caused a decrease in the porosity (98.0–93.3 %). This phenomenon was due to the more compact structure of the cellulose aerogels.

Table 4.1 The morphology control of the cellulose aerogels by changing the cellulose concentrations, with the concentrations of NaOH and urea fixed at 1.9 wt. % and 13.7 wt. % respectively.

Cellulose fibres (wt. %)	Density (g/cm^3)	Porosity (%)
1.5	0.026 ±0.004	98.0 ±0.2
2.0	0.039 ±0.004	97.3 ±0.3
3.0	0.049 ±0.006	96.7 ±0.4
4.0	0.104 ±0.015	93.3 ±1.0

4.2.1.2 Effects of the sodium-hydroxide concentration

The morphological effects of the sodium-hydroxide concentration on the cellulose aerogels are summarized in Table 4.2 below. The results suggest that the amount of sodium hydroxide may slightly affected the density and porosity of the cellulose aerogels in the range from 1.5 to 3 wt. %. As discussed earlier in Section 2.2.1, sodium hydroxide can partially bond to cellulose, which improves the dissolution. A possible explanation is that a larger amount of sodium hydroxide, resulting in less bonding in the cellulose, leads to cellulose aerogels with less porosity.

Table 4.2 The morphological effects of the sodium-hydroxide concentration on the cellulose aerogels, with the concentrations of cellulose fibres and urea fixed at 2.0 wt. % and 13.7 wt. % respectively.

Sodium hydroxide (wt.%)	Density (g/cm^3)	Porosity (%)
1.5	0.036 ±0.004	97.6 ±0.2
1.9	0.036 ±0.004	97.6 ±0.3
2.5	0.039 ±0.007	97.4 ±0.4
3.0	0.040 ±0.006	97.3 ±0.4

4.2.1.3 Effects of the urea concentration

As shown in Table 4.3 below, the density and porosity of the cellulose aerogels were not significantly changed when the amount of urea was adjusted. The urea amount had no obvious influence on the morphology of the cellulose aerogels in the range from 10 to 20 wt. %. Urea helps the dissolution of cellulose, since urea hydrates serve as hydrogen-bonding donors and receptors

to keep the cellulose apart. However, the results suggest that the amount of urea may have an insignificant effect on the porosity of cellulose aerogels.

Table 4.3 Morphological effects of the urea concentration on the cellulose aerogels, with the concentrations of cellulose fibres and NaOH fixed at 2.0 wt. % and 1.9 wt. % respectively.

Urea (wt. %)	Density (g/cm^3)	Porosity (%)
10.0	0.036 ±0.004	97.6 ±0.3
13.7	0.036 ±0.004	97.6 ±0.3
15.0	0.036 ±0.001	97.6 ±0.1
20.0	0.033 ±0.004	97.8 ±0.3

4.2.1.4 Hydrophobicity of the cellulose aerogels

Hydrophilicity is a natural feature of cellulose due to its hydroxyl groups, as discussed in Section 2.2.2. Therefore, a hydrophobic coating was applied to the recycled cellulose aerogel to make it oleophilic. To achieve this, a simple but effective chemical vapour–deposition procedure was performed for the aerogel with MTMS at 70 ℃, as described in Section 3.2.3 [46]. After the silanation reaction between the aerogel and MTMS, the excess MTMS was removed using a vacuum oven until the pressure fell below 0.03 mbar. As shown in Figure 4.2 below, the open porous structure of the material was still preserved after the coating was applied.

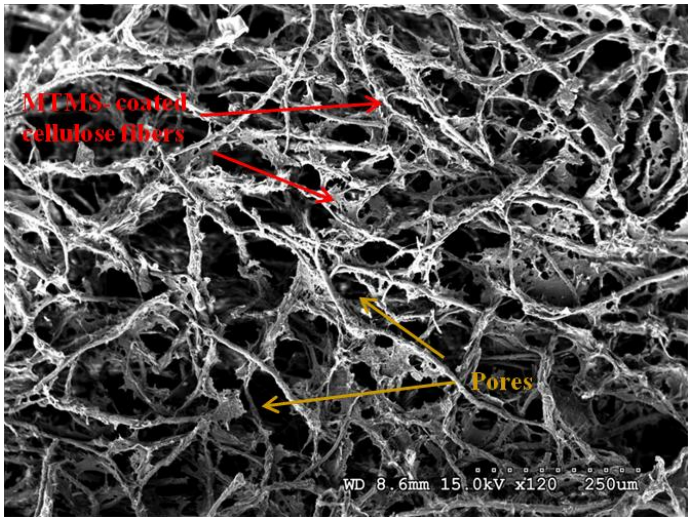

Figure 4.2 The FE-SEM image of the recycled cellulose aerogel after MTMS-coating.

To determine the effect of the coating on the hydrophobicity of the aerogel, water contact angle measurements were performed for the uncoated and coated aerogels. The uncoated sample immediately absorbed the water droplets in the test, and no measurable contact angle could be recorded. By contrast, as shown in Figure 4.3(a) below, a high contact angle of 145 ° was measured for the aerogel coated with MTMS, indicating the hydrophobicity of the material. To ensure that the internal surfaces of the pores were fully coated with MTMS, the sample was cut into two pieces, and a water contact angle of 143 ° was obtained on the cross-section of the cellulose aerogel, as shown in Figure 4.3(b), proving that the whole porous structure was hydrophobic and that the MTMS coating was effective.

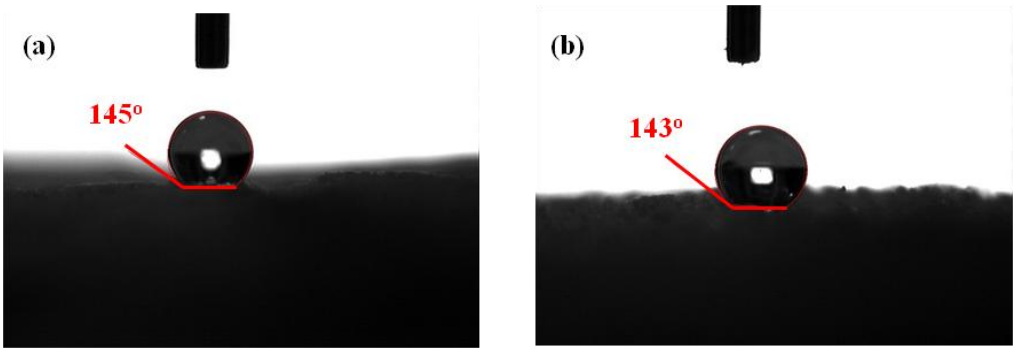

Figure 4.3 Water contact angle (a) on the external surface of the coated aerogel and (b) on the cut surface of the coated aerogel.

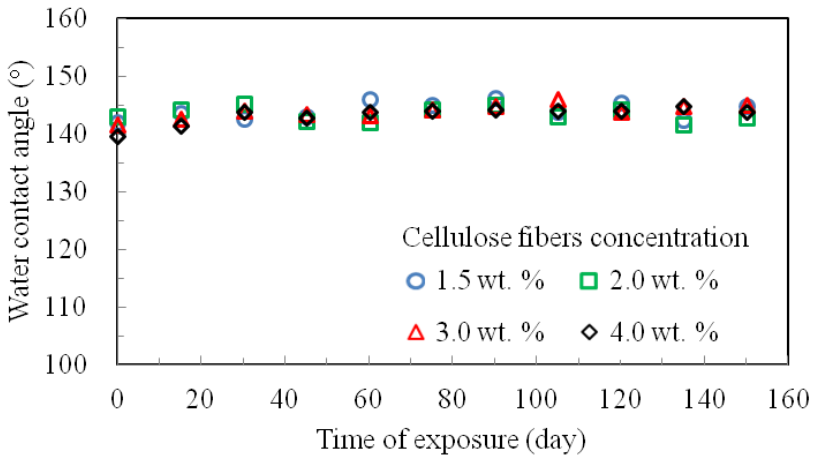

Figure 4.4 Effects of exposure time on the water contact angles of the cellulose aerogels with different cellulose fibre concentrations.

The stability of the hydrophobicity of the coated cellulose aerogels with cellulose concentrations of 1.5–4.0 wt. % was also examined. During the test, the coated aerogels were exposed to ambient conditions for 150 days. Their water contact angles (measured every 15 days) were 135–150^{o} over the examined period, as shown in Figure 4.4 above. The water contact angles of samples with different cellulose concentrations did not show any obvious change over time. These results confirmed the excellent stability of the hydrophobic coating of the MTMS-coated recycled cellulose aerogels used for this thesis.

4.2.2 Oil absorption properties of the cellulose aerogels

All the studies described in this section were based on recycled cellulose aerogels with a cellulose concentration of 2.0 wt. %. There were two main reasons for this: (1) after oil absorption, the recycled cellulose aerogels with 1.5 wt. % cellulose concentration were observed to have low rigidity; and (2) the oil absorption capacity of the cellulose aerogels with a cellulose concentration of 2.0 wt. % was the highest of all the cellulose aerogels with cellulose concentrations of 2.0–4.0 wt. %, because of the high porosity of the former..

4.2.2.1 Absorption capacities of the cellulose aerogels

a. Absorption capacities of the cellulose aerogels with different oils

The crude oil–absorption behaviour of the MTMS-coated aerogel was investigated with three different crude oils: Ruby (RB), Te Giac Trang (TGT), and Rang Dong (RD). The absorption capacities of the aerogels of RB, TGT,

and RD were 18.4, 18.5, and 20.5 g/g, respectively, at the end of the absorption test, as calculated by Equation 3.6. The absorption capacities were nearly double those obtained with polypropylene fibrous mats, which are widely used as absorbents for crude oil–spill cleaning [11, 19, 47–52]. The highest absorption capacity value was for RD, while the aerogel showed similar oil absorption behaviour for RB and TGT. This was probably due to the fact that RD has the lowest viscosity, while RB and TGT have comparable viscosity values, as shown in Table 4.4 below.

Table 4.4 The relevant specifications of the crude-oil samples in this thesis.

Crude oil	Density at 25 ^{o}C (g/cm^{3})	Viscosity (Pa.s)			
		10 ^{o}C	25 ^{o}C	40 ^{o}C	60 ^{o}C
RB	0.8236	42	0.0090	0.0049	0.0027
TGT	0.8264	n/a	0.0088	n/a	n/a
RD	0.8153	n/a	0.0062	n/a	n/a

It is well known that the absorption process of oils by absorbents is controlled by the capillary effect, van der Waals forces, hydrophobic interaction between the oils and absorbents, pore morphology, and oil viscosity [17, 24, 31, 48, 50, 53]. In this case, oil viscosity seemed to be the main factor responsible for the absorption-capacity difference between the three crude oils. A lower viscosity facilitates the penetration of the oil into the porous network of the aerogel, thus resulting in a higher oil absorption capacity [17, 31, 49]. Similar studies of absorption capacity were conducted using motor and cooking oils, and the cellulose aerogels showed strong affinity with both oils, with absorption capacities of 18 and 17.6 g/g respectively.

b. Absorption capacities of the cellulose aerogels at different temperatures

The effect of temperature on the crude-oil absorption capacity of the MTMS-coated recycled cellulose aerogel was examined with RB. The tests

were conducted at 10, 25, 40, and 60 ℃. The results are summarized in Figure 4.5 below, and displayed with the viscosities.

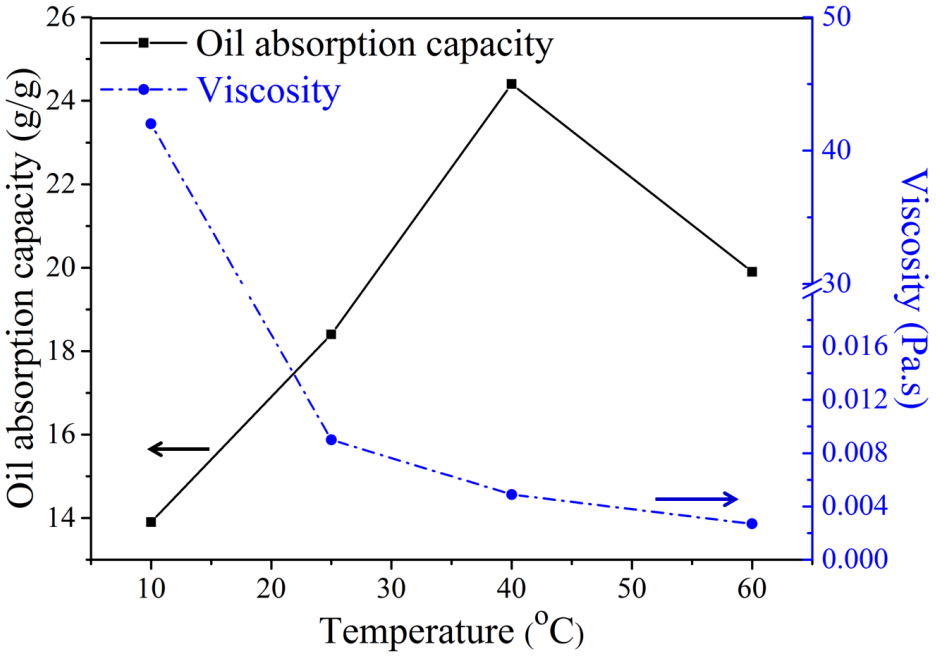

Figure 4.5 Effect of temperature on crude-oil absorption capability of the MTMS-coated recycled cellulose aerogel, and on the viscosity of RB.

As shown in Figure 4.5, the oil absorption capacity increased from 13.9 to 18.4 g/g when the temperature was increased from 10 to 25 ℃. The highest absorption capacity was 24.4 g/g, achieved at 40 ℃; the absorption capacity decreased to 19.9 g/g when the temperature was increased to 60 ℃. This can be explained by the change of oil viscosity with temperature, as displayed in Figure 4.5 and Table 4.4. At 10 ℃, the oil formed a gel with a high viscosity value of 42 Pa.s. This high viscosity impeded the diffusion of the oil into the pores of the absorbent, and led to a low absorption capacity. When the testing temperature was increased from 10 to 25, to 40, and to 60 ℃, a reduction in the crude-oil viscosity from 42 to 0.0090, to 0.0049, and to 0.0027 Pa.s, respectively, was observed. The reduced viscosities made the oil diffuse into the porous matrix of the aerogel much faster and more easily [17, 31,

[49, 54]. However, the large decrease in the oil viscosity at 60 ℃ resulted in low adherence of the oil to the pore walls, and as a consequence, more oil was drained out during the drainage step [17, 31, 49, 54]. The maximum oil absorption capacity was achieved at 40 ℃, at which the optimal oil-viscosity value facilitated the penetration of the crude oil into the pores, and the retention of oil in the structure of the aerogel.

c. Reusability of the cellulose aerogels

The effect of cycles of sorption on the oil absorption capacity of the aerogel was explored. Figures 4.6(a) and (b) below show images of the aerogel sample before and after the first oil absorption test cycle. It can be observed that the size of the sample was nearly unchanged after the oil was absorbed. This is confirmed by the aerogel sample having a volume ratio of 1.05 before and after the first oil absorption test cycle. To remove the absorbed oil, a simple squeezing was performed, as shown in Figure 4.6(c), and the absorbed oil was removed by finger pressure. Figures 4.6(d) and (e) show the sample after squeezing and the good flexibility of the sample, respectively. The squeezed sample was then used for the next absorption test cycle. The oil absorption capacities of the sample after five sorption cycles are displayed in Figure 4.7(a) below. The sample achieved a high absorption capacity of 18.4 g/g in cycle 1. However, the capacity dropped to 0.96, 0.68, 0.59, and 0.63 g/g in cycles 2, 3, 4, and 5, respectively. This phenomenon can be explained by the change in the sample volume, as calculated by Equation 3.7; the change in the sample volume is also displayed in Figure 4.7(a).

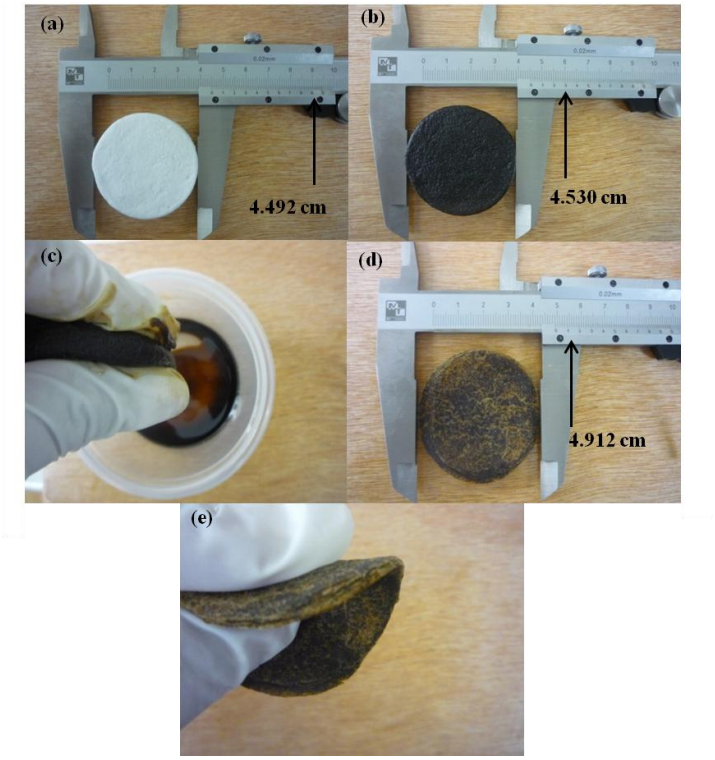

Figure 4.6 (a) Aerogel sample before first absorption cycle. (b) Aerogel sample after first absorption cycle. (c) Squeezing out the oil from the cellulose aerogel. (d) Aerogel sample after squeezing. (e) Flexibility of the sample after squeezing.

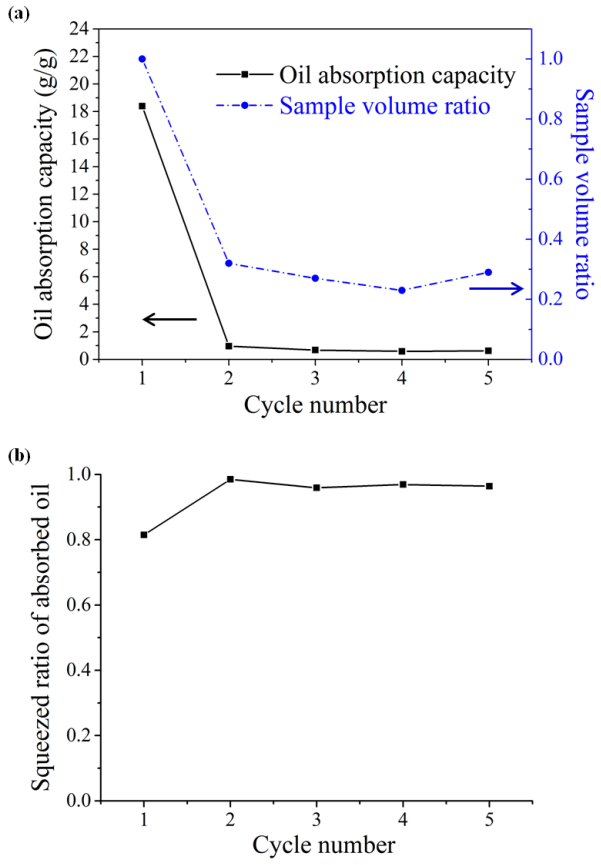

Figure 4.7 Effect of cycles of sorption on (a) Oil absorption capacity and sample volume of the aerogel (b) Squeezed ratio of absorbed oil.

After cycle 1, the sample was squeezed to remove the absorbed oil, and the squeezed sample was used for cycle 2. After this squeezing, the ratio of the volume of the squeezed sample to its original volume was 0.32, indicating that the porous structure of the sample had largely collapsed. As a result, the oil absorption capacity of the aerogel sharply decreased to 0.96 g/g in cycle 2. In later cycles, the volume ratio values (0.27, 0.23 and 0.29) were similar to the value after the first cycle, suggesting that the sample structure did not change anymore. Regarding the squeezed ratio of the absorbed oil, as calculated by Equation 3.8, 81.5, 98.5, 95.9, 96.9, and 96.4 % of the absorbed oil was released after cycles 1, 2, 3, 4, and 5, respectively, as presented in Figure 4.7(b) above. The reusability could be improved by enhancing the elasticity of the cellulose aerogels in future.

4.2.2.2 Absorption kinetics of the cellulose aerogels with different oils

Figure 4.8 below demonstrates the crude-oil absorption test of the material with a mixture of RB (crude oil) and DI water (40 mL of water/5 mL of RB). The crude oil formed a coloured layer on the water surface. It was observed that the hydrophobic aerogel floated on the mixture and rapidly absorbed the crude oil. After about 4 min, most of the oil (99.4%) was absorbed by the hydrophobic aerogel. The test indicated that the MTMS-coated aerogel was promising candidate for crude oil spill–cleaning applications. The crude-oil absorption behaviour of the MTMS-coated aerogel was studied, and three different crude oils, RB, TGT, and RD, were used. Figure 4.9 below shows the first 250 minutes of the sorption process.

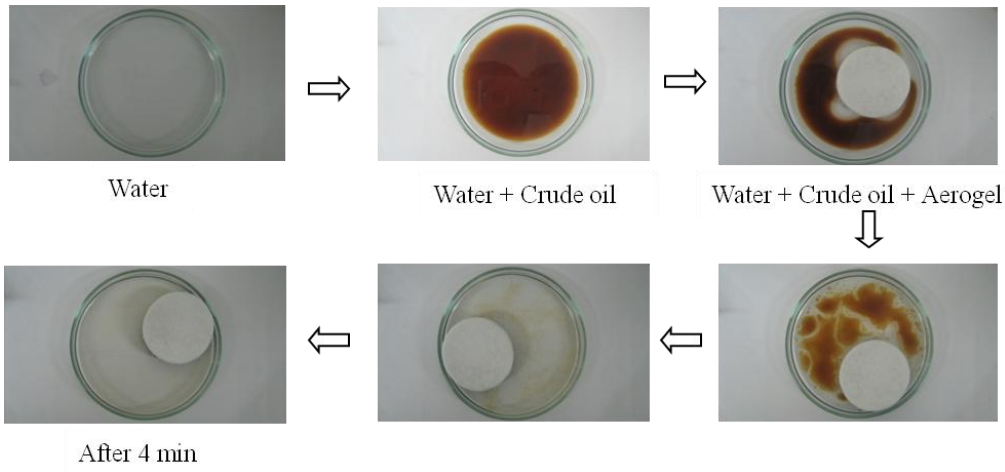

Figure 4.8 Oil absorption process of the recycled cellulose aerogel in the mixture of RB (5 mL) and DI water (40 mL).

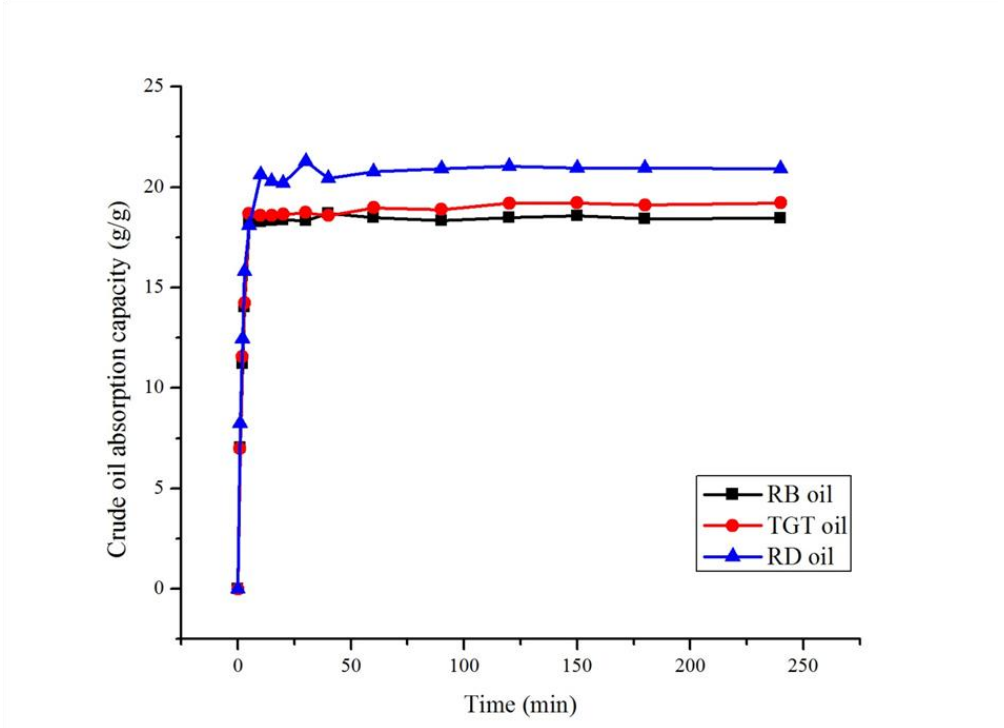

Figure 4.9 The absorption kinetics of crude oils on the coated aerogel.

It can be observed that the material easily absorbed the crude oil and was completely immersed in the oil after about 3 min, indicating the high affinity of the absorbent with crude oil. The sorption kinetics of the three crude oils on the aerogel are also shown in Figure 4.9 above. The absorption rates were very high at the first stage, and saturation was achieved after about 10 min. According to Equation 3.9, the absorption rate constants for the pseudo-first-order model were 0.014, 0.017, and 0.016 for the three different

crude oils, RB, TGT, and RD, respectively. In addition, according to Equation 3.10, the absorption rate constants for the pseudo-second-order model were 0.0005, 0.0004, and 0.0004, respectively. The correlation coefficient R^2 values of the pseudo-second-order model (RD: 0.999, TGT: 0.997, and RB: 0.997) were higher than those of the pseudo-first-order model (RD: 0.934, TGT: 0.871, and RB: 0.888), which suggests that the pseudo-second-order model can better predict the crude-oil absorption behaviour of the cellulose aerogels.

4.2.3 Mechanical properties of the cellulose aerogels

A qualitative test was performed on the sample to investigate its mechanical strength by loading a 200 g weight on the sample for 1 h, 5 h, one day, and five days, as shown in Figure 4.10(a) below. No shape change of the aerogel was observed after the test durations.

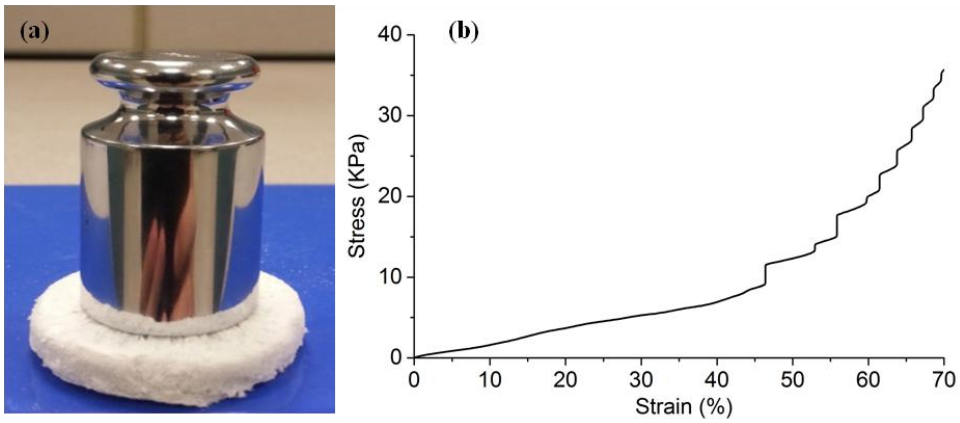

Figure 4.10 Mechanical properties of the aerogel. (a) A 200g load on the aerogel (b) Compressive curve of the aerogel.

For further understanding of the mechanical property of the material, compression tests were performed with an Instron 5500 microtester, as described in Section 3.3.9. As shown in Figure 4.10(b) above, the cellulose

aerogels showed a ductile behaviour. The compression modulus was approximately 22 KPa.

The compression modules of the cellulose aerogels were comparable to those of the scaffolds prepared from poly ether ester multi-block copolymer based on polyethylene oxide and polybutylene terephthalate (13.0–21.4 KPa), silk fibroin (18 KPa), sodium alginate (25 KPa), and poly ε -caprolactone (44.6–90.9 KPa) via freeze drying [55, 56]. The value of the compression modulus of the cellulose aerogel was also similar to those of the poly acrylic acid-clay composite aerogel (43 KPa) [57].

However, the value of the compression modulus was lower than those of the cellulose aerogels prepared from bacterial cellulose (150 KPa) and cellulose nanofibres (35–2800 KPa), since bacterial cellulose and cellulose nanofibres have high mechanical strengths as source materials [58, 59]. On the other hand, recycled cellulose aerogels have the advantages of cost–effectiveness and eco-friendliness, due to having recycled paper–waste cellulose as a source. In addition, recycled cellulose aerogels are rigid enough for conventional handling, and can be used in oil-spill applications.

4.3 Summary

In conclusion, recycled cellulose aerogels were successfully prepared from recycled paper-waste cellulose fibres by freeze drying, using an alkaline–urea aqueous solution. For the first time, paper waste could be successfully converted into green cellulose aerogels. Morphology control of the recycled cellulose aerogels could be achieved by adjusting the cellulose concentration inside the cellulose aqueous suspension. To improve the

hydrophobicity of the hydrophilic cellulose aerogels, a simple chemical vapour deposition method using MTMS was successfully developed, and the coating stability was tested. The crude-oil absorption behaviour of the MTMS-coated aerogel with cellulose concentration of 2.0 wt. % was investigated with the three different crude oils, RB, TGT, and RD, at three different temperatures, 25, 40, and 60 ℃. The aerogel showed a maximum absorption capacity of 24.4 g/g, with RB crude oil at 40 ℃, due to the optimal viscosity of the oil at this temperature.

The absorption kinetics of the material with the three different crude oils have been briefly described. It was observed that the material could easily absorb crude oil and was completely immersed in the oil after approximately 3 min, indicating a high affinity between crude oil and the coated aerogels. In addition, the compressive modulus of the sample with cellulose concentration of 2.0 wt. % was tested and calculated to be approximately 22 KPa. The oil absorption properties indicated that the material is a promising candidate for oil spill–cleaning applications.

References

[1] O. A. Centeno-Chale, M. L. Aguirre-Macedo, G. Gold-Bouchot, V. M. Vidal-Martinez, Effects of oil spill related chemical pollution on helminth parasites in Mexican flounder Cyclopsetta chittendeni from the Campeche Sound, Gulf of Mexico, *Ecotox. Environ. Safe.*, 2015, **119**, 162-169.

[2] D. Li, F. Z. Zhu, J. Y. Li, P. Na, N. Wang, Preparation and Characterization of Cellulose Fibers from Corn Straw as Natural Oil Sorbents, *Ind. Eng. Chem. Res.*, 2012, 121224103114008.

[3] H. Li, L. Liu, F. Yang, Hydrophobic modification of polyurethane foam for oil spill cleanup, *Mar. Pollut. Bull.*, 2012, **64**, 1648-1653.

[4] V. Singh, R. J. Kendall, K. Hake, S. Ramkumar, Crude Oil Sorption by Raw Cotton, *Ind. Eng. Chem. Res.*, 2013, **52**, 6277-6281.

[5] J. Wang, Y. Zheng, Y. Kang, A. Wang, Investigation of oil sorption capability of PBMA/SiO2 coated kapok fiber, *Chem. Eng. J.*, 2013, **223**, 632-637.

[6] N. Xiao, Y. Zhou, Z. Ling, J. Qiu, Synthesis of a carbon nanofiber/carbon foam composite from coal liquefaction residue for the separation of oil and water, *Carbon*, 2013, **59**, 530-536.

[7] K. Zhu, Y.-Y. Shang, P.-Z. Sun, Z. Li, X.-M. Li, J.-Q. Wei, K.-L. Wang, D.-H. Wu, A.-Y. Cao, H.-W. Zhu, Oil spill cleanup from sea water by carbon nanotube sponges, *Front. Mater. Sci.*, 2013, **7**, 170-176.

[8] Q. Zhu, Y. Chu, Z. Wang, N. Chen, L. Lin, F. Liu, Q. Pan, Robust superhydrophobic polyurethane sponge as a highly reusable oil-absorption material, *J. Mater. Chem. A*, 2013, **1**, 5386.

[9] D. Cormack, B. W. J. Lynch, B. D. Dowsett, Evaluation of dispersant effectiveness, *Oil Chem. Pollut.*, 1986, **3**, 87-103.

[10] M. F. Fingas, R. Stoodley, N. Laroche, Effective testing of spill - treating agents, *Oil Chem. Pollut.*, 1990, **7**, 337-348.

[11] A. Bayat, S. F. Aghamiri, A. Moheb, G. R. Vakili-Nezhaad, Oil spill cleanup from sea water by sorbent materials, *Chem. Eng. Technol.*, 2005, **28**, 1525-1528.

[12] R. M. Atlas, Petroleum biodegradation and oil spill bioremediation, *Mar. Pollut. Bull.*, 1995, **31**, 178-182.

[13] D. Dave, A. E. Ghaly, Remediation technologies for marine oil spills: a critical review and comparative analysis, *Am. J. Environ. Sci.*, 2011, **7**, 423-440.

[14] A. A. Al-Majed, A. R. Adebayo, M. E. Hossain, A sustainable approach to controlling oil spills, *J. Environ. Manage.*, 2012, **113**, 213-227.

[15] Y. Chu, Q. Pan, Three-dimensionally macroporous Fe/C nanocomposites as highly selective oil-absorption materials, *ACS Appl. Mater. Inter.*, 2012, **4**, 2420-2425.

[16] C. Cojocaru, M. Macoveanu, I. Cretescu, Peat-based sorbents for the removal of oil spills from water surface: Application of artificial neural network modeling, *Colloid. Surface. A*, 2011, **384**, 675-684.

[17] X. Gui, H. Li, K. Wang, J. Wei, Y. Jia, Z. Li, L. Fan, A. Cao, H. Zhu, D. Wu, Recyclable carbon nanotube sponges for oil absorption, *Acta Mater.*, 2011, **59**, 4798-4804.

[18] X. Gui, Z. Zeng, Z. Lin, Q. Gan, R. Xiang, Y. Zhu, A. Cao, Z. Tang, Magnetic and highly recyclable macroporous carbon nanotubes for spilled oil sorption and separation, *ACS Appl. Mater. Inter.*, 2013, **5**, 5845-5850.

[19] M. O. Adebajo, R. L. Frost, J. T. Kloprogge, O. Carmody, S. Kokot, Porous Materials for Oil Spill Cleanup: A Review of Synthesis and Absorbing Properties, *J. Porous Mat.*, 2003, **10**, 159-170.

[20] D. Peng, Z. Lan, C. Guo, C. Yang, Z. Dang, Application of cellulase for the modification of corn stalk: leading to oil sorption, *Bioresource Technol.*, 2013, **137**, 414-418.

[21] D. Bastani, A. A. Safekordi, A. Alihosseini, V. Taghikhani, Study of oil sorption by expanded perlite at 298.15K, *Sep. Purif. Technol.*, 2006, **52**, 295-300.

[22] O. K. Karakasi, A. Moutsatsou, Surface modification of high calcium fly ash for its application in oil spill clean up, *Fuel*, 2010, **89**, 3966-3970.

[23] V. Rajakovic, G. Aleksic, M. Radetic, L. Rajakovic, Efficiency of oil removal from real wastewater with different sorbent materials, *J. Hazard. Mater.*, 2007, **143**, 494-499.

[24] G. Deschamps, H. Caruel, M. E. Borredon, C. Bonnin, C. Vignoles, Oil Removal from Water by Selective Sorption on Hydrophobic Cotton Fibers. 1. Study of Sorption Properties and Comparison with Other Cotton Fiber-Based Sorbents, *Environ. Sci. Technol.*, 2003, **37**, 1013-1015.

[25] R. Wahi, L. A. Chuah, T. S. Y. Choong, Z. Ngaini, M. M. Nourouzi, Oil removal from aqueous state by natural fibrous sorbent: An overview, *Sep. Purif. Technol.*, 2013, **113**, 51-63.

[26] X. Yuan, T. C. M. Chung, Novel Solution to Oil Spill Recovery: Using Thermodegradable Polyolefin Oil Superabsorbent Polymer (Oil–SAP), *Energ. Fuel.*, 2012, **26**, 4896-4902.

[27] N. T. Cervin, C. Aulin, P. T. Larsson, L. Wågberg, Ultra porous nanocellulose aerogels as separation medium for mixtures of oil/water liquids, *Cellulose*, 2011, **19**, 401-410.

[28] J. T. Korhonen, M. Kettunen, R. H. Ras, O. Ikkala, Hydrophobic nanocellulose aerogels as floating, sustainable, reusable, and recyclable oil absorbents, *ACS Appl. Mater. Inter.*, 2011, **3**, 1813-1816.

[29] K. C. Payne, C. D. Jackson, C. E. Aizpurua, O. J. Rojas, M. A. Hubbe, Oil spills abatement: factors affecting oil uptake by cellulosic fibers, *Environ. Sci. Technol.*, 2012, **46**, 7725-7730.

[30] J. Wang, Y. Zheng, A. Wang, Effect of kapok fiber treated with various solvents on oil absorbency, *Ind. Crop. Prod.*, 2012, **40**, 178-184.

[31] J. Wang, Y. Zheng, A. Wang, Coated kapok fiber for removal of spilled oil, *Mar. Pollut. Bull.*, 2013, **69**, 91-96.

[32] J. Cai, S. Kimura, M. Wada, S. Kuga, L. Zhang, Cellulose aerogels from aqueous alkali hydroxide-urea solution, *ChemSusChem*, 2008, **1**, 149-154.

[33] W. Chen, H. Yu, Q. Li, Y. Liu, J. Li, Ultralight and highly flexible aerogels with long cellulose I nanofibers, *Soft Matter*, 2011, **7**, 10360.

[34] F. Liebner, E. Haimer, M. Wendland, M. A. Neouze, K. Schlufter, P. Miethe, T. Heinze, A. Potthast, T. Rosenau, Aerogels from unaltered bacterial cellulose: application of scCO2 drying for the preparation of shaped, ultra-lightweight cellulosic aerogels, *Macromol. Biosci.*, 2010, **10**, 349-352.

[35] Z. Wang, S. Liu, Y. Matsumoto, S. Kuga, Cellulose gel and aerogel from LiCl/DMSO solution, *Cellulose*, 2012, **19**, 393-399.

[36] C. Chang, L. Zhang, Cellulose-based hydrogels: Present status and application prospects, *Carbohyd. Polym.*, 2011, **84**, 40-53.

[37] N. Isobe, S. Kimura, M. Wada, S. Kuga, Mechanism of cellulose gelation from aqueous alkali-urea solution, *Carbohyd. Polym.*, 2012, **89**, 1298-1300.

[38] H. Jin, M. Pääkkö, J. Netral, L. A. Berglund, C. Neagu, P. E. Bourban, M. Ankerfors, T. Lindström, O. Ikkala, Effects of different drying methods on textural properties of nanocellulose aerogels, 17th International conference on composite materials, Edinburgh, Scotland, 2009.

[39] H. Jin, Y. Nishiyama, M. Wada, S. Kuga, Nanofibrillar cellulose aerogels, *Colloid. Surface. A*, 2004, **240**, 63-67.

[40] D. Klemm, F. Kramer, S. Moritz, T. Lindstrom, M. Ankerfors, D. Gray, A. Dorris, Nanocelluloses: a new family of nature-based materials, *Angew. Chem. Int. Edit.*, 2011, **50**, 5438-5466.

[41] I. M. Low, J. Somers, H. S. Kho, I. J. Davies, B. A. Latella, Fabrication and Properties of Recycled Cellulose Fibre-Reinforced Epoxy Composites, *Compos. Interface.*, 2009, **16**, 659-669.

[42] M. S. Huda, L. T. Drzal, M. Misra, A. K. Mohanty, K. Williams, D. F. Mielewski, A study on biocomposites from recycled newspaper fiber and poly(lactic acid), *Ind. Eng. Chem. Res.*, 2005, **44**, 5593-5601.

[43] R. Bhardwaj, A. K. Mohanty, L. T. Drzal, F. Pourboghrat, M. Misra, Renewable resource-based green composites from recycled cellulose fiber and

poly(3-hydroxybutyrate-co-3-hydroxyvalerate) bioplastic, *Biomacromolecules*, 2006, **7**, 2044-2051.

[44] R.-B. Adusumali, M. Reifferscheid, H. Weber, T. Roeder, H. Sixta, W. Gindl, Mechanical Properties of Regenerated Cellulose Fibres for Composites, *Macromol. Symp.*, 2006, **244**, 119-125.

[45] M. Pääkkö, J. Vapaavuori, R. Silvennoinen, H. Kosonen, M. Ankerfors, T. Lindström, L. A. Berglund, O. Ikkala, Long and entangled native cellulose I nanofibers allow flexible aerogels and hierarchically porous templates for functionalities, *Soft Matter*, 2008, **4**, 2492.

[46] H. Jin, M. Kettunen, A. Laiho, H. Pynnonen, J. Paltakari, A. Marmur, O. Ikkala, R. H. Ras, Superhydrophobic and superoleophobic nanocellulose aerogel membranes as bioinspired cargo carriers on water and oil, *Langmuir : the ACS journal of surfaces and colloids*, 2011, **27**, 1930-1934.

[47] C.Teas, S. Kalligeros, F. Zanikos, S. Stournas, E. Lois, G. Anastopoulos, Investigation of the effectiveness of absorbent materials in oil spills clean up, *Desalination*, 2001, **140**, 259-264.

[48] H. M. Choi, H. J. Kwon, Cotton nonwovens as oil spill cleanup sorbents, *Text. Res. J.* , 1993, **63**, 211-218.

[49] H. M. Choi, R. M. Cloud, Natural sorbents in oil spill cleanup *Environ. Sci. Technol.*, 1992, **26**, 772-776.

[50] J. Lin, Y. Shang, B. Ding, J. Yang, J. Yu, S. S. Al-Deyab, Nanoporous polystyrene fibers for oil spill cleanup, *Mar. Pollut. Bull.*, 2012, **64**, 347-352.

[51] H. Moriwaki, S. Kitajima, M. Kurashima, A. Hagiwara, K. Haraguchi, K. Shirai, R. Kanekatsu, K. Kiguchi, Utilization of silkworm cocoon waste as

a sorbent for the removal of oil from water, *J. Hazard. Mater.*, 2009, **165**, 266-270.

[52] Q. F. Wei, R. R. Mather, A. F. Fotheringham, R. D. Yang, Evaluation of nonwoven polypropylene oil sorbents in marine oil-spill recovery, *Mar. Pollut. Bull.*, 2003, **46**, 780-783.

[53] J. Wu, N. Wang, L. Wang, H. Dong, Y. Zhao, L. Jiang, Electrospun porous structure fibrous film with high oil adsorption capacity, *ACS Appl. Mater. Inter.*, 2012, **4**, 3207-3212.

[54] D. M. J. M. M. Radetić, P. M. Jovancić, Z. L. Petrović, H. F. Thomas, Recycled Wool-Based Nonwoven Material as an Oil Sorbent, *Environ. Sci. Technol.*, 2003, **37**, 1008-1012.

[55] Q. Hou, D. W. Grijpma, J. Feijen, Preparation of interconnected highly porous polymeric structures by a replication and freeze-drying process, *J. Biomed. Mater. Res. B*, 2003, **67**, 732-740.

[56] J. Ming, B. Zuo, A novel silk fibroin/sodium alginate hybrid scaffolds, *Polym. Eng. Sci.*, 2014, **54**, 129-136.

[57] M. D. Gawryla, L. Liu, J. C. Grunlan, D. A. Schiraldi, pH Tailoring Electrical and Mechanical Behavior of Polymer-Clay-Nanotube Aerogels, *Macromol. Rapid Comm.*, 2009, **30**, 1669-1673.

[58] R. T. Olsson, M. A. S. Azizi Samir, G. Salazar-Alvarez, L. Belova, V. Strom, L. A. Berglund, O. Ikkala, J. Nogues, U. W. Gedde, Making flexible magnetic aerogels and stiff magnetic nanopaper using cellulose nanofibrils as templates, *Nat. Nanotechnol.*, 2010, **5**, 584-588.

[59] H. Sehaqui, Q. Zhou, L. A. Berglund, High-porosity aerogels of high specific surface area prepared from nanofibrillated cellulose (NFC), *Compos. Sci. Technol.*, 2011, **71**, 1593-1599.

CHAPTER 5: Recycled Cellulose Aerogels Using Kymene Binder for Oil Spill–Cleaning Applications

5.1 Introduction

This chapter describes the successful development of an advanced and cost-effective method for fabrication of recycled cellulose aerogels. This novel method synthesizes the recycled cellulose aerogels from paper waste by using Kymene as a cross-linker, instead of using sodium hydroxide and urea [1–3]. The synthesis procedures are discussed in Section 3.2.2. This method can significantly reduce the toxicity of raw materials, and reduce the entire synthesis duration from the nine days of previous methods to three days [4, 5]. After being freeze dried and coated with methyltrimethoxysilane (MTMS) via chemical vapour deposition, the recycled cellulose aerogels exhibited ultra-flexibility, high porosity, super-hydrophobicity, and outstanding oil absorption capability.

5.2 Results and discussion

5.2.1 Morphology and hydrophobicity of the recycled cellulose aerogels

In this section, the morphologies and hydrophobic properties of the recycled cellulose aerogels are discussed. The recycled cellulose aerogels exhibited macropore structures. Moreover, the aerogel with the higher cellulose concentration (1.0 wt. %) had a more compacted network and lower porosity. The aerogel with high stability was also observed to have super-hydrophobicity.

5.2.1.1 Effects of the cellulose concentrations

The photographs and SEM images of the developed recycled cellulose aerogels are shown in Figure 5.1 below. The aerogel sample in Figure 5.1a had dimensions of 45 mm (diameter) × 11 mm (thickness), and the same shape as that of its reaction container. As reported previously, the recycled cellulose aerogels were formed via hydrogen bonding between the self-assembled cellulose fibres [2, 4].

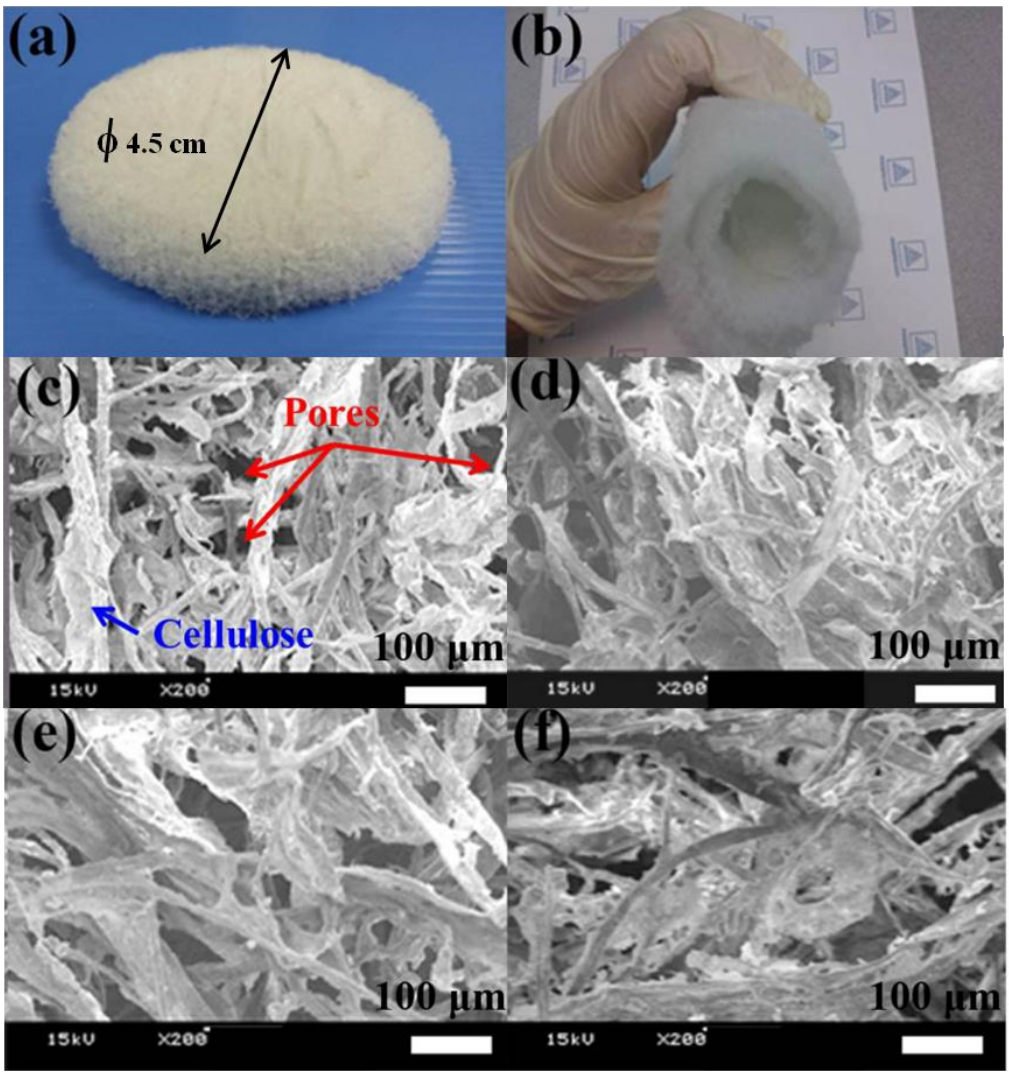

Figure 5.1 (a) Super-hydrophobic recycled cellulose aerogel, (b) Flexibility of the large-scale cellulose aerogel (38 cm × 38 cm × 1 cm) containing 0.60 wt. % of cellulose fibres, SEM images of the cellulose aerogels with different ratios of cellulose fibres (wt. %) and Kymene (µl): (c) 0.25:5, (d) 1.00:5, (e) 0.60:5, and (f) 0.60:20.

In addition, for this work, Kymene strengthened the cellulose aerogels by providing a protection mechanism and reinforcement mechanism [6]. For the protection mechanism, some Kymene molecules reacted with other Kymene molecules, and the formed Kymene networks wrapped the cross-linking points between the cellulose fibres to improve the strength of the cellulose network [6]. Moreover, Kymene molecules also bonded with the cellulose fibres to enhance the strength of the cellulose network, providing the reinforcement mechanism [6]. The utilization of Kymene as a cross-linker ensured that the resultant aerogels had a robust structure [6, 7].

In contrast to the mesopores (2–70 nm) of the aerogels formed by the cellulose nanofibers, the cellulose aerogels with macropores (>50 nm) had highly porous structure, which can be clearly observed in the SEM images of Figures 5.1c–f [8-10]. Their macropores were possibly caused by the larger size of the recycled cellulose fibres, obtained from the paper waste [4]. Figures 5.1c and d show the morphologies of the cellulose aerogels with cellulose concentrations of 0.25 and 1.00 wt. %, respectively. The aerogel with the higher cellulose concentration (1.0 wt. %) had a more compacted network and lower porosity. However, an increase in the amount of Kymene from 5 to 20 µl in a 30 ml reaction mixture did not significantly impact the aerogel structures, as shown in Figures 5.1e and f, as the amount of Kymene was small compared to that of the cellulose fibres and the possible minor structure changes might not have been observed.

5.2.1.2 Hydrophobicity of the cellulose aerogels

In order to investigate the super-hydrophobicity of the developed

cellulose aerogels, the water contact angles were measured on both the external surface and cross-section of the MTMS-coated cellulose aerogels. As shown in Figures 5.2a and b, large contact angles of 153.5^{o} and 150.8^{o}, respectively, were obtained, thus proving that the hydrophobic coating successfully covered the whole aerogel network. The water contact angle values of the external surface were slightly higher than those of the cross section, possibly due to the greater accessibility of the external surface.

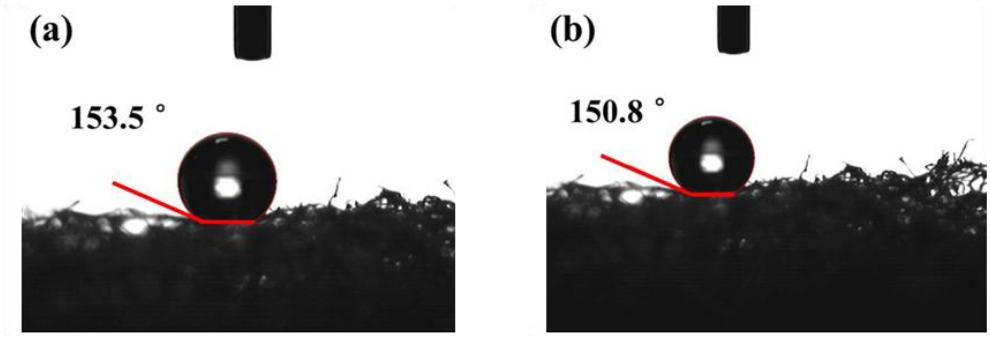

Figure 5.2 Water contact angles on (a) the external surface and (b) the cross-section of the super-hydrophobic recycled cellulose aerogel.

To examine the hydrophobic stability of the cellulose aerogels, they were then exposed to the normal ambient atmosphere for five months. Their water contact angles of 145–155^{o} over this period were examined, as shown in Figures 5.3a and b below. The effects of the reagent ratios on the super-hydrophobic properties of the aerogels with different compositions are presented in Figure 5.3a. Interestingly, all the cellulose aerogels exhibited similar water contact angles of approximately 150^{o}, regardless of their cellulose concentrations or Kymene amounts. It is well known that the water contact angles strongly depend on the functional groups on the aerogel surfaces. Therefore, in this case, such a small variation in the water contact angles may likely have been a consequence of the identical functional groups (-Si-O-CH_3-) induced by the MTMS coating [4]. Furthermore, the water

contact angles of the cellulose aerogels on the external surface and the cross-section did not show any obvious change with time, as shown in Figure 5.3b. These results further confirm the uniformity of the MTMS coating and the excellent stability of the hydrophobicity of the MTMS-coated recycled cellulose aerogels examined for this work. The hydrophobic properties of the aerogels discussed in this section are similar to those of the aerogels described in Chapter 4, demonstrating the excellent performance of the MTMS coating on different types of cellulose aerogels.

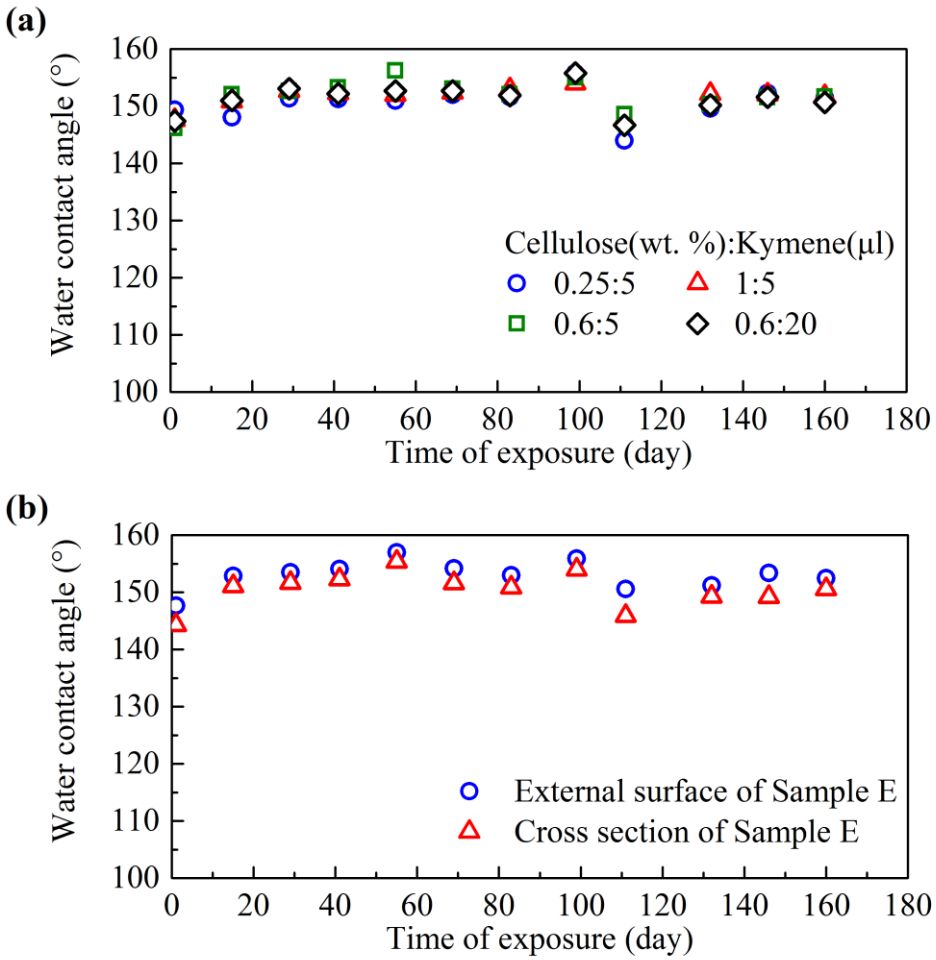

Figure 5.3 Effects of exposure time on the water contact angles: (a) of the cellulose aerogels with different ratios of cellulose fibres and Kymene, and (b) on the external surface and cross-section of the same aerogel sample, sample E (0.6 wt. % cellulose fibres and 5 µL Kymene inside the cellulose aqueous suspension).

5.2.2 Oil absorption properties of the cellulose aerogels

The oil absorption properties of the recycled cellulose aerogels are discussed in this section. Several factors, such as the type of oil, the initial cellulose fibre concentration, the temperature, and the seawater effect with different pH values, were investigated with regard to their effects on the oil absorption capacity of the cellulose aerogels. The absorption kinetics and the activation energy values of cellulose aerogels are also investigated in detail in this section.

5.2.2.1 Absorption capacities with different oils

A 5w40 motor oil was used to investigate the oil absorption capabilities of the recycled cellulose aerogels listed in Table 5.1 below. This chapter focuses on motor oils instead of crude oils, as it aims to show the excellent absorption properties of cellulose aerogels with oil products containing additives.

Table 5.1 Chemical compositions of the various recycled cellulose aerogels.

Sample label	Cellulose fibres (wt. %)	Kymene (μl)	Porosity (%)
Sample A	0.25	5	99.4±0.0
Sample B	0.50	5	98.9±0.0
Sample C	0.75	5	98.1±0.0
Sample D	1.00	5	97.2±0.1
Sample E	0.60	5	98.4±0.0
Sample F	0.60	20	98.4±0.0
Sample G	1.00	10	97.4±0.0
Sample H	2.00	20	96.9±0.0
Sample I	4.00	40	96.1±0.3

When the Kymene amount was kept at 5 μl and the cellulose concentration was increased from 0.25 to 0.50 to 0.75 to 1.00 wt. %, the measured absorption capacities of the aerogels (Samples A, B, C, and D in Table 5.1) were 95, 73, 58, and 49 g/g, respectively, at 25 ^{o}C. The maximum

absorption capacity of 95 g/g was achieved with the 0.25 wt. % cellulose aerogel, because it had the lowest density (9×10^{-3} g/cm^3) and a highest porosity (99.4%).

The absorption capacities of all the MTMS-coated cellulose aerogels were one order greater than those of the natural sorbents, two to ten times greater than those of the commercial polypropylene sorbents, and five times greater than those of the recycled cellulose aerogels (approximately 20 g/g) reported in previous works using that used the sodium hydroxide/urea method [4, 5, 11–13]. The significant enhancement of the absorption capacity may be largely ascribed to the reduced densities and increased porosities of the cellulose aerogels.

The cellulose aerogels fabricated with Kymene binder can achieve a high porosity (up to 99.4 %), while the cellulose aerogels using sodium hydroxide and urea can achieve only 98.0 % porosity. When further decreased the cellulose amounts in the syntheses mixture using sodium hydroxide and urea, rigid aerogels could not be successfully formed.

Temperature is also a major factor affecting the viscosity and the diffusion capability of the oils into the porous aerogel structures. Therefore, the absorption behaviour of the different oils with each aerogel was examined at three different temperatures of 25, 50, and 70 ^{o}C. As shown in Table 5.2 and Figure 5.4 below, the maximum oil absorption capacity increased when the temperature was increased from 25 to 50 ^{o}C, but then decreased when the temperature was further increased from 50 to 70 ^{o}C. This trend holds for the absorption behaviour of all the oils with the 0.50, 0.75, and 1.00 wt. % cellulose aerogels.

Table 5.2 Summary of the maximum oil absorption capacities and the absorption rate constants of the cellulose aerogels at different temperatures, with various cellulose fibre concentrations, using the pseudo-first-order and pseudo-second-order models.

	Cellulose concentration (wt. %)		0.50			0.75			1.00		
	Temperature (^oC)		25	50	70	25	50	70	25	50	70
5w50 Motor oil	Maximum absorption capacity, Q_m (g/g)		62.6	64.9	59.2	48.1	53.8	46.3	45.9	46.5	46.2
	Pseudo-first-order	R^2	0.986	0.970	0.972	0.977	0.954	0.966	0.986	0.993	0.944
		K_1	0.293	0.324	0.355	0.254	0.319	0.367	0.218	0.287	0.357
	Pseudo-second-order	R^2	0.996	0.996	0.998	0.995	0.998	0.996	0.996	0.995	0.998
		K_2	0.006	0.008	0.009	0.008	0.010	0.015	0.005	0.007	0.013
Singer Machine oil	Maximum absorption capacity, Q_m (g/g)		59.3	61.0	58.2	46.1	48.8	47.6	40.4	43.1	42.4
	Pseudo-first-order	R^2	0.983	0.978	0.980	0.981	0.956	0.994	0.978	0.970	0.987
		K_1	0.297	0.311	0.351	0.273	0.306	0.343	0.278	0.377	0.425
	Pseudo-second-order	R^2	0.994	0.999	0.999	0.996	0.995	0.999	0.993	0.994	0.996
		K_2	0.008	0.010	0.012	0.008	0.011	0.015	0.007	0.009	0.016

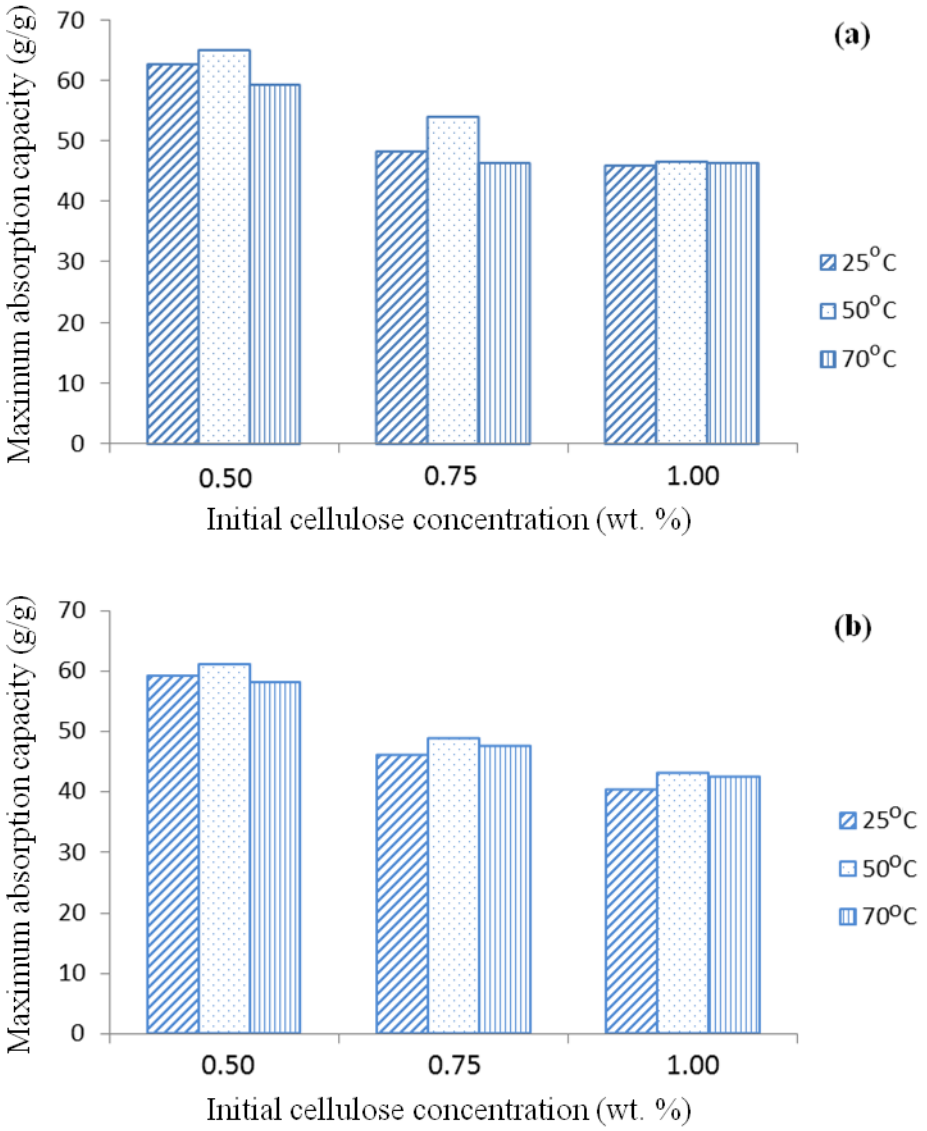

Figure 5.4 Maximum absorption capacities, Q_m, of (a) the 5w50 motor oil and (b) the Singer machine oil with the recycled cellulose aerogels with various cellulose fibre concentrations of 0.50, 0.75, and 1.00 wt. % at 25, 50, and 70 ^{o}C.

The explanation for this may be that the temperature increase reduced the oil viscosities (shown in Table 5.3 below), which in turn facilitated oil penetration into the porous aerogel networks. However, the lower viscosities of the oils also had a negative effect on their ability to anchor to the pore walls, reducing the amounts of oil retained in the porous absorbents during drainage. Comparing the maximum oil absorption capacity with the tested temperatures,

it can be concluded that 50 ^{o}C is the optimum temperature for maximizing the oil absorption performance of the recycled cellulose aerogels.

Table 5.3 The relevant viscosities of the tested oils at different temperatures.

Viscosity (Pa.s)	25^{o}C	50^{o}C	70^{o}C
5w40 motor oil	0.140	n.a.	n.a.
5w50 motor oil	0.160	0.054	0.029
Singer machine oil	0.026	0.009	0.006

Besides the temperature effects, the porosity of cellulose aerogels also significantly affects their oil absorbency. Table 5.2 and Figure 5.4 show that the oil absorption capacity of the aerogels was reduced when the initial cellulose concentration increased from 0.50 to 1.00 wt. %. This can be explained by the porosity of the cellulose aerogels. Table 5.1 shows that the aerogel porosity reduced from 98.9 to 97.2% when the cellulose concentration increased from 0.50 to 1.00 wt. %. As the aerogel porosity was lower, there was less space in the aerogel network for oil occupation, and therefore the oil absorbency was lower.

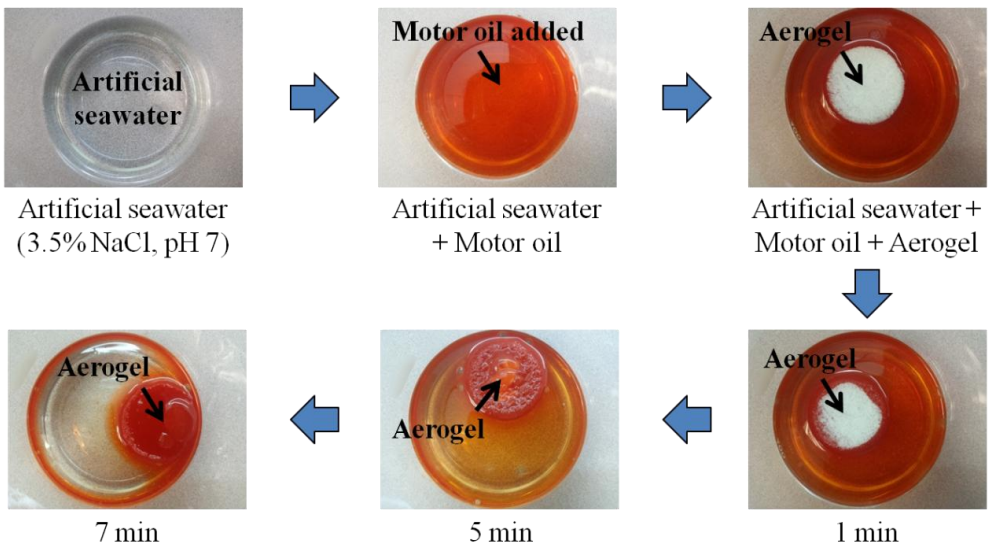

Figure 5.5 Oil absorption process of the recycled cellulose aerogel with 0.5 wt. % of cellulose fibres in artificial seawater (3.5 wt. % NaCl and pH=7) mixed with 5w40 motor oil and dyed with Sudan Red G before testing.

To evaluate the practical oil absorption performance of the recycled cellulose aerogels in the sea, a 3.5% NaCl solution was prepared to imitate the seawater. Figure 5.5 above illustrates the absorption process over several minutes. The cellulose aerogel was loaded on the top of the mixture, and quickly absorbed most of the motor oil within 7 min.

In addition, the effects of pH on the oil absorption capacities of the cellulose aerogels were investigated different pH values prepared from HCl or NaOH. The oil absorption capacities of the 0.50 wt. % cellulose aerogels under pH = 3, 5, 7, and 9 environments were measured to be 63.00, 62.85, 63.06, and 62.98 g/g, respectively. The absorption results indicated pH-insensitive behaviour of the aerogels during the oil absorption tests, possibly because the oil capacities of aerogels are mostly controlled by their porosities and tested oil viscosities, both of which are independent of environmental pH values.

5.2.2.2 Absorption kinetics with different oils

The absorption kinetics of the 5w50 motor oil and Singer machine oil on the recycled cellulose aerogels were investigated, and are summarized in Table 5.2. Although sample A, with a cellulose fibre concentration of 0.25 wt. % (Table 5.1), had the highest oil absorption capacity, it possessed a less rigid structure and was easy to disintegrate after repeated draining and absorbing of oil. Therefore, three different aerogel samples, marked B, C, and D (Table 5.1) and with cellulose fibre concentrations of 0.50, 0.75, and 1.00 wt. % respectively, were prepared for the oil absorption kinetics tests at 25 ^{o}C.

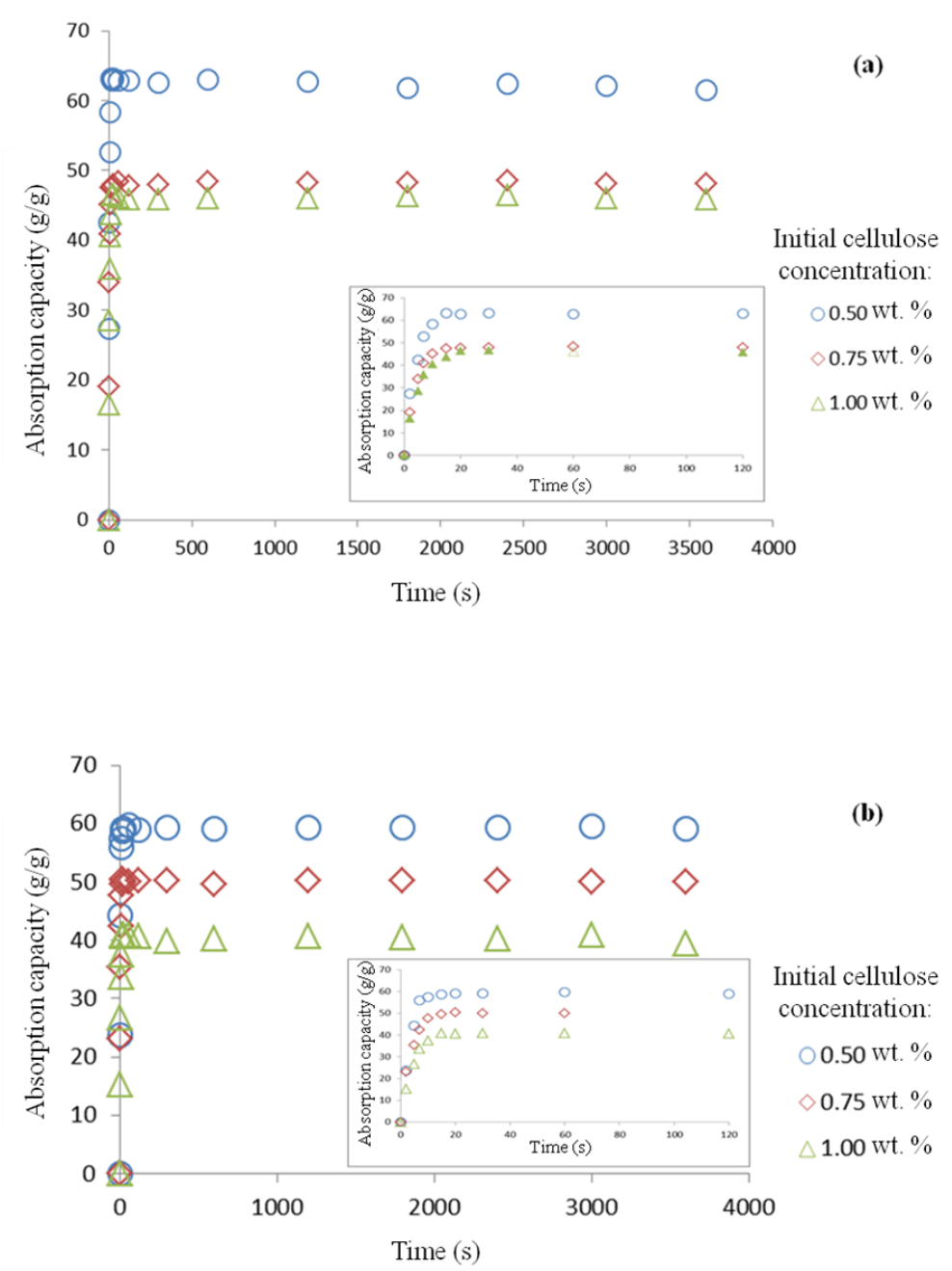

Figure 5.6 Absorption kinetics of (a) the 5w50 motor oil and (b) the Singer machine oil on the recycled cellulose aerogels with various cellulose fibre concentrations of 0.50, 0.75, and 1.00 wt. % at 25°C. The magnified images show the absorption kinetics of the initial 2 min of the absorption processes.

As shown in Figure 5.6 above, the sorption capacity of each oil on the cellulose aerogels was plotted as a function of absorption time. The sorption rate was fast during the first 10 s, and the absorption reached the equilibrium state at 30 s for both the two oils. Figure 5.7 below shows the absorption kinetics of the 5w50 motor oil and Singer machine oil on the 0.50 wt. %

cellulose aerogel at 25 ^{o}C, respectively. The plots of $\ln[Q_m/(Q_m-Q_t)]$ versus time t using the pseudo-first-order model are shown in Figures 5.7a and b, while Figures 5.7c and d display the plots of (t/Q_t) against t using the pseudo-second-order model.

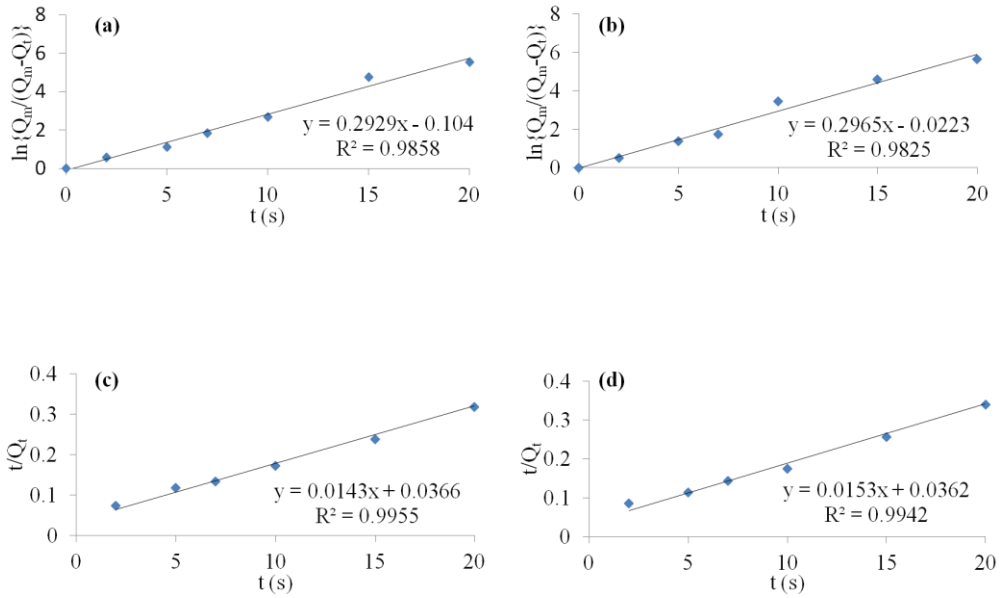

Figure 5.7 Pseudo-first-order absorption linear fitting of (a) the 5w50 motor oil and (b) the Singer machine oil, and pseudo-second-order absorption linear fitting of (c) the 5w50 motor oil and (d) the Singer machine oil on the aerogel with 0.50 wt. % of cellulose fibres at 25^{o}C [14, 15].

From the plots of Figure 5.7, the sorption rate constants k_1 and k_2 and the correlation coefficient R^2 were calculated, and are presented in Table 5.2. It can be observed that the correlation coefficient values of the pseudo-second-order model are higher than those of the pseudo-first-order model for both tested oils. Therefore, for this work, the pseudo-second-order model could better predict the oil absorption behaviour. Most of the absorption rate constants (k_1 and k_2) for the Singer oil were bigger than those for the 5w50 motor oil. In addition, the absorption rate constants at a higher temperature were larger than those of the same oil and sample at a lower temperature. These suggest the oil absorption processes of the Singer oil, and those at the higher temperature occur faster.

Figures 5.8a and b below show the experimental absorption kinetics data and the two fitted model curves for the absorption of the two oils on the 0.50 wt. % cellulose aerogels, which show a good agreement.

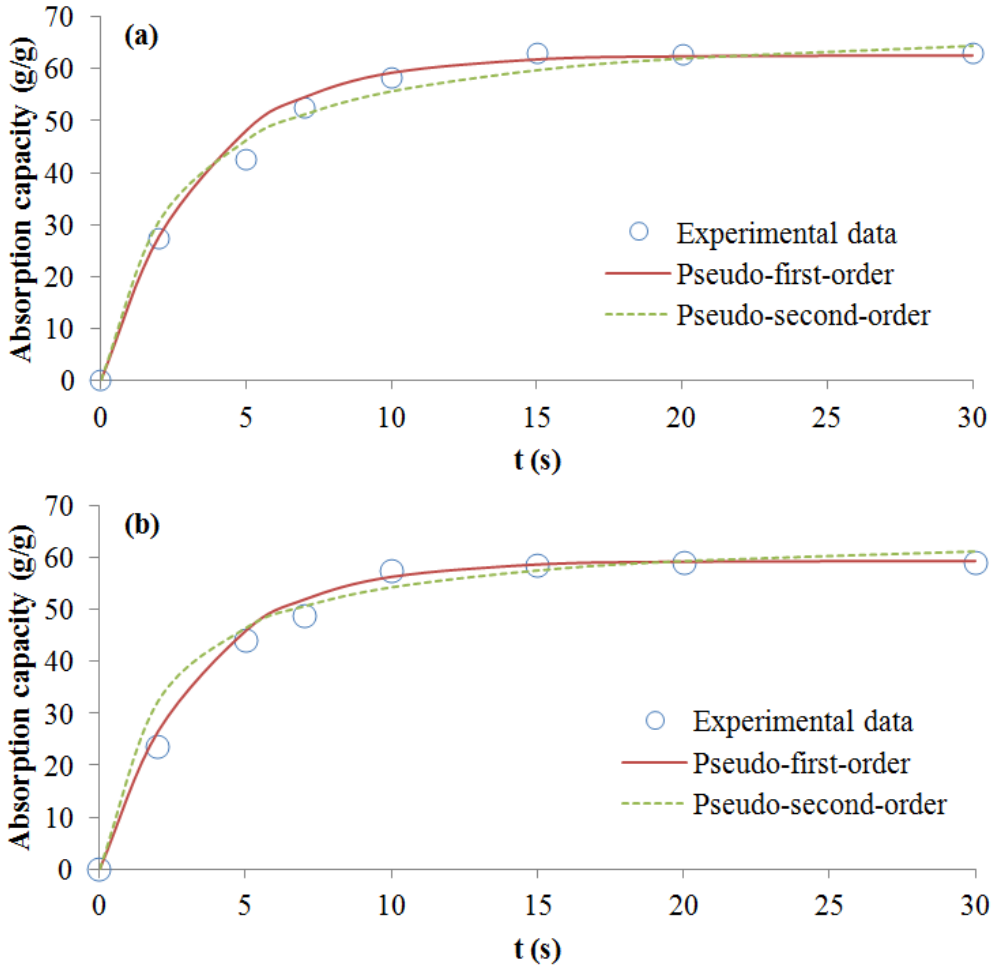

Figure 5.8 Experimental data fitted with the pseudo-first-order and pseudo-second-order models for the absorption kinetics of (a) the 5w50 motor oil and (b) the Singer machine oil on the aerogel with 0.50 wt. % of cellulose fibres at 25°C [14, 15].

The values of k_1 and k_2 in this chapter are generally much larger than those in Chapter 4. This phenomenon indicates that the absorption speed of the cellulose aerogels described in this chapter, with 5w50 motor oil and Singer oil, were much higher than those of the cellulose aerogels described in the previous chapter, with crude oils. This may be explained by the high porosities of the cellulose aerogels described in this chapter.

The activation energy, E_a, is an important parameter in a thermodynamic study [16]. For example, during a successful absorption process, the activation energy must be overcome by an absorbate to interact with functional groups on the sorbent surface. The activation energy, E_a, can be determined from the change in the absorption rate constant, k, with temperature, T (K), using the Arrhenius equation [16, 17]:

$$\ln k = \ln A - \frac{E_a}{RT} \tag{5.3}$$

in which A is the pre-exponential factor and R is the gas constant (8.314 J/mol K). By plotting ln[k] against 1/T, E_a can be calculated from the slope.

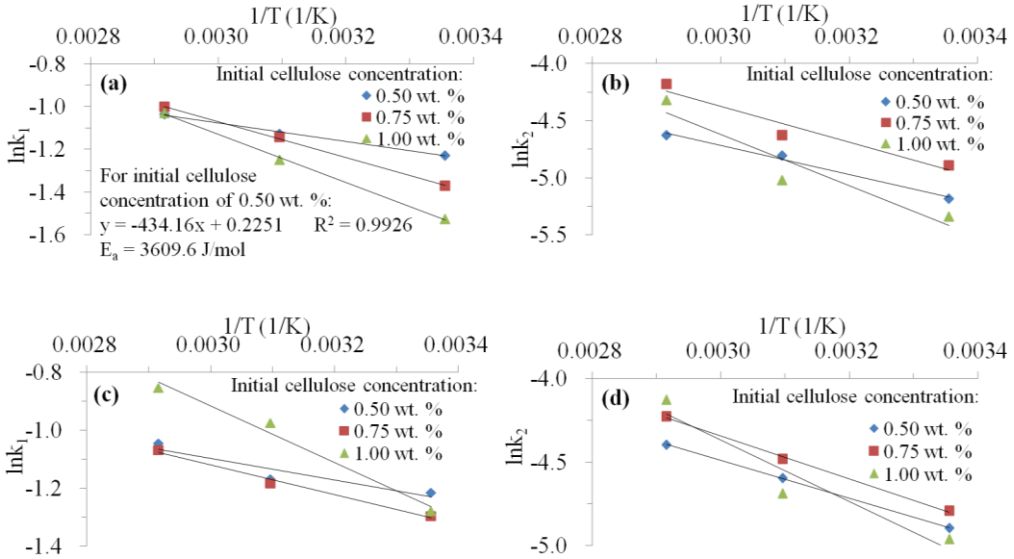

Figure 5.9 Plots of $\ln(k_1)$ and $\ln(k_2)$ against reciprocal temperature for the absorption of (a, b) the 5w50 motor oil and (c, d) the Singer machine oil, respectively, on the cellulose aerogels with various cellulose fibre concentrations of 0.50, 0.75, and 1.00 wt. %.

Plots of $\ln[k_1]$ and $\ln[k_2]$ versus 1/T are presented in Figure 5.9 above, and the activation energy values are presented in Table 5.4 below. It can be observed that the activation energy values of the pseudo-second-order model are higher than those of the pseudo-first-order model. This is because the pseudo-second-order model was used for the absorption process controlled by

chemi-sorption, which involves higher forces than in physic-sorption [18]. In addition, compared with the 5w50 motor oil, the Singer machine oil had the lower activation energy values, which made the oil absorption on the cellulose aerogels more effective.

Table 5.4 Activation energies of the absorption of the cellulose aerogels with various cellulose concentrations on the oils, using the pseudo-first-order and pseudo-second-order models.

Activation energies (J/mol)	Initial cellulose concentration (wt. %)	0.50	0.75	1.00
5w50 motor oil	Pseudo-first-order	3609.6	6984.6	9331.6
	Pseudo-second-order	10682.7	13120.3	18612.6
Singer machine oil	Pseudo-first-order	3090.5	4248.0	8130.2
	Pseudo-second-order	9354.9	10610.3	15240.4

5.2.3 Mechanical properties of the recycled cellulose aerogels

Good flexibility was observed for the recycled cellulose aerogels. As can be observed in Figure 5.1b, the large-scale cellulose aerogel could be easily bent or rolled without damaging its shape. However, when the cellulose concentration increased slightly, its flexibility tended to decrease slightly, as it became more difficult for the cellulose fibres to slide and bend.

The mechanical properties of the recycled cellulose aerogels are discussed in this section. As shown in Figure 5.10a below, the cellulose aerogels with different cellulose fibre concentrations could be compressed to large strains (up to 70%), demonstrating a ductile behaviour. The Young's moduli of the cellulose aerogels with cellulose fibre concentrations of 0.5 and 1 wt. % were 4 and 13 KPa, respectively. To further improve the Young's modulus of the cellulose aerogels, cellulose aerogels with higher cellulose fibre concentrations (up to 4%) were fabricated and tested. The cellulose

aerogels with cellulose fibre concentrations of 2.0 and 4.0 wt. % had Young's modulus values of 21 and 39 KPa, respectively.

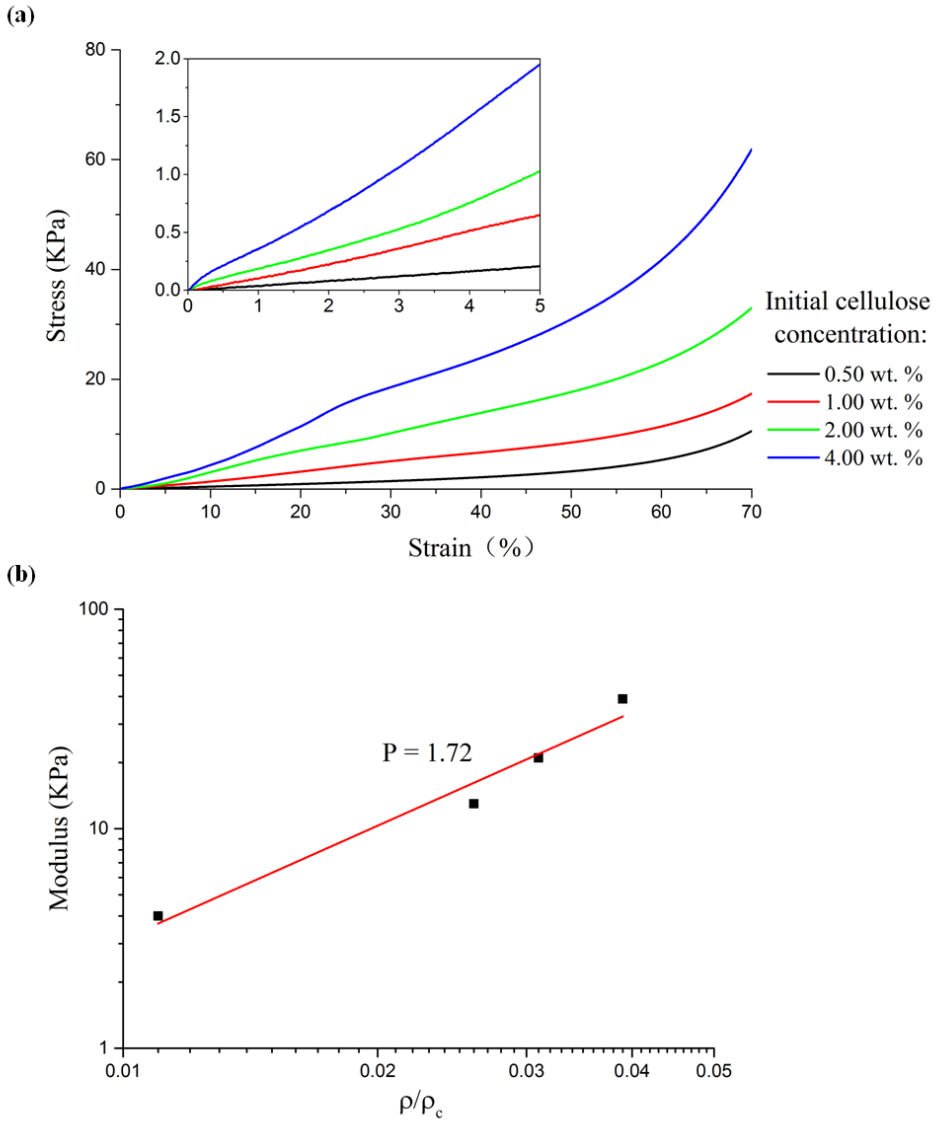

Figure 5.10 (a) The compression stress–strain curves of the cellulose aerogels with different cellulose fibre concentrations. The magnified section shows the compressive curves at the low strain (up to 5%) for the cellulose aerogels with different initial cellulose concentrations. (b) The modulus as a function of the relative density (ρ/ρ_c) of the cellulose aerogels.

The Young's modulus values of the recycled cellulose aerogels were lower than those of the cellulose nanofibre (CNF) aerogels (35–2800 KPa), possibly due to the weak mechanical strength of the recycled cellulose fibres [19–21]. Meanwhile, the Young's modulus value (21 KPa) of the cellulose

aerogels with 2.0 wt. % cellulose fibres fabricated by the Kymene binder method was similar to the value measured by the previous study using a sodium hydroxide–urea aqueous suspension with the same cellulose fibre concentration (22 KPa), this study is described in Section 4.2.3.

A power-law relationship was observed between the Young's modulus and the relative density of all the investigated cellulose aerogels. The relative density is defined as the ratio of the cellulose-aerogel density (ρ) to the density of the cellulose fibres (ρ_c). The proportionality factor was approximately 1.7, that is $E \sim (\rho/\rho_c)^{1.7}$, as shown in Figure 5.10b. The proportionality factor of the cellulose aerogels (1.7) was similar to that of the CNF foam fabricated by Sehaqui *et al.* (1.8) [20]. This phenomenon might be explained by the model proposed by Clyne *et al.* [19]: when the density of the cellulose aerogels increases, the fibre volume fraction (ρ/ρ_c) of the cellulose aerogels is increased, and the ratio of the fibre-joint-to-fibre-joint length to the fibre diameter of the cellulose aerogels is decreased, which contributes to the increase in the Young's modulus.

5.3 Summary

In conclusion, the advanced and cost-effective fabrication method of the recycled cellulose aerogels was further improved. The MTMS-coated cellulose aerogels exhibited stable hydrophobicity during the test period of over five months. Their excellent oil absorption capacities were demonstrated with motor oil and Singer oil. It was found that the initial cellulose fibre concentration significantly affected the oil absorption capability of the developed cellulose aerogels. The 0.25 wt. % cellulose aerogel yielded a

maximum absorption capacity of 95 g/g with the 5w40 motor oil. The maximum absorption capacity of the cellulose aerogels could be reached at 50 ^{o}C, regardless of the pH values of the seawater/oil suspensions, and decreased with an increase in the cellulose fibre concentration.

The pseudo-first-order and pseudo-second-order kinetics models were applied to describe the oil absorption behaviour of the recycled cellulose aerogels for the first time. The pseudo-second-order model was more suited to the oil absorption kinetics study of the aerogels, due to its chemi-sorption nature.

Moreover, the recycled cellulose aerogels displayed excellent flexibility: the large-scale cellulose aerogel could be easily bent or rolled without damaging its shape. All the tested cellulose aerogels could also be compressed to up to 70% strain. The experimental results of this work demonstrate that the super-hydrophobic recycled cellulose aerogels described in this thesis could be very promising sorbents for oil-spill cleaning.

References

[1] S. Hoepfner, L. Ratke, B. Milow, Synthesis and characterisation of nanofibrillar cellulose aerogels, *Cellulose*, 2007, **15**, 121-129.

[2] N. Isobe, S. Kimura, M. Wada, S. Kuga, Mechanism of cellulose gelation from aqueous alkali-urea solution, *Carbohyd. Polym.*, 2012, **89**, 1298-1300.

[3] J. Cai, L. Zhang, Unique Gelation Behavior of Cellulose in NaOH/Urea Aqueous Solution, *Biomacromolecules*, 2006, **7**, 183-189.

[4] S. T. Nguyen, J. Feng, N. T. Le, A. T. T. Le, N. Hoang, V. B. C. Tan, H. M. Duong, Cellulose Aerogel from Paper Waste for Crude Oil Spill Cleaning, *Ind. Eng. Chem. Res.*, 2013, **52**, 18386-18391.

[5] S. T. Nguyen, J. Feng, S. K. Ng, J. P. W. Wong, V. B. C. Tan, H. M. Duong, Advanced thermal insulation and absorption properties of recycled cellulose aerogels, *Colloid. Surface. A.*, 2014, **445**, 128-134.

[6] H. H. Epsy, Mechanism of wet-strength development in paper: a review, *Tappi J.*, 1995, **78**, 90-99.

[7] P. Nordell, Wet strength development of paper, Departemnt of Applied Physics and Mechanical Engineering, *Lulea University of Technology*, 2006.

[8] J. Cai, S. Kimura, M. Wada, S. Kuga, L. Zhang, Cellulose aerogels from aqueous alkali hydroxide-urea solution, *ChemSusChem*, 2008, **1**, 149-154.

[9] W. Chen, H. Yu, Q. Li, Y. Liu, J. Li, Ultralight and highly flexible aerogels with long cellulose I nanofibers, *Soft Matter*, 2011, **7**, 10360.

[10] R. T. Olsson, M. A. S. Azizi Samir, G. Salazar-Alvarez, L. Belova, V. Strom, L. A. Berglund, O. Ikkala, J. Nogues, U. W. Gedde, Making flexible

magnetic aerogels and stiff magnetic nanopaper using cellulose nanofibrils as templates, *Nat. Nanotechnol.*, 2010, **5**, 584-588.

[11] A. Bayat, S. F. Aghamiri, A. Moheb, G. R. Vakili-Nezhaad, Oil spill cleanup from sea water by sorbent materials, *Chem. Eng. Technol.*, 2005, **28**, 1525-1528.

[12] M. O. Adebajo, R. L. Frost, J. T. Kloprogge, O. Carmody, S. Kokot, Porous Materials for Oil Spill Cleanup: A Review of Synthesis and Absorbing Properties, *J. Porous Mat.*, 2003, **10**, 159-170.

[13] R. Wahi, L. A. Chuah, T. S. Y. Choong, Z. Ngaini, M. M. Nourouzi, Oil removal from aqueous state by natural fibrous sorbent: An overview, *Sep. Purif. Technol.*, 2013, **113**, 51-63.

[14] Y. Chen, D. Zhang, Adsorption kinetics, isotherm and thermodynamics studies of flavones from Vaccinium Bracteatum Thunb leaves on NKA-2 resin, *Chem. Eng. J.*, 2014, **254**, 579-585.

[15] B. Wu, M. H. Zhou, Recycling of waste tyre rubber into oil absorbent, *Waste Manage.*, 2009, **29**, 355-359.

[16] P. Saha, S. Chowdhury, Insight into adsorption thermodynamics, in: M. Tadashi (Ed.), Thermodynamics, *InTech*, 2011, p. 450.

[17] P. Sharma, B. K. Saikia, M. R. Das, Removal of methyl green dye molecule from aqueous system using reduced graphene oxide as an efficient adsorbent: Kinetics, isotherm and thermodynamic parameters, *Colloid. Surface. A.*, 2014, **457**, 125-133.

[18] A. M. M. Vargas, A. L. Cazetta, M. H. Kunita, T. L. Silva, V. C. Almeida, Adsorption of methylene blue on activated carbon produced from

flamboyant pods (Delonix regia): Study of adsorption isotherms and kinetic models, *Chem. Eng. J.*, 2011, **168**, 722-730.

[19] T. Clyne, A. Markaki, J. Tan, Mechanical and magnetic properties of metal fibre networks, with and without a polymeric matrix, *Compos. Sci. Technol.*, 2005, **65**, 2492-2499.

[20] H. Sehaqui, M. Salajkova, Q. Zhou, L. A. Berglund, Mechanical performance tailoring of tough ultra-high porosity foams prepared from cellulose I nanofiber suspensions, *Soft Matter*, 2010, **6**, 1824-1832.

[21] H. Sehaqui, Q. Zhou, L. A. Berglund, High-porosity aerogels of high specific surface area prepared from nanofibrillated cellulose (NFC), *Compos. Sci. Technol.*, 2011, **71**, 1593-1599.

CHAPTER 6: Cellulose-Based Aerogels for Heat-Insulation Applications

6.1 Introduction

The greenhouse effect is gradually warming up the earth and potentially threatening human life. It was found that CO_2 emissions from buildings contributed approximately 31% of global greenhouse-gas emissions in 2010 [1, 2]. Improving thermal insulation of buildings is one of the most effective solutions for the issue. Therefore, many efforts have been made to develop new insulation materials [3]. Silica aerogels have been investigated as insulation materials for buildings [4]. However, they are very brittle. A flexible, aerogel-based insulation material has been developed by Aspen Aerogels (USA), but it is much more expensive than conventional insulation materials [4]. As a result, there is considerable need for insulation materials with reasonably low thermal conductivities and costs. These materials should also have high thermal stability for fire safety.

This chapter focuses on the thermal properties, such as thermal conductivity and thermal stability, of the recycled cellulose aerogels and their silica composites. This is the first time that the benchmark data of the thermal properties of recycled cellulose-based aerogels have been reported. Of the recycled cellulose-based materials in this thesis, the recycled cellulose aerogels using sodium hydroxide–urea aqueous solutions showed the lowest thermal conductivities (0.032 W/mK); however, the cellulose aerogels display a continuous weight loss from below 100 ^{o}C, during the thermogravimetric

(TGA) test. The cellulose–silica composite aerogels displayed the best thermal stability; however, their thermal conductivities (0.039–0.041 W/mK) are much higher than those of the cellulose aerogels using sodium hydroxide–urea aqueous solutions (0.032 W/mK). In summary, the recycled cellulose aerogels using a Kymene binder (the aerogels with the lowest cost), exhibiting lower thermal conductivities (0.034–0.037 W/mK) than those of the composite aerogels (0.039–0.041 W/mK), and a higher thermal stability (with a decomposition temperature of approximately 300 ^{o}C) surpassing that of the cellulose aerogels using sodium hydroxide–urea aqueous solutions, is the most promising thermal insulation material developed in this thesis.

6.2 Thermal properties of the recycled cellulose aerogels using sodium hydroxide–urea aqueous solutions

6.2.1 Thermal conductivity of the recycled cellulose aerogels using sodium hydroxide–urea aqueous solutions

To investigate the thermal insulation ability of our recycled cellulose aerogel fabricated from a sodium hydroxide–urea aqueous solution, a thermal conductivity measurement was carried out with a C-Therm TCi Thermal Conductivity Analyzer System, as described in Section 3.3.8. The measured thermal conductivity of the material was 0.0320 (±0.0003) W/mK, which was much better than that of the recycled cellulose fibres (0.050 W/mK, provided by Insul-Dek Engineering Pte Ltd and tested by PSB Corporation). This phenomenon was because the recycled cellulose fibres were in aerogel form, which has a large volume fraction of air, and air has a low thermal conductivity (0.026 W/mK) [5, 6]. The thermal conductivity of recycled cellulose aerogels is comparable to those of good insulation materials such as

wool (0.03–0.04 W/mK), silica aerogels (0.026 W/mK), and Aspen Aerogels products (0.021W/mK) [7, 8]. The low thermal conductivity of the cellulose aerogel might be attributed to the high porosity of the material, as shown in Figures 4.1c and 4.2. This low thermal conductivity, the eco-friendliness of the cellulose aerogels, and the cost-effectiveness of paper waste make recycled cellulose aerogels promising candidates for thermal-insulation applications.

6.2.2 Thermal stability of the recycled cellulose aerogels using sodium hydroxide–urea aqueous solutions

For safety concerns, the practical thermal insulation materials of buildings need to have high thermal stability. To evaluate the thermal stability of the cellulose aerogel fabricated from a sodium hydroxide–urea aqueous solution, a TGA test was performed on the cellulose aerogel sample in air, as described in Section 3.3.7. The results are displayed in Figure 6.1 below.

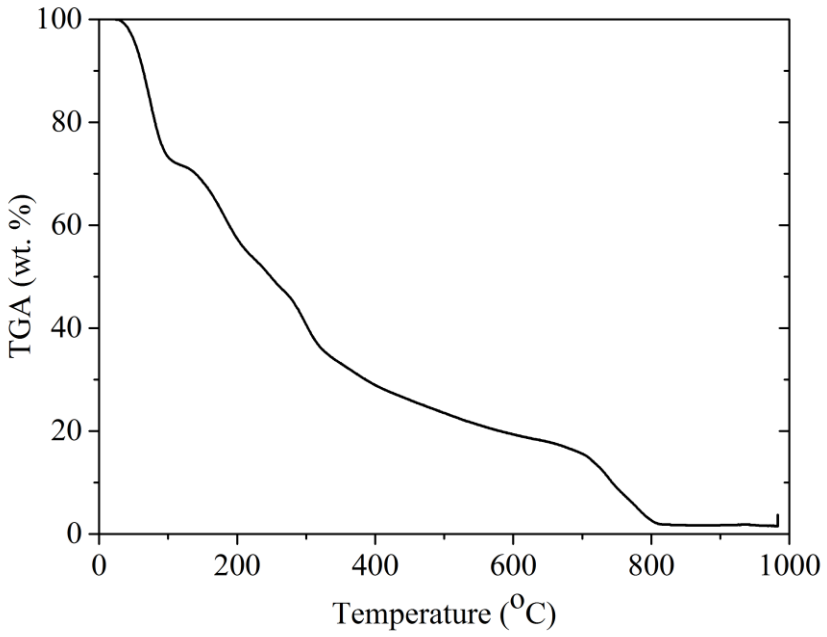

Figure 6.1 The thermogravimetric analysis (TGA) curve of the cellulose aerogel using sodium hydroxide–urea aqueous solution in the range of 25 to 1000 °C.

It can be observed from Figure 6.1 that a weight loss of approximately 32 wt. % occurred in the temperature range of 25 to 150 ^{o}C due to the removal of the absorbed water, and the degradation of cellulose. Following this, a weight loss of approximately 28 wt. % occurred in the range of 150 to 300 ^{o}C, due to the oxidative decomposition of cellulose, the formation of carbonaceous products, and the decomposition of some urea traces left in the tested cellulose-aerogel sample [9, 10]. In the temperature range of 300 to 700 ^{o}C, a slow mass loss of the residual substances was observed. There was then a small drop in the sample weight from 700 to 815 ^{o}C, possibly due to the oxidation of the charred residue [11].

6.3 Thermal properties of the recycled cellulose aerogels using a Kymene binder

6.3.1 Thermal conductivity of the recycled cellulose aerogels using a Kymene binder

Using the same approach as that described in Section 6.2.1, the thermal conductivities of the recycled cellulose aerogels fabricated with a Kymene binder were measured. The porosity of the cellulose aerogels using a Kymene binder significantly affected their thermal conductivities. Table 6.1 below shows that the thermal conductivity of the aerogels using a Kymene binder increased from 0.034 to 0.037 W/mK when the initial cellulose fibre concentration increased from 1.0 to 4.0 wt. %. As discussed in Section 5.2.1.1, increases in the initial cellulose fibre concentration lead to decreases in the porosity of the resultant cellulose aerogels. When the porosity is lower, there

is more solid substance to promote thermal conduction and reduce thermal insulation.

Table 6.1 Effects of cellulose fibre concentrations on the thermal conductivities of the cellulose aerogels using a Kymene binder.

Cellulose fibre concentration (wt. %)	Density (g/cm^3)	Thermal conductivity (W/mK)
1.0	0.0392 ± 0.0005	0.0340 ± 0.0003
2.0	0.0473 ± 0.0004	0.0353 ± 0.0006
4.0	0.0592 ± 0.0032	0.0366 ± 0.0003

6.3.2 Thermal stability of the recycled cellulose aerogels using a Kymene binder

Comparing Figure 6.1 with Figure 6.2 (below), the thermal stability of the cellulose aerogels using a Kymene binder was much better than that of the cellulose aerogels fabricated from the sodium hydroxide–urea aqueous solution. A weight loss of 6.5 wt. %, corresponding to the water release, was observed in the temperature range of 25–150 ^{o}C for the cellulose aerogel using a Kymene binder. Slow decomposition of the material was observed between 150 and 300 ^{o}C, and 86.3 wt. % remained of the cellulose aerogel using a Kymene binder at 300 ^{o}C. In comparison, 40.7 wt. % remained of the cellulose aerogel fabricated from the sodium hydroxide–urea aqueous solution at the same temperature.

The obvious differences suggest that the thermal stability of the cellulose aerogel using a Kymene binder was much better than that of the cellulose aerogel synthesized via the sodium hydroxide–urea route. The differences between the thermal stabilities of these two cellulose aerogels could possibly be explained by two major factors: (1) there was no urea involved in the fabrication of the cellulose aerogels via the Kymene route, and

so there was no urea residue [12]; and (2) the sonication method applied with the Kymene route, as a mechanical approach, had an advantage over the chemical treatment methods regarding thermal stability of the cellulose materials [13, 14].

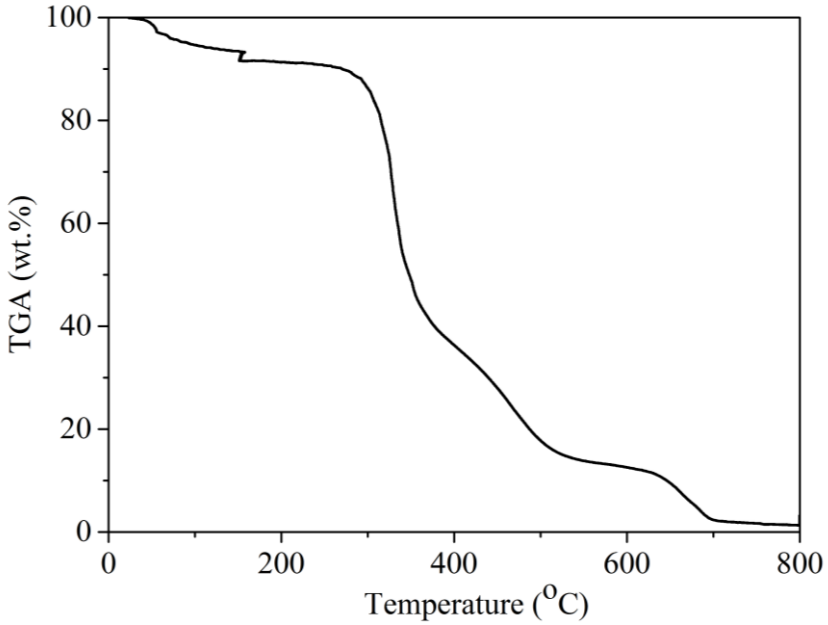

Figure 6.2 A typical image of the thermogravimetric analysis (TGA) curve of the cellulose aerogel using a Kymene binder. There were no observable differences between the TGA curves of the cellulose aerogels with different initial cellulose concentrations.

6.4 Properties of the silica–cellulose aerogels

The silica–cellulose composite aerogels were fabricated by immersing the cellulose matrixes inside the solutions containing a silica precursor, as described in Section 3.2.4. The cellulose matrixes were the recycled cellulose aerogels (obtained after hydrophobic coating) fabricated with a Kymene binder described in Section 3.2.2. The main purpose of the development of the silica–cellulose aerogels was to further improve the thermal stability and mechanical strength of the pure cellulose aerogels, which are extensively discussed in Sections 4.2.3, 5.2.3, 6.2.2 and 6.3.2. The different silica–cellulose aerogels are synthesized from the varied cellulose matrixes with

different initial recycled cellulose fibre concentrations (1.0–4.0 wt. %) in the initial cellulose suspensions. In this section, the morphology, structure, thermal, and mechanical properties of the different composites are discussed.

6.4.1 Morphology and hydrophobicity of the silica–cellulose aerogels

6.4.1.1 Morphology and structure of the silica–cellulose aerogels

The morphologies of the silica–cellulose composite aerogels were investigated with FE-SEM. Figures 6.3a–c display the SEM images of the silica–cellulose aerogels fabricated with the cellulose matrixes with different cellulose fibre concentrations in the initial cellulose aqueous suspensions. The images in Figures 6.3a–c suggest that the cellulose matrix served as the three-dimensional supporting frame.

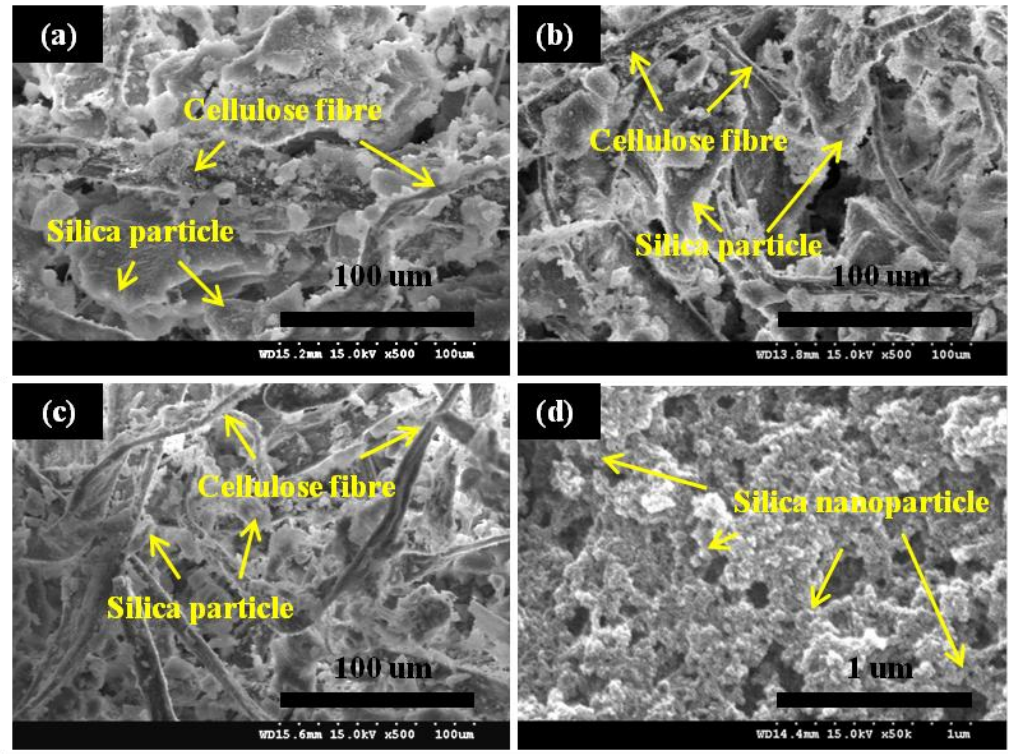

Figure 6.3 SEM images of the silica–cellulose aerogels fabricated with the cellulose matrixes with different cellulose fibre concentrations (a) 1.0 wt. %, (b) 2.0 wt. %, and (c) 4.0 wt. % in the initial cellulose aqueous suspensions. (d) is a typical image of the zoomed-in silica region of the composites.

The intersection points between the cellulose fibres were strengthened by a great number of hydrogen-bond links, which helped the formation of the strong supporting frame [15]. The strong supporting frame restricted the silica particles firmly within it by a confinement effect [16]. Meanwhile, the interconnected silica particles reinforced the cellulose matrix by attaching themselves to the matrix. As a result, a more rigid structure was formed.

The structures of the silica–cellulose aerogels using different cellulose aerogel matrixes are compared in Figures 6.3a–c. When the cellulose content was higher, silica particles with a smaller particle size and more uniform distribution were found. This phenomenon might be explained by the following speculations proposed in this thesis. Before the freeze drying, the cellulose fibres were embedded in the silica hydrogel. During the freeze drying (including the freezing pre-treatment), the silica particles away from the cellulose fibres experienced less force from the cellulose matrix than the silica particles next to the cellulose fibres. The denser cellulose matrix led to a more uniform distribution of small silica particles because of the more uniformly distributed force exerted by the cellulose matrix. On the other hand, the loose cellulose matrix with many large pores yielded a number of large silica particles located away from the cellulose fibres because of the small force exerted by the cellulose matrixes. At the same time, inside the loose cellulose matrix, the large silica particles located away from the cellulose fibres coexisted with the small silica particles that formed near the cellulose fibres, yielding a less uniform distribution.

The mesostructures of the silica–cellulose aerogels using different cellulose aerogel matrixes were nearly identical, and a typical image of the

magnified silica region of the silica–cellulose aerogels is shown in Figure 6.3d. The mesostructure of the silica particles was similar to the findings of other groups that developed silica–cellulose aerogels [16, 17].

The nitrogen adsorption of the silica–cellulose aerogels was studied, and the adsorption–desorption isotherms are displayed in Figure 6.4 below. As shown in Table 6.2 below, the BET surface areas of the silica–cellulose composite aerogels were between approximately 198 and 296 m^2/g, comparable to the surface areas found in similar studies conducted by Demilecamps *et al.* (90–170 m^2/g) [18] and Litschauer *et al.* (220–290 m^2/g) [19].

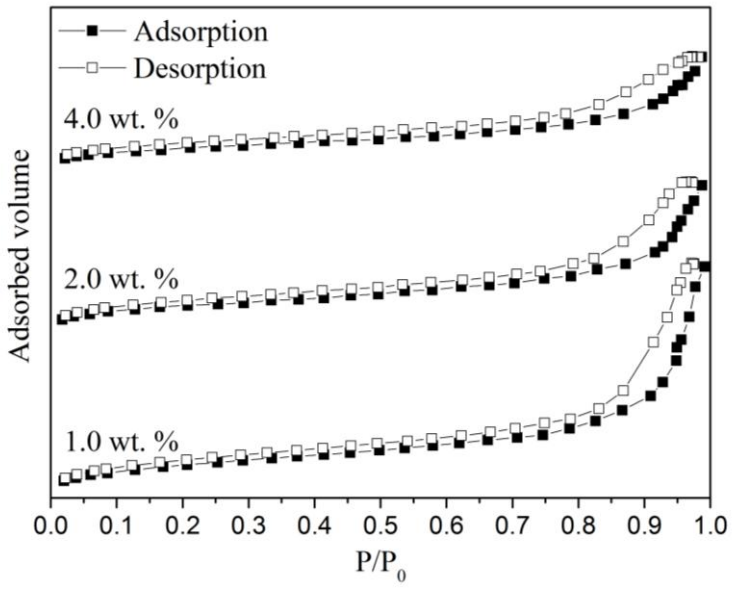

Figure 6.4 The nitrogen adsorption/desorption isotherms of the silica–cellulose aerogels fabricated with different cellulose matrixes. The different cellulose matrixes were fabricated with different cellulose fibre concentrations (1.0, 2.0, and 4.0 wt. %) inside the initial cellulose aqueous suspensions.

Table 6.2 Morphology studies of the cellulose–silica composites.

Cellulose fibre concentration inside the initial suspension for cellulose matrix fabrication (wt. %)	Density (g/cm^3)	SiO_2 in composite aerogel (wt. %)	BET surface area (m^2/g)	Porosity (%)
1.0	0.149 ±0.005	79 ±4	296 ±31	93.8 ±0.0
2.0	0.146 ±0.005	73 ±5	248 ±28	93.8 ±0.0
4.0	0.138 ±0.002	60 ±3	198 ±24	93.7 ±0.0

A moderate linear relationship was observed between the silica mass concentration and the BET surface area of the composite, as shown in Figure 6.5 below. The silica mass concentration was calculated as the ratio of the mass of the composite aerogel excluding the mass of the cellulose matrix (before embedding) to the mass of the silica–cellulose aerogel. This relationship indicated that the different cellulose matrixes played a minor role in the meso-porous structure of the silica–cellulose aerogels, which is consistent with previous SEM findings.

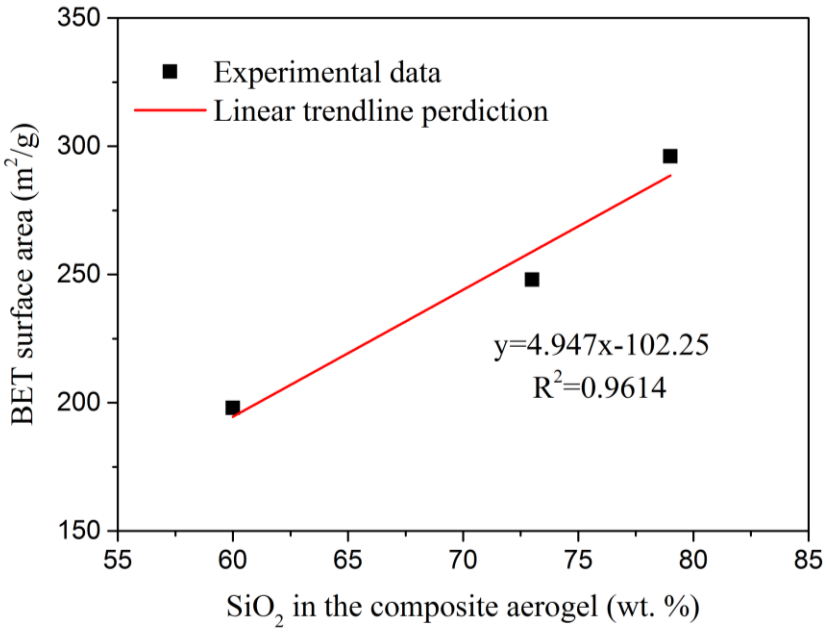

Figure 6.5 The moderate linear relationship between the silica mass concentration and the BET surface area of the composite.

As can be observed in Figure 6.6 below, the X-ray diffraction patterns of the silica–cellulose composite aerogels seem to be the superposition of those of the pure cellulose aerogels and the pure silica aerogels, which is similar to the findings of Cai *et al.* [20]. This XRD finding implies that the extent of chemical reaction between the cellulose fibres and the silica components was quite limited as no new compound was detected. The XRD

results suggest that it was reasonable for the meso-porous structure of the silica–cellulose aerogels to be controlled only by the silica components as the cellulose matrix did not possess a detectable BET surface area, and no new compound was formed. In addition, the XRD results indicate that the attachments between the cellulose fibres and the silica particles observed in the SEM images were physical instead of chemical.

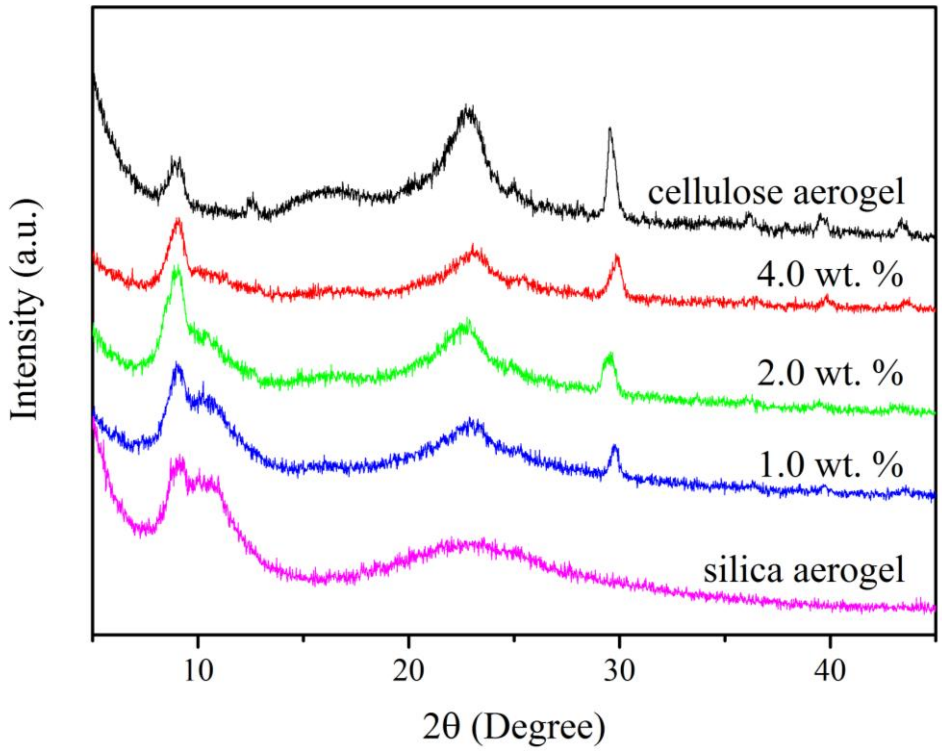

Figure 6.6 XRD patterns of the silica aerogel, the cellulose aerogel, and the silica–cellulose aerogels fabricated from cellulose matrixes with different cellulose fibre concentrations (1.0, 2.0, and 4.0 wt. %) inside the initial suspensions.

6.4.1.2 Hydrophobicity of the silica–cellulose aerogels

According to *Shi et al.* [17], the hydrophobicity of the composite could improve the stability of the heat-insulation performance of the material. To date, research on hydrophobic modifications of silica–cellulose composite aerogels has been limited. In 2013, Shi *et al.* [17] applied a CCl4 cold-plasma modification approach using gas ionization. In the same year, Sai *et al.* [16]

proposed a solvent-immersion method involving a 24 h aging followed by freeze drying. Both methods might be considered uneconomical because of either the expensive equipment or the large amount of chemicals and the long duration involved. Moreover, the water contact angles of the modified composite aerogels from the above two methods were similar (132 ^{o} and 133^{o}), indicating that the aerogels were not super-hydrophobic [16, 17].

However, the silica–cellulose composite aerogels developed for this thesis exhibited the super-hydrophobic property. The average water contact angle was approximately 151 ^{o} for all three composites. Figure 6.7 below shows a typical image of the water contact angle measurements of the composites. This excellent water-repelling property was inherited from both the hydrophobic cellulose matrix and the silica precursor (MTMS). The hydrophobic property of the cellulose matrix is discussed extensively in Section 5.2.1.2. Meanwhile, the stable methyl group of MTMS was responsible for the excellent hydrophobicity of the silica components [21]. Further modification of the fabricated composite aerogels was not required to achieve the super-hydrophobicity, which could be considered a remarkable advantage.

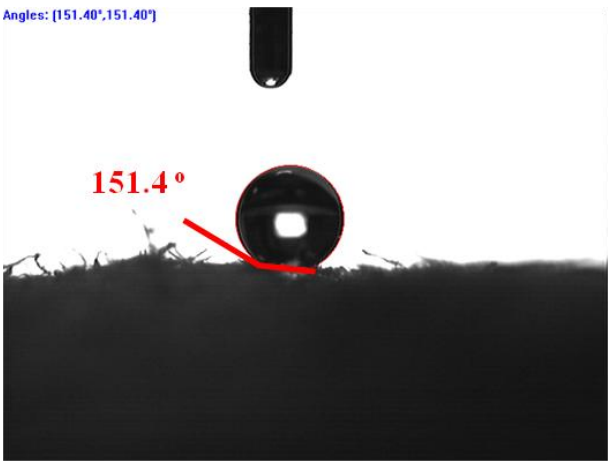

Figure 6.7 A typical image of the water contact angle measurements of the silica–cellulose aerogels.

6.4.2 Thermal conductivity of the silica–cellulose aerogels

As suggested by table 6.3, the thermal conductivities of the silica–cellulose aerogels (0.0385–0.0410 W/mK) increase with the increases in density (0.138–0.149 g/cm^3). With references to Table 6.1, and Table 6.3 below, the thermal conductivities and the densities of the silica–cellulose aerogels (0.0385–0.0410 W/mK; 0.138–0.149 g/cm^3) were higher than those of the cellulose aerogels using a Kymene binder (0.034–0.037 W/mK; 0.039–0.059 g/cm^3). One possible reason is that thermal conductivities increase with densities [22, 23].

The thermal conductivities of the silica–cellulose aerogels (0.0385–0.0410 W/mK) were lower than those of the silica–cellulose composites fabricated by other groups (0.15 W/mK), and comparable to those of conventional insulation materials, such as polyurethane foams (0.02–0.04 W/mK) and insulation boards (0.035–0.16 W/mK) [7].

Table 6.3 The thermal conductivities of the silica–cellulose aerogels fabricated from cellulose matrixes with different cellulose fibre concentrations in the initial suspensions.

Cellulose fibre concentration in the initial suspension for cellulose-matrix fabrication (wt. %)	Density (g/cm^3)	Thermal conductivity (W/mK)
1.0	0.149 ±0.005	0.0410 ±0.0003
2.0	0.146 ±0.005	0.0390 ±0.0006
4.0	0.138 ±0.002	0.0387 ±0.0003

6.4.3 Thermal stability of the silica–cellulose aerogels

As shown in Figure 6.8 below, it is clear that the thermal stability of the composite was better than that of the pure cellulose aerogel without the silica embedment. A small weight loss of approximately 2 wt. % of the composites before 150 ^{o}C corresponds to the water release. The cellulose aerogel using a Kymene binder showed an approximately 7 wt. % weight loss

up to 150 ^{o}C, which is greater than that of the composite. This smaller weight loss from the desorbed water was due to the super-hydrophobicity of the composite.

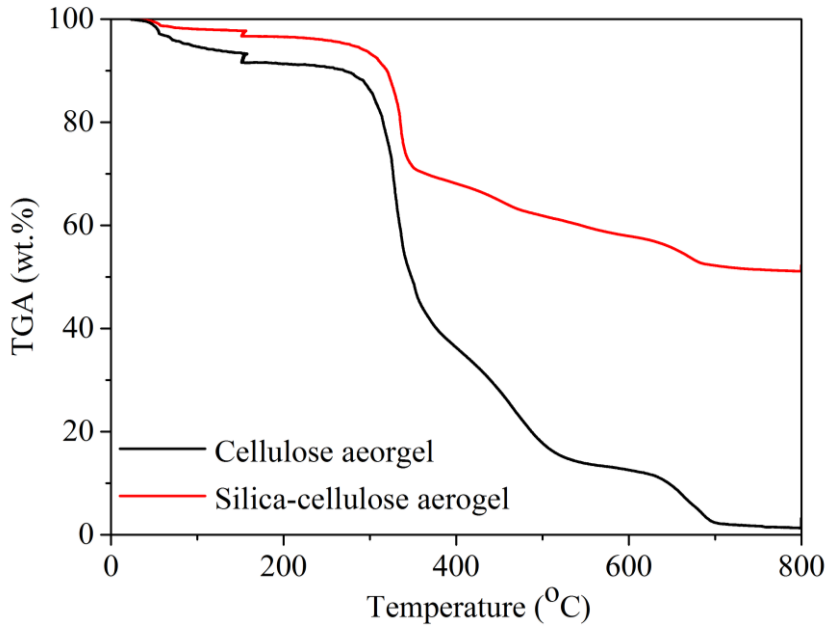

Figure 6.8 The thermogravimetric analysis (TGA) curve of the silica–cellulose aerogel, compared with that of the cellulose aerogel using a Kymene binder. The composite aerogels were fabricated from cellulose matrixes with different cellulose fibre concentration of 4.0 wt. % in the initial suspensions.

A 25 ^{o}C delay in the thermal degradation of the cellulose component of the composite was observed at 325 ^{o}C, compared with 300 ^{o}C before the silica modification. This increase in the degradation temperature might have been due to an interaction between the silica and the cellulose matrix at higher temperatures, and the interaction showed a positive effect on the thermal resistance of the composite [7, 24]. At 300 ^{o}C, 93 wt. % silica–cellulose aerogels was remained, as opposed to 86 wt. % of cellulose aerogels using Kymene binder, demonstrating a better thermal stability.

The slow mass loss of the residual substances followed the rapid oxidative decomposition stage, after which the oxidation of the charred

residue occurred and continued to the plateau. At the plateau, 51 wt. % of the silica–cellulose aerogel was preserved, mainly containing the silica.

6.4.4 Mechanical properties of the silica–cellulose aerogels

The silica modification did not impede the ductile behaviour of the silica–cellulose aerogels. The compressive strain–stress curves of the silica–cellulose aerogels fabricated from different cellulose matrixes are displayed in Figure 6.9 below.

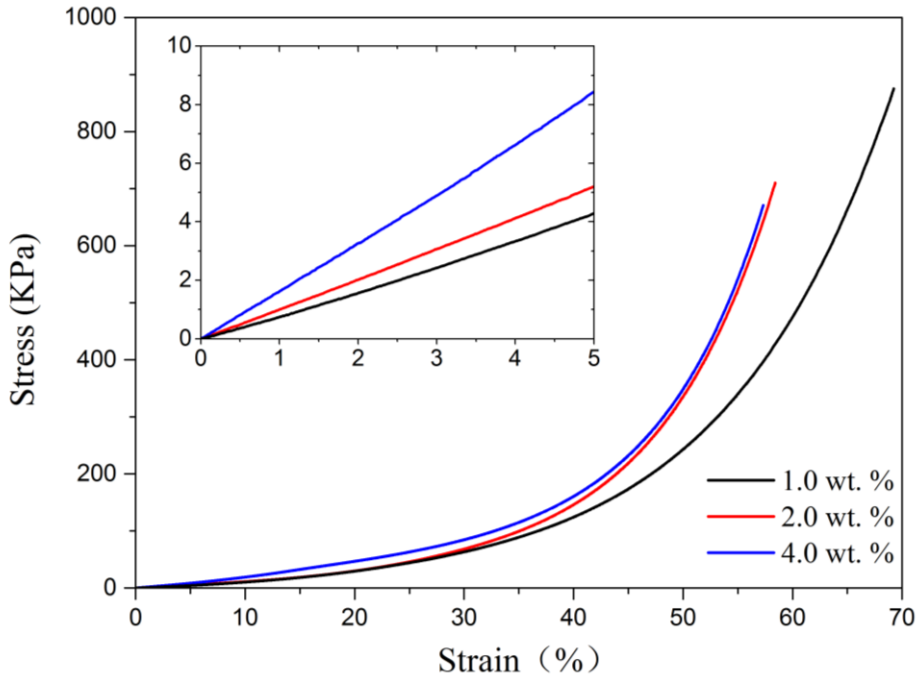

Figure 6.9 The compressive strain–stress curves of the silica–cellulose aerogels fabricated from the cellulose matrixes with different cellulose fibre concentrations (1.0, 2.0, and 4.0 wt. %) in the initial suspensions. The magnified section shows the compressive curves at the low strain (up to 5%) for the composite aerogels.

Silica embedment improved the mechanical strength of the aerogels dramatically. The compressive Young's moduli of the composites were three to five times greater than those of their cellulose aerogel matrixes, as shown in Table 6.4 below. One contributing factor to the high mechanical strength of

the silica–cellulose aerogels was their high densities compared with those of the cellulose matrixes, which is typical for many material systems, as the materials are more rigid and stiff, with a higher density [25, 26]. From microcosmic aspect, the silica particles restrained the bending of the cellulose fibres, improving the mechanical strength of the silica–cellulose aerogels.

Table 6.4 The Young's modulus of the silica–cellulose composites and their cellulose aerogel matrixes.

Cellulose fibre concentration in the initial suspension for cellulose matrix fabrication (wt. %)	Young's modulus of cellulose matrix (KPa)	Density of composite (g/cm^3)	Young's modulus of composite (KPa)
1.0	13 ±1	0.149 ±0.005	86 ±3
2.0	21 ±1	0.146 ±0.005	104 ±3
4.0	39 ±2	0.138 ±0.002	169 ±5

For the silica–cellulose aerogels, the Young's modulus increased with slight decreases in density, as suggested in Table 6.4. This might possibly be explained by the increased cellulose content of the silica–cellulose aerogels, as proposed by this thesis. The cellulose matrix reinforces and constrains the silica granules, and the higher cellulose content leads to a more rigid cellulose matrix; thus the Young's modulus of the composite increases with the increases in the cellulose content.

6.5 Summary

In summary, the three recycled cellulose-based aerogels with three different thermal property combinations have been discussed. The thermal conductivity of the cellulose aerogel using a sodium hydroxide–urea aqueous solution was 0.032 W/mK, which was the lowest among the recycled cellulose fibre–based aerogels discussed in this thesis. However, the cellulose content of

this material begins to degrade at 150 ^{o}C; therefore the material will require substantial modifications if the thermal stability is a major concern.

The recycled cellulose aerogels using a Kymene binder with cost-effective fabrication displayed better thermal stability than the cellulose aerogels using a sodium hydroxide–urea aqueous solution. However, the thermal conductivities of the aerogels using a Kymene binder were between 0.034 and 0.037 W/mK. These thermal conductivity values are slightly higher than those of the cellulose aerogels using a sodium hydroxide–urea aqueous solution.

To improve the thermal stability of the recycled cellulose-based aerogels further, the silica–cellulose composite aerogels were successfully developed. A 25 ^{o}C delay in the cellulose degradation was also observed for the composites. The developed silica–cellulose aerogels also had better mechanical strengths (compressive Young's modulus: 86–169 KPa) than those of the cellulose aerogels (compressive Young's modulus: 13–39 KPa). Moreover, the inherent super-hydrophobic property of the silica–cellulose aerogels is also desirable for reliable and long-term thermal insulation. The thermal conductivities of the silica–cellulose aerogels were approximately 0.04 W/mK, comparable to those of commercial insulation products and lower than those of the cellulose aerogels described in this thesis, as discussed in Section 6.4.3.

References

[1] S. de la Rue du Can, L. Price, T. Zwickel, Understanding the full climate change impact of energy consumption and mitigation at the end-use level: A proposed methodology for allocating indirect carbon dioxide emissions, *Appl. Energ.*, 2015, **159**, 548-559.

[2] V. Krey, O. Masera, G. Bllanford, T. Bruckner, R. Cooke, Climate change 2014: mitigation of climate change, *Cambridge University Press*, Cambridge, 2014.

[3] B. P. Jelle, Traditional, state-of-the-art and future thermal building insulation materials and solutions – Properties, requirements and possibilities, *Energ. Buildings*, 2011, **43**, 2549-2563.

[4] R. Baetens, B. P. Jelle, A. Gustavsen, Aerogel insulation for building applications: A state-of-the-art review, *Energ. Buildings*, 2011, **43**, 761-769.

[5] I. H. Tavman, Effective thermal conductivity of granular porous materials, *Int. Comm. Heat Mass Transfer*, 1996, **23**, 169-176.

[6] Z.-Y. Deng, J. M. F. Ferreira, Y. Tanaka, Y. Isoda, Microstructure and thermal conductivity of porous ZrO2 ceramics, *Acta Mater.*, 2007, **55**, 3663-3669.

[7] S. Sequeira, D. V. Evtuguin, I. Portugal, Preparation and properties of cellulose/silica hybrid composites, *Polym. Composite.*, 2009, **30**, 1275-1282.

[8] J. W. S. Hearle, A fringed fibril theory of structure in crystalline polymers, *J. Polym. Sci.*, 1958, **28**, 432-435.

[9] S. Soares, N. M. P. S. Ricardo, S. Jones, F. Heatley, High temperature thermal degradation of cellulose in air studied using FTIR and ^{1}H and ^{13}C solid-state NMR, *Eur. Polym. J.*, 2001, **37**, 737-745.

[10] P. M. Schaber, J. Colson, S. Higgins, D. Thielen, B. Anspach, J. Brauer, Thermal decomposition (pyrolysis) of urea in an open reaction vessel, *Thermochimica Acta*, 2004, **424**, 131-142.

[11] B. Kaur, I. S. Gur, H. L. Bhatnagar, Studies on thermal degradation of cellulose and cellulose phosphoramides, *J. Appl. Polym. Sci.*, 1986, **31**, 667-683.

[12] J. Feng, S. T. Nguyen, Z. Fan, H. M. Duong, Advanced fabrication and oil absorption properties of super-hydrophobic recycled cellulose aerogels, *Chem. Eng. J.*, 2015, **270**, 168-175.

[13] S. Y. Cho, Y. Choi, D. Park, S. Heo, D. H. Kim, H.-J. Jin, Cellulose nanocrystals with high thermal stability and their nanocomposites with poly(lactic acid), ICCM18, Korea, 2011.

[14] G. H. Tonoli, E. M. Teixeira, A. C. Correa, J. M. Marconcini, L. A. Caixeta, M. A. Pereira-da-Silva, L. H. Mattoso, Cellulose micro/nanofibres from Eucalyptus kraft pulp: preparation and properties, *Carbohydrate polymers*, 2012, **89**, 80-88.

[15] D. Klemm, B. Heublein, H. P. Fink, A. Bohn, Cellulose: fascinating biopolymer and sustainable raw material, *Angewandte Chemie*, 2005, **44**, 3358-3393.

[16] H. Sai, L. Xing, J. Xiang, L. Cui, J. Jiao, C. Zhao, Z. Li, F. Li, Flexible aerogels based on an interpenetrating network of bacterial cellulose and silica by a non-supercritical drying process, *J. Mater. Chem. A*, 2013, **1**, 7963.

[17] J. Shi, L. Lu, W. Guo, J. Zhang, Y. Cao, Heat insulation performance, mechanics and hydrophobic modification of cellulose-SiO2 composite aerogels, *Carbohydrate polymers*, 2013, **98**, 282-289.

[18] A. Demilecamps, G. Reichenauer, A. Rigacci, T. Budtova, Cellulose–silica composite aerogels from “one-pot” synthesis, *Cellulose*, 2014, **21**, 2625-2636.

[19] M. Litschauer, M.-A. Neouze, E. Haimer, U. Henniges, A. Potthast, T. Rosenau, F. Liebner, Silica modified cellulosic aerogels, *Cellulose*, 2011, **18**, 143-149.

[20] J. Cai, S. Liu, J. Feng, S. Kimura, M. Wada, S. Kuga, L. Zhang, Cellulose-silica nanocomposite aerogels by in situ formation of silica in cellulose gel, *Angewandte Chemie*, 2012, **51**, 2076-2079.

[21] A. Venkateswara Rao, M. M. Kulkarni, D. P. Amalnerkar, T. Seth, Superhydrophobic silica aerogels based on methyltrimethoxysilane precursor, *J. Non-Cryst. Solids*, 2003, **330**, 187-195.

[22] S. B. H. Simmler, U. Heinemann, H. Schwab, K. Kumaran, P. Mukhopadhyaya, et al, Vaccum insulation panels: study on VIP-components and panels for service life prediction of VIP in building applications (subtask A), 2005.

[23] M. C. Kiran, A. Nandanwar, M. V. Naidu, K. C. V. Rajulu, Effects of density on thermal conductivity of bamboo mat board, *Int. J. Agric. For.* , 2012, **2**, 257-261.

[24] N. Jia, S.-M. Li, M.-G. Ma, J.-F. Zhu, R.-C. Sun, Synthesis and characterization of cellulose-silica composite fiber in ethanol/water mixed solvents, *BioResources*, 2011, **6**, 1186-1195.

[25] K. E. Parmenter, F. Milstein, Mechanical properties of silica aerogels, *J. Non-Cryst. Solids*, 1998, **223**, 179-189.

[26] A. H. Alaoui, T. Woignier, G. W. Scherer, J. Phalippou, Comparison between flexural and uniaxial compression tests to measure the elastic modulus of silica aerogel, *J. Non-Cryst. Solids*, 2008, **354**, 4556-4561.

CHAPTER 7: Conclusions and Recommendations

7.1 Conclusions

For the first time, paper waste can be successfully converted into cellulose-based aerogels with high oil absorption capacities (95 g/g), good thermal-insulation performances (0.032 W/mK), and excellent water-repellent properties (151^{o}). Recycled cellulose-based aerogels utilizing paper waste are promising and economical candidates for several applications, such as oil-spill cleaning and building thermal insulation.

For this thesis, two methods were successfully explored for the fabrication of recycled cellulose aerogels: (1) the method using a sodium hydroxide–urea aqueous solution; and (2) the approach using a Kymene binder. In addition, morphology control of the recycled cellulose aerogels could be efficiently achieved by changing the cellulose concentration. To obtain the hydrophobic coating, a simple but effective chemical vapour deposition method via MTMS was developed, and the stability of the hydrophobic coating was tested. The recycled cellulose aerogels generated from both fabrication methods demonstrated stable hydrophobic properties over the tested time span of five months.

The crude oil–absorption behaviour of the recycled cellulose aerogels fabricated from a sodium hydroxide–urea aqueous suspension (cellulose fibre concentration: 2.0 wt. %) was studied. During this study, the sorption capacities of the cellulose aerogels of three different crude oils (RB, TGT, and RD) at three different temperatures (25, 40 and 60 ℃) were investigated. For all the cellulose aerogels, RB at 40 ℃ had the highest absorption capacity,

24.4 g/g; the absorption capacities depended on the viscosities of the oils. The absorption kinetics of the cellulose aerogels using a sodium hydroxide–urea aqueous suspension with the three different crude oils were investigated. The aerogels easily absorbed crude oil and were completely immersed in the oil after approximately 3 min, indicating high affinity between the absorbent and the crude oils. Furthermore, the compressive modulus of the aerogel (cellulose fibre concentration: 2.0 wt. %) was calculated as approximately 22 KPa from the strain–stress curve. The recycled cellulose aerogels fabricated from the sodium hydroxide–urea aqueous solution method are good candidates for oil-spill cleaning because of their reasonable oil absorption properties and compressive modulus. However, the fabrication cost and time of these cellulose aerogels need to be further reduced for industrial oil spill–cleaning applications.

Because of these limitations, the oil absorption properties of the recycled cellulose aerogels fabricated with a Kymene binder were also investigated. The initial cellulose fibre concentration played a critical role in the absorption capacities: the decreases in the initial cellulose fibre concentration led to increases in the absorption capacities due to the reduced porosities. The maximum absorption capacity of 95 g/g (for 5w40 motor oil) was achieved by the cellulose aerogels with a cellulose fibre concentration of 0.25 wt. % in the initial cellulose aqueous suspension.

The optimum temperature for high oil absorption capacity was 50 ^{o}C (of 25, 50, and 70 ^{o}C) because of the favourable viscosities of the oils at this temperature, as the viscosities were low enough for the oils to efficiently penetrate the porous aerogel networks and high enough for the oils to

effectively anchor to the pore walls of the cellulose aerogels. In addition, the pH values of the seawater/oil suspension had negligible effects on the oil absorption capacities of the cellulose aerogels, as the key factors affecting absorption capacity (the porosities of the cellulose aerogels and the viscosities of the oils) were independent of the environmental pH values.

The oil absorption kinetics of the cellulose aerogels were investigated via both the pseudo-first-order and pseudo-second-order kinetics models. Benchmark values for the absorption rate constant and the activation energy of the oil absorption behaviour of cellulose aerogels using a Kymene binder have been provided in this thesis, with these two kinetics models. The pseudo-second-order model can better predict the oil absorption behaviour due to its chemi-sorption nature.

The raw-material toxicity of the cellulose aerogels using a Kymene binder was significantly lower than that of the aerogel using sodium hydroxide–urea. This is because only a few micro-litres of Kymene, instead of a few grams of sodium hydroxide and urea, was required during the fabrication. In addition, the Kymene method made it possible to shorten the synthesis duration from the nine days of the previous method (using sodium hydroxide–urea) to three days. Furthermore, cellulose aerogels (cellulose fibre concentration: 0.6%) of industrial-scale size (38 cm by 38 cm by 1 cm) and using a Kymene binder were fabricated, and could be easily bent or rolled without damaging their shape, indicating excellent flexibility.

In conclusion, the recycled cellulose aerogels using a Kymene binder, which are cost-effective and have excellent oil absorption properties and high flexibility, could be very promising sorbents for oil spill–cleaning applications.

In addition, the thermal insulation and thermal stability of three types of recycled cellulose-based aerogels were explored: (1) the recycled cellulose aerogels using a sodium hydroxide–urea aqueous suspension; (2) the recycled cellulose aerogels using a Kymene binder; and (3) the silica–cellulose aerogels. The cellulose aerogels using a sodium hydroxide–urea aqueous suspension showed the lowest thermal conductivity (0.032 W/mK) of the three types of cellulose-based aerogels due to their high porosity. However, the thermal stability of these aerogels was the worst, with continuous degradation observed at a relatively low temperature (below 150 ^{o}C), because of the chemical treatment method and the fact that urea was involved in the fabrication.

The most cost-effective cellulose aerogels using a Kymene binder showed an observable improvement in thermal stability over the previous cellulose aerogels, because the Kymene method mainly applies a mechanical approach and no urea is involved. However, their thermal-conductivity values (0.034–0.037 W/mK) were slightly higher than those of the cellulose aerogels using the sodium hydroxide–urea method, due to their lower porosity and highly compressible nature.

To improve thermal stability further, the silica–cellulose aerogels were successfully developed. A significant improvement in thermal stability was achieved: the thermal degradation of the cellulose component shifted from 300 ^{o}C for the cellulose aerogels using a Kymene binder to 325 ^{o}C for the silica–cellulose aerogels. This shift might have been due to the interaction between the silica and cellulose matrixes under the heating conditions; at 800 ^{o}C, approximately 58–72 wt. % of the silica–cellulose aerogels was

preserved, compared with 20 wt. % of the cellulose aerogels using a Kymene binder, due to the thermally stable silica component. The major DTA peak also shifted from 352 ^{o}C for the cellulose aerogels to 530–550 ^{o}C for the silica–cellulose aerogels, as the major DTA peak of the composites is caused by the oxidation of the methyl group of the silica component. In addition, the silica–cellulose aerogels displayed an inherent super-hydrophobic property and better mechanical strength (Young's modulus: 86–169 KPa) than the cellulose aerogels using a Kymene binder (4–39 KPa). However, the thermal conductivities (approximately 0.04 W/mK) of the silica–cellulose aerogels were higher than those of the cellulose aerogels using a Kymene binder, due to their high density and low porosity.

7.2 Future work recommendations

This thesis focuses on synthesizing cellulose-based aerogels from recycled paper cellulose fibres and testing their properties. Other cellulosic sources for aerogel fabrication would also be of interest for some specific applications, such as the components of thermal-insulation lunch boxes and wound dressings for medical uses. Both these applications require a high standard of hygiene, which the recycled cellulose fibre described in this thesis cannot meet without further modifications. Moreover, the most effective way to further improve the mechanical properties of the cellulose-based aerogels would be to change the cellulose source, for example to bacterial cellulose or plant cellulose, with its inherent high mechanical strength. However, the synthesis methods introduced in this thesis may also be applicable to other similar cellulosic sources.

In addition, the only cellulose aerogel–based composite investigated for this thesis was the silica–cellulose aerogels, for the purpose of improving thermal stability and mechanical strength, compared with pure cellulose aerogels. Other cellulose-based composites would also be interesting subjects for other purposes, for example the absorbents that undergo swelling during a sorption process. This type of material has the advantages of easy storage and fast-rate absorption. One possible approach to creating such materials is to develop cellulose–carboxymethylcellulose (CMC) composite aerogels. Cellulose–CMC hydrogels have been successfully fabricated, and shown swelling properties [1]. The aerogels that are based on these swelling hydrogels might therefore display a higher swelling rate and ratio than the hydrogels. However, one possible problem is the brittleness of the new material, which will need to be carefully handled.

The recycled cellulose-based aerogels in this thesis may also be promising materials for acoustic insulation, as cellulose materials are well known for their good acoustic insulation properties [2–4]. To test the acoustic insulation properties of the cellulose-based aerogels, standing wave tube methods could be applied, as they could provide the acoustic absorption coefficients [5, 6]. However, when only rough estimates are needed, it might be possible to use a sound-signal generator producing known sound signals at the appropriate frequency range, and a sound meter to investigate the acoustic insulation properties of the cellulose-based aerogels.

With this approach, the sound generator may be placed both inside and outside an insulation box fabricated from the testing material, and the incident sound signal measured at the same distance from the sound generator in both

situations. The sound absorption efficiency might be defined as the ratio of the absorbed sound intensity to the known sound intensity. After the absorption efficiencies of the different cellulose-based aerogels and reference materials are obtained, it would be straightforward to evaluate the acoustic insulation performances of the cellulose-based aerogels.

References

[1] C. Chang, B. Duan, J. Cai, L. Zhang, Superabsorbent hydrogels based on cellulose for smart swelling and controllable delivery, *Eur. Polym. J.*, 2010, **46**, 92-100.

[2] J. P. Arenas, J. Rebolledo, R. d. Rey, J. Alba, Sound absorption properties of unbleached cellulose loose-fill insulation material, *BioResources*, 2014, **9**, 6227-6240.

[3] F. Asdrubali, S. Schiavoni, K. V. Horoshenkov, A review of sustainable materials for acoustic applications, *Build. Acoust.*, 2012, **19**, 283-312.

[4] J.-O. Yeon, K.-W. Kim, K.-S. Yang, J.-M. Kim, M.-J. Kim, Physical properties of cellulose sound absorbers produced using recycled paper, *Constr. Build. Mater.*, 2014, **70**, 494-500.

[5] Y. Lu, Q. Sun, D. Yang, X. She, X. Yao, G. Zhu, Y. Liu, H. Zhao, J. Li, Fabrication of mesoporous lignocellulose aerogels from wood via cyclic liquid nitrogen freezing–thawing in ionic liquid solution, *J. Mater. Chem.*, 2012, **22**, 13548.

[6] K. W. Oh, D. K. Kim, S. H. Kim, Ultra-porous flexible PET/Aerogel blanket for sound absorption and thermal insulation, *Fiber. Polym.*, 2009, **10**, 731-737.

LIST OF PUBLICATIONS

1. JOURNAL PAPERS

(1) **Jingduo Feng**, Son T. Nguyen, Zeng Fan, Hai M. Duong, Advanced fabrication and oil absorption properties of super-hydrophobic recycled cellulose aerogels, *Chemical Engineering Journal*, 2015, **270**, 168-175.

(2) Son T. Nguyen[#], **Jingduo Feng**[#], Shao Kai Ng, Janet P. W. Wong, Vincent B. C. Tan, Hai M Duong, Advanced thermal insulation and absorption properties of recycled cellulose aerogels, *Colloids and Surfaces A: Physicochemical and Engineering Aspects*, 2014, **445**, 128-134. ([#]Contribute equally.)

(3) **Jingduo Feng**, Son T. Nguyen, Hai M. Duong, Recycled paper cellulose aerogels synthesis and water absorption properties, *Advanced Materials Research*, 2014, **936**, 938-941.

(4) Son T. Nguyen[#], **Jingduo Feng**[#], Nhat T. Le, Ai T. T. Le, Nguyen Hoang, Vincent B. C. Tan, Hai M. Duong, Cellulose aerogel from paper waste for crude oil spill cleaning, *Industrial & Engineering Chemistry Research*, 2013, **52**, 18386-18391. ([#]Contribute equally.)

2. CONFERENCES PROCEEDINGS

(1) **Jingduo Feng**, Son T. Nguyen, Hai M. Duong, Recycled paper cellulose aerogels synthesis and water absorption properties, MSET 2014, 28th–29th June 2014, Shanghai, China.

(2) **Jingduo Feng**, Son T. Nguyen, Shao Kai Ng, Janet P. W. Wong, Nhat T. Le, Ai T. T. Le, Nguyen Hoang, Vincent B. C. Tan, Hai M. Duong,

Cellulose aerogels from paper waste and their applications, PFAM XXII, 18th–20th December 2013, Singapore.

(3) **Jingduo Feng**, Son T. Nguyen, Shao Kai Ng, Janet P. W. Wong, Vincent B. C. Tan, Hai M. Duong, Industrial applications of paper waste aerogels, TechInnovation 2013, 24th September 2013, Singapore.

(4) **Jingduo Feng**, Son T. Nguyen, Shao Kai Ng, Janet P. W. Wong, Vincent B. C. Tan, Hai M. Duong, InnovFest, 14th–16th May 2013, Singapore.